UNIVERSITY OF OKLAHOMA

GRADUATE COLLEGE

SATELLITE REMOTE SENSING AND HYDROLOGIC MODELING FOR FLOOD MONITORING IN DATA POOR ENVIRONMENTS

A DISSERTATION

SUBMITTED TO THE GRADUATE FACULTY

in partial fulfillment of the requirements for the

Degree of

DOCTOR OF PHILOSOPHY

By

SADIQ IBRAHIM KHAN
Norman, Oklahoma
2011

SATELLITE REMOTE SENSING AND HYDROLOGIC MODELING FOR FLOOD MONITORING IN DATA POOR ENVIRONMENTS

A DISSERTATION APPROVED FOR THE
DEPARTMENT OF GEOGRAPHY AND ENVIRONMENTAL SUSTAINABILITY

BY

Dr. Jason Julian, Chair

Dr. Yang Hong, Co-Chair

Dr. Sally Gros

Dr. Xiangming Xiao

Dr. Aondover Tarhule

TABLE OF CONTENTS

List of Figures

List of Tables

CHAPTER 1 : INTRODUCTION

Natural disasters cannot be completely avoided, but the impacts and aftereffects can be managed by developing effective risk reduction strategies through application of geospatial tools and decision support systems. Disasters, such as floods, can cause loss of life and bring about extensive economic losses and social disruptions throughout the world. It was not long ago that the international community fully recognized that sustainable development framework should integrate natural disaster risk reduction strategies. This concept was in the “reducing disaster risk” report from the United Nations Development Programme (Pelling et al. 2004) that provides the groundwork for incorporating hazard assessment at an early stage of natural disaster risk mitigation. This insight is made possible because of the natural disaster risk scholarship that was established half a century ago by geographers and natural and social scientists through sound understanding of natural hazards and disasters.

The pioneering work of Gilbert White from the 1950s till 1980s is the keystone for contemporary natural hazard risk reduction research. During this time, the notion of human adjustment to natural hazards in relation to floods was introduced. This opened new dimensions to flood hazard management. White and his colleagues listed different forms of human coping mechanisms, ranging

from sociological to technological means for flood risk mitigation (White 1957; White 1973; Harris 1978). Their research revealed that early flood warning with adequate lead time facilitates disaster risk reduction and is crucial in reducing the loss of life and economic damages.

Among all geophysical disasters, floods are considered to produce the most devastating effects on a global scale. On average, floods cause more than 20,000 deaths and adversely affect about 140 million people per year around the globe (Adhikari et al. 2010). It is not surprising, thus, that intensive research efforts have been devoted to the monitoring of such natural hazards, especially in flood prone regions. Flood prediction requires data that describes the dynamic hydrologic states and topographic factors (i.e. slope, aspect, curvature). Topographic factors are relatively static in comparison to hydrologic processes, which require frequent measurements.

One of the proven technological mitigation measures for flood disaster is to predict flood events with a sufficient lead time to minimize the loss and damage of life and property. Getting satisfactory ground data for flood prediction has been a major constraint in the past despite the availability of numerous hydrological models. In the regions where installation of the ground instruments is limited by the available resources and rugged terrain, satellite remote sensing products with global coverage have made it possible to set-up flood monitoring systems.

The National Aeronautics and Space Administration (NASA) has taken a leading role in the research and development of natural hazards warning systems such as the internet-based Global Flood Monitoring (GFM) system (Hong et al. 2007); (http://trmm.gsfc.nasa.gov/) and the Regional Monitoring and Visualization System (SERVIR) for Africa and Mesoamerica (http://www.servir.net/). Although the general deployment of SERVIR has been highly successful, its flood warning system component is still under development and invites the research community for participation. GFM and SERVIR systems are based on the Tropical Rainfall Measurement Mission (TRMM), which is near real-time satellite precipitation data, with a temporal resolution of three hours and a spatial resolution of 0.25 degrees. This data exhibits potential for hydro-meteorological applications.

Current satellite remote sensing based precipitation estimation techniques represent an important advantage for flood prediction purposes, especially in sparsely or ungauged regions. The recent development and improvement in precipitation estimates from space involves a combination of infrared measurements from geostationary satellites and passive microwave measurements from polar-orbiting satellites (Marzano et al. 2004; Tapiador et al. 2004). These developments in satellite based remote sensing techniques can be used to report the spatial and temporal aspects of floods hazards cost effectively. Moreover, flood risks can be managed with consistent and timely information through an early warning system.

Tropical Rainfall Measurement Mission (TRMM) based Multi-satellite Precipitation Analysis (TMPA) products have been heavily used with rainfall runoff models for flood monitoring. Although several hydrologically-based evaluations of TMPA data have been performed over different regions (Hong et al., 2007; Hossain and Lettenmaier, 2006; Collischonn et al., 2008; Li et al., 2008; Su et al., 2009; Yong et al., 2009), the use of satellite precipitation as an input to hydrologic models for flood prediction is still an active area of research, particularly over sparsely or un gauged regions.

The primary advantage of using remotely sensed precipitation data over surface rain gauge measurements is the high spatial and temporal, coverage. Satellite based precipitation estimates provide near real time precipitation at a fine spatial temporal resolution (Hong et al 2007). The use of satellite remote sensing and forecasting models reduces the dependency for in-situ precipitation and other observations in parts of the world where surface networks are critically deficient. These advantages are more pronounced in unreachable areas, where rugged terrain hampers the installation of rain gauge networks.

1.1 Problem statement

Precipitation triggered floods are among the most devastating natural disasters around the globe, impacting human lives and causing severe economic damage through livelihood and property loss. Moreover, floods, unlike other natural disasters, repeat the dreadful toll on human life and property annually worldwide. It is understood that flood risks will not subside in the near future in developing regions due to an increasing population and settlements in vulnerable areas. In 2004, the United Nations University (UNU) warned that the number of people vulnerable to floods (mostly in developing countries) might reach two billion by 2050 due to population growth, unsustainable development, and climate change impacts in flood-prone regions.

The burgeoning population in flood plains and the lack of flood contingency plans will intensify the associated flood risks. The current trend and future scenarios of flood risks demand accurate spatial and temporal information on the potential of flood hazards and risks. This is a challenge in data scarce environments. The unavailability of local (on-the-ground) observations in many regions around the world hampers pre flood risk reduction measures. In data poor regions, flood early warning systems are nonexistent due to the lack of surface based networks, financial and human resources for flood prediction. Moreover, the flood monitoring and reporting is not systematic and mainly depends on the international media and international organizations. Therefore, with the increase in frequency and intensity of precipitation, it can be assumed

that the potential for loss of life and property will rise in the future as the extreme events will increase in number and intensity.

To address the limited data availability issue in data poor environments, the Predictions in Ungauged Basins (PUB) initiative was launched in 2003 by the International Association of Hydrological Science. In addition to other technological measures, the PUB plan accentuates new techniques and data for hydrologic prediction. It draws attention to the understanding and potential of satellite remote sensing to provide a first order analysis of the hydrologic extremes.

The success of current satellite data on revealing spatial patterns at scales unachievable by ground observations is accompanied by uncertainties associated with the indirect nature of remote radiance estimates. A key research component of this dissertation is to test the feasibility of remote sensing products and quantification of uncertainties in the context of a hydrologic assessment. The latter seeks to enable a better understanding of satellite-based precipitation and other estimates into hydrologic modeling.

1.2 Research objective

The overarching goal of this research is to evaluate the hydrological capabilities of the multispectral and microwave satellite remote sensing products within a hydrologic modeling framework for flood prediction systems in SERVIR-Africa domain.

1.3 Research questions

Based on the overall objective, the following research questions are formulated and addressed in this dissertation:

1. How can satellite precipitation products and in-situ data be used to study hydroclimatology in data poor environments?

2. What is the viability of multispectral sensors to supplement in-situ observations to calibrate a rainfall runoff model for flood monitoring?

3. Can a combined geospatial approach based on microwave remote sensing data assist in flood prediction in ungauged basins?

1.4 Outline of the Dissertation

The dissertation is structured into the introductory chapter, three main chapters followed by the fifth chapter; which serves as an overall conclusion. Chapter 2 and 3 are published as two independent peer reviewed journal articles, and chapter 4 is recently submitted to a journal. There is some repetition in

chapters 3 and 2, but this is done so that the manuscripts can stand alone. Findings from this research work are organized into the following main chapters.

Chapter 2: **Hydroclimatology of Lake Victoria using in-situ and satellite data**

This chapter presents the hydroclimatology of the sub basin of Lake Victoria in East Africa, using observed and simulated data with particular emphasis on distributed hydrology of the watershed. First, this chapter examines the basin scale hydroclimatology at decadal, annual, monthly and daily temporal scales using observed gauge data. Second, it studies the hydrological capability of remote sensing data, primarily the satellite precipitation to study the hydrology. Using a semi-distributed hydrologic model and multiple years satellite remote sensing data, the water cycle components were simulated and analyzed.

Chapter 3: **Multispectral Remote Sensing for Flood Detection**

This chapter seeks to investigate the utility of flood spatial extent information obtained from orbital sensors to calibrate and evaluate the hydrologic model. This is done in an effort to potentially improve hydrologic prediction and flood management strategies in ungauged catchments. The goal of this exercise was to formulate an approach to evaluate the satellite based flood inundation areas with the hydrologic model flood extent. In this chapter, an attempt is made to address the question on how the multispectral sensor based flood extent can be used to calibrate the semi- distributed hydrologic model.

Chapter 4: Microwave Sensors for Flood Predictions in Ungauged Basins

This chapter introduces a novel framework that integrates microwave satellite remote sensing and the hydrologic model for flood Prediction in Ungauged Basin (PUB). The objective is to use the unconventional satellite remote sensing based river discharge signal to calibrate the hydrologic model for flood forecasting in sparsely gauged catchments. Therefore, for this research work the Okavango basin, which is a poorly gauged catchment, will serve as a testbed. First, a rainfall runoff model is implemented with observed data. Second, the passive microwave based river discharge signal is used to calibrate and validate the model. Finally, the simulations from the two approaches are compared to test the efficacy of the new method.

1.5 List of Publications from the Dissertation

CHAPTER 2:

Khan, S. I., P. Adhikari, Y. Hong, H. Vergara, R. F Adler, F. Policelli, D. Irwin, T. Korme & L. Okello (2011) Hydroclimatology of Lake Victoria region using hydrologic model and satellite remote sensing data. *Hydrol. Earth Syst. Sci*., 15, 107-117. 10.5194/hess-15-107-2011.

CHAPTER 3:

Khan, S. I., Y. Hong, J. Wang, K. K. Yilmaz, J. J. Gourley, R. F. Adler, G. R. Brakenridge, F. Policelli, S. Habib & D. Irwin (2011b) Satellite Remote Sensing and Hydrologic Modeling for Flood Inundation Mapping in Lake Victoria Basin: Implications for Hydrologic Prediction in Ungauged Basins. *Geoscience and Remote Sensing, IEEE Transactions* on, 49, 85-95. doi: 10.1109/TGRS.2010.2057513.

CHAPTER 4:

Khan, S. I., Y. Hong, H. Vergara, J. J. Gourley, G. R. Brakenridge, Z. L. Flamig, T. De Groeve & F. Policelli (2011) Microwave satellites remote sensing for flood prediction in un-gauged basins. *Geoscience and Remote Sensing Letters, IEEE* (under review).

References

Adhikari, P., Y. Hong, K. R. Douglas, D. B. Kirschbaum, J. Gourley, R. Adler & G. Robert Brakenridge (2010) A digitized global flood inventory (1998–2008): compilation and preliminary results. *Natural Hazards***,** 1-18.

Collischonn, B., Collischonn, W., Morelli, C.E., 2008., Daily hydrological modeling in the Amazon basin using TRMM rainfall estimates, *Journal of Hydrology* (2008) 360, 207– 216.

Harriss, R.C., Hohenemser, C., and Kates, R.W. 1978. Our Hazardous Environment. Environment 20: 6-15, 38-40.

Hong, Y., Adler, R. F., Hossain, F., Curtis, S., and Huffman, G. J., 2007, A First Approach to Global Runoff Simulation using Satellite Rainfall Estimation, *Water Resources Research*, Vol. 43, No.8, W08502, doi: 10.1029/2006WR005739.

Hossain, F., and D. P. Lettenmaier (2006), Flood prediction in the future: Recognizing hydrologic issues in anticipation of the Global Precipitation Measurement mission, *Water Resources Research*., 42, W11301, doi:10.1029/2006WR005202.

Li, L., Hong, Y., Wang, J., Adler, R., Policelli, F.S., Habib, S., Irwn, D., Korme, T., Okello, L., 2008, Evaluation of the Real-time TRMM-based Multi-satellite Precipitation Analysis for anOperational Flood Prediction System in Nzoia Basin, Lake Victoria, Africa, *Journal of Natural Hazards* doi 10.1007/s11069-008-9324-5.

Marzano, F. S., M. Palmacci, D. Cimini, G. Giuliani, and F. J. Turk, 2004: Multivariate statistical integration of satellite infrared and microwave radiometric measurements for rainfall retrieval at the geostationary scale. *IEEE Transactions on Geoscience and Remote Sensing,* 42, 1018–1032.

Pelling, M., A. Maskrev, P. Ruiz & L. Hall (2004) Reducing disaster risk: a challenge for development. *UNDP global report. New York: United Nations Development Program*.

Su, F., H. Gao, G. J. Huffman & D. P. Lettenmaier (2010) Potential utility of the real-time TMPA-RT precipitation estimates in Streamflow prediction. *Journal of Hydrometeorology,* doi/10.1175/2010JHM1353.1.

Tapiador, F. J., C. Kidd, V. Levizzani, and F. S. Marzano, 2004: A neural networks–based fusion technique to estimate halfhourly rainfall estimates at 0.1° resolution from satellite passive microwave and infrared data. J. Appl. Meteor., 43, 576–594.

White, Gilbert F. "A Perspective of River Basin Development." Law and Contemporary Problems 22, no. 2 (1957):157–184.

White, Gilbert F. 1973. Natural Hazards Research. In Richard J. Chorley (ed.) Directions in Geography. London: Methuen. Pp. 193-216.

Yong, B., L. Ren, Y. Hong, J. Wang, W. Wang, and X. Chen (2010) Hydrologic Evaluation of TRMM Standard Precipitation Products in Basins Beyond its Inclined Latitude Band: a Case Study in Laohahe Basin, China, *Water Resour. Res*, doi:10.1029/2009WR008965

CHAPTER 2 : HYDROCLIMATOLOGY OF LAKE VICTORIA USING HYDROLOGIC MODEL AND REMOTE SENSING DATA

Abstract

Study of hydroclimatology at a range of temporal scales is important in understanding and ultimately mitigating the potential severe impacts of hydrological extreme events such as floods and droughts. Using daily in-situ data combined with the recently available satellite remote sensing data, the hydroclimatology of Nzoia basin, one of the contributing sub-catchments of Lake Victoria in the East African highlands is analyzed. The basin, with a semi-arid climate, has no sustained base flow contribution to Lake Victoria. The short spell of high discharge showed that rain is the primary cause of floods in the basin. There is only a marginal increase in annual mean discharge over the last 21 years. The 2-, 5- and 10- year peak discharges, for the entire study period showed that more years since the mid 1990s have had high peak discharges despite having relatively less annual rain.

The study also presents the hydrologic model calibration and validation results over the Nzoia basin. The spatiotemporal variability of the water cycle components were quantified using a hydrologic model, with in-situ and multi-

satellite remote sensing datasets. The model is calibrated using daily observed discharge data for the period between 1985 and 1999, for which model performance is estimated with a Nash Sutcliffe Efficiency (NSCE) of 0.87 and 0.23% bias. The model validation showed an error metrics with NSCE of 0.65 and 1.04% bias. Moreover, the hydrologic capability of satellite precipitation (TRMM-3B42 V6) is evaluated. In terms of reconstruction of the water cycle components the spatial distribution and time series of modeling results for precipitation and runoff showed considerable agreement with the monthly model runoff estimates and gauge observations. Runoff values responded to precipitation events that occurred across the catchment during the wet season from March to early June. The spatially distributed model inputs, states, and outputs, were found to be useful for understanding the hydrologic behavior at the catchment scale. The monthly peak runoff is observed in the months of April, May and November. The analysis revealed a linear relationship between rainfall and runoff for both wet and dry seasons. Satellite precipitation forcing data showed the potential to be used not only for the investigation of water balance but also for addressing issues pertaining to sustainability of the resources at the catchment scale.

2.1 Introduction

Climatologically most of East Africa is considered as a sub humid landscape that comprises arid and semi-arid regions, grasslands, savannahs, as well as a Mediterranean environment. East African climate is mainly influenced by the seasonal shift of the Intertropical Convergence Zone (ITCZ). However other regional factors that influence the climate are topographical variations, large inland lakes, land cover/land use, as well as the proximity to the Indian Ocean. Oscillations in the ITCZ, shapes two rainy seasons in the equatorial East Africa, one from March to May and the second from October to December (Kaspar et al., 2008). This precipitation pattern can result in floods in this region with impacts on the food and agricultural security, human health, infrastructure, tourism, and other sectors.

The rainy season that onsets from October through early December brings devastating floods in Uganda, Kenya, Tanzania, and other countries in East Africa almost every year. This region, surrounding Lake Victoria, is heavily populated with around thirty million people (Osano et al., 2003). These floods are a serious problem in East Africa, particularly in the Lake Victoria Basin, which impacts the livelihood of many people every year. Since the 1950's East African countries like Kenya, Uganda, and Tanzania showed an increase in population as well as unsustainable development. Due to economic pressure, much of the forest land is converted to agriculture or settlement purposes. Moreover, the Lake Victoria region experiences rising demands for its depleting water resources.

Hydro-climatology deals with the interactions of climate with hydrology. It recognizes that climate is the driving force of the hydrologic cycle. One of the main focuses of the hydro-climatic study is the interactions between precipitation, evapotranspiration, soil moisture storage, groundwater recharge, and stream flow (Shelton, 2009). The study of the water budget at a given location and time period essentially deals with the components of hydro-climatology. Hydrologic modeling is one of the efficient and valuable approaches for understanding the relationship between climate, hydrologic cycle, and water resources.

In East Africa, the current trend and future scenarios of unsustainable water resource utilization demands modeling studies that provide accurate spatial and temporal information on hydrological and climatological variables. The main obstacles for these investigations are the lack of sufficient geospatial data for distributed hydrologic model input and validation. Availability of observed data in regions with sparse ground based networks for hydrologic estimations is the key limitation in hydroclimatologic studies.

Hydrologic modeling has been constrained by the difficulty in precisely estimating precipitation, the key forcing factor, over a range of spatial and temporal scales. However, advances in satellite remote sensing data can provide objective estimates on precipitation, evapotranspiration and land surface controlling factors for water budget calculations. The recent availability of virtually real time and uninterrupted satellite-based rainfall estimates is becoming a cost-effective source of

data for hydro climatologic investigations in many under-gauged regions around the world. Furthermore, application of remotely sensed spatially distributed datasets has made possible the transition from lumped to distributed hydrologic models that accounts for the spatial variability of the model parameters and inputs. The question remains whether with the existing spatial and temporal coverage of satellite precipitation and other estimates, how can we achieve their optimal use to compute a less uncertain water budget?

The aim of this chapter is to provide the hydro-climatology of the Nzoia basin, a sub catchment of the Lake Victoria region using observed and simulated data with particular emphasis on distributed hydrology of the watershed. The specific objectives are to 1) quantify the hydroclimatology of Nzoia basin at decadal, annual, monthly and daily time scale using in-situ dataset; 2) model the rainfall-runoff relationship using a semi-distributed hydrological model, calibrated by long-term observations, in terms of predictability at the daily scale; 3) investigate the hydrological capability of remote sensing data (primarily the precipitation) in terms of the reconstruction of water cycle components.

In this study, Coupled Routing and Excess Storage (CREST) (Wang et al. 2011) a semi-distributed hydrologic model, is used to simulate the spatial and temporal variation of atmospheric, land surface, and subsurface water fluxes and storages. This chapter follows with a brief description of the study basin, data, and model in section 2. The hydroclimatology based on observational datasets are

discussed in section 3, followed by section 4 with a model set-up, calibration, and verification. The hydrological model reconstruction results are outlined in section 5, and finally summary and discussions are given in section 6.

2.2 Study area and In-situ Data

The study area is the Nzoia River located at latitudes 34°–36℄E and longitudes 0℃03′–1℃15′N in East Africa. It drains into the Lake Victoria and Nile river basins. Lake Victoria, with an area of 68,600 km^2, is the second largest freshwater lake in the world (Swenson and Wahr, 2009). Nzoia, a sub-basin of Lake Victoria, is chosen as the study area because of its regional importance as it is a flood-prone basin and also one of the major tributaries to Lake Victoria (Figure 2.1).

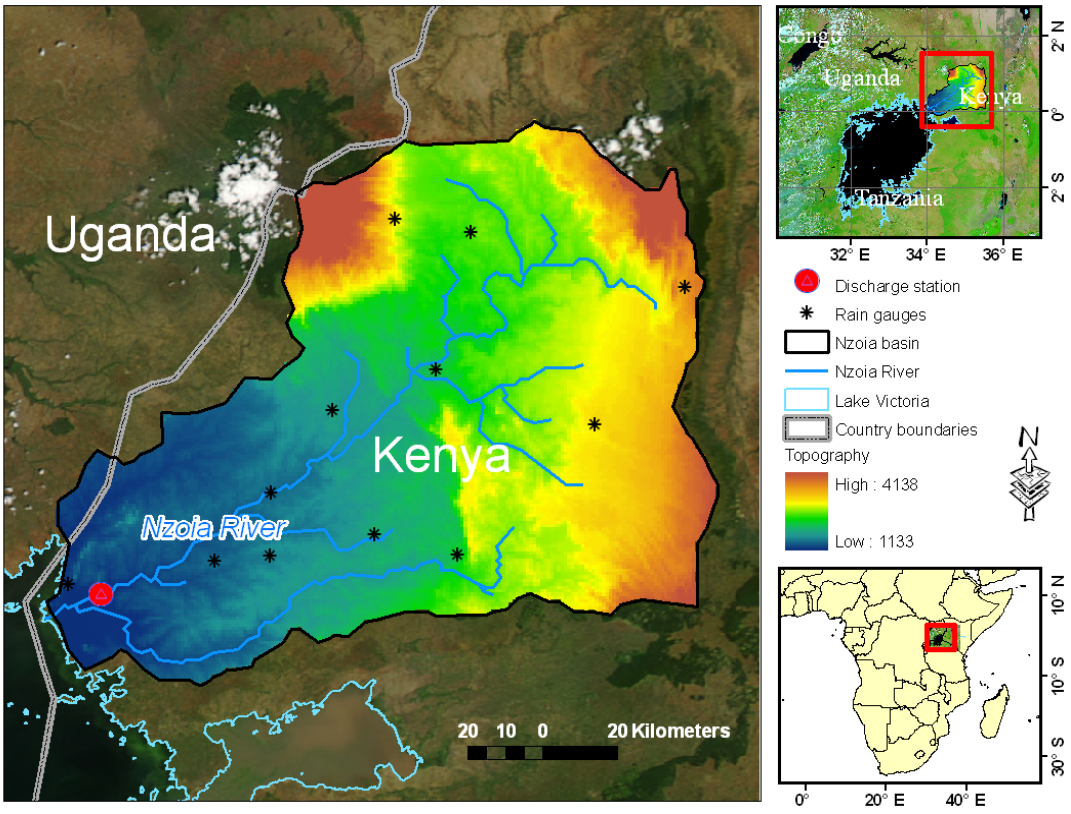

Figure 2.1: Map of Nzoia river basin in Lake Victoria region, East Africa.

The Nzoia sub-basin covers approximately 12,900 km^2 of area with an elevation ranging between 1,100 to 3,000 m. The Nzoia River originates in the southern part of the Mt. Elgon and Western slopes of Cherangani Hills (Li et al., 2009). The lowlands are characterized by predominant clayey soils at 77%. The other main soil type of the catchment is sand at 14%. Soil data is used from the Food and Agriculture Organization of the United Nations (FAO; http://www.fao.org/AG/agl/agll/dsmw.htm). The land use land cover data is from the Moderate Resolution Imaging Spectroradiometer (MODIS) land classification map. It is used in this study as a representation of land use/cover, with 17 classes of land cover based on the International Geosphere–Biosphere Programme classification (Friedl et al., 2002).

2.3 Satellite remote sensing datasets

NASA's Tropical Rainfall Measuring Mission data.

Precipitation is a critical forcing variable to hydrologic models, and therefore accurate measurements of precipitation on a fine space and time scale is very important for simulating land-surface hydrologic processes, and monitoring water resources, especially for semiarid regions (Sorooshian et al., 2005; Gebremichael et al., 2006). For the past decade, there have been several multi-satellite based precipitation retrieval algorithms for operational and research purposes (Hong et al., 2004; Huffman et al., 2007; Joyce et al., 2004; Sorooshian et al., 2000). For this study, we used one of the Tropical Rainfall

Measuring Mission (TRMM) Multi-satellite Precipitation Analysis (TMPA) product, 3B42 V6 given its 10+ year data availability.

Satellite precipitation product (3B42 V6) is used to drive the CREST model to simulate the water budget components such as runoff, evapotranspiration and, change in storage for the study basin. The standard TMPA provides precipitation estimates from multiple satellites at a 3-hourly, $0.25^{o}\times0.25^{o}$ latitude-longitude resolution covering the globe between the latitude band of 50^{o} N-S (Huffman et al., 2007). This TRMM standard precipitation product has been widely used for hydrological applications such as flood and landslide prediction at the global and regional scope (Su et al. 2008; Hong et al. 2006; Hong et al. 2007; Yong et al. 2010).

Evapotranspiration

The process of water flux from the land surface soils, vegetation, or directly from overland water to the atmosphere is referred to as evapotranspiration. Potential evapotranspiration (Ep) is the amount of evapotranspiration that would occur if there were an unlimited supply of land surface water, and is often estimated from atmospheric thermodynamics, wind and radiation conditions. In the model, Potential Evapotranspiration (PET) values are from the global dataset based on the Famine Early Warning Systems Network (FEWS). Further details on these estimates can be found at (http://earlywarning.usgs.gov/Global/product.php?image=pt). The PET are

estimates of climate parameter data that is extracted from the Global Data Assimilation System (GDAS) analysis fields. FEWS PET is at a 1-degree spatiotemporal resolution calculated using global-scale meteorological datasets.

In-Situ data

Daily observed rainfall data are obtained from the Africa Regional Centre for Mapping of Resources for Development (RCMRD) from 1985 to 2006 for the 12 rain gauge stations located within the Nzoia basin. They are then interpolated to fit the model grid resolution using the Thiessen polygon method (Kopec, 1963). Also obtained are the daily discharge data (in m^3/sec) at the basin outlet for the same time period.

The mean monthly rainfall over Nzoia shows dual peaks over the year which is common to parts of the immediate equatorial zone especially in East Africa (Hulme, 2006). The first and second maxima occurred in April-May and July-November respectively. It is observed that for the given time period of 1985-2006, the basin average rainfall per annum is about 1,500 mm. Observations of the rainfall since 1985 do not show any significant change. It is observed that half of the recorded rainfalls are below 5mm/d (Figure 2.2a, b)

The highest river discharges occurred in the months of May through September, while the lowest river discharges occurred in the months of December through February (Table 2.1). From 1985-2006, the average daily

discharge is 134 m^3/sec. The flow duration curve shows the average percentage of time that specific daily flows (Figure 2.3a) are equaled or exceeded at Nzoia. The discharge histogram is skewed towards the lower values and more than half of the recorded daily discharges are less than 120 m^3/sec (Figure 2.3b).

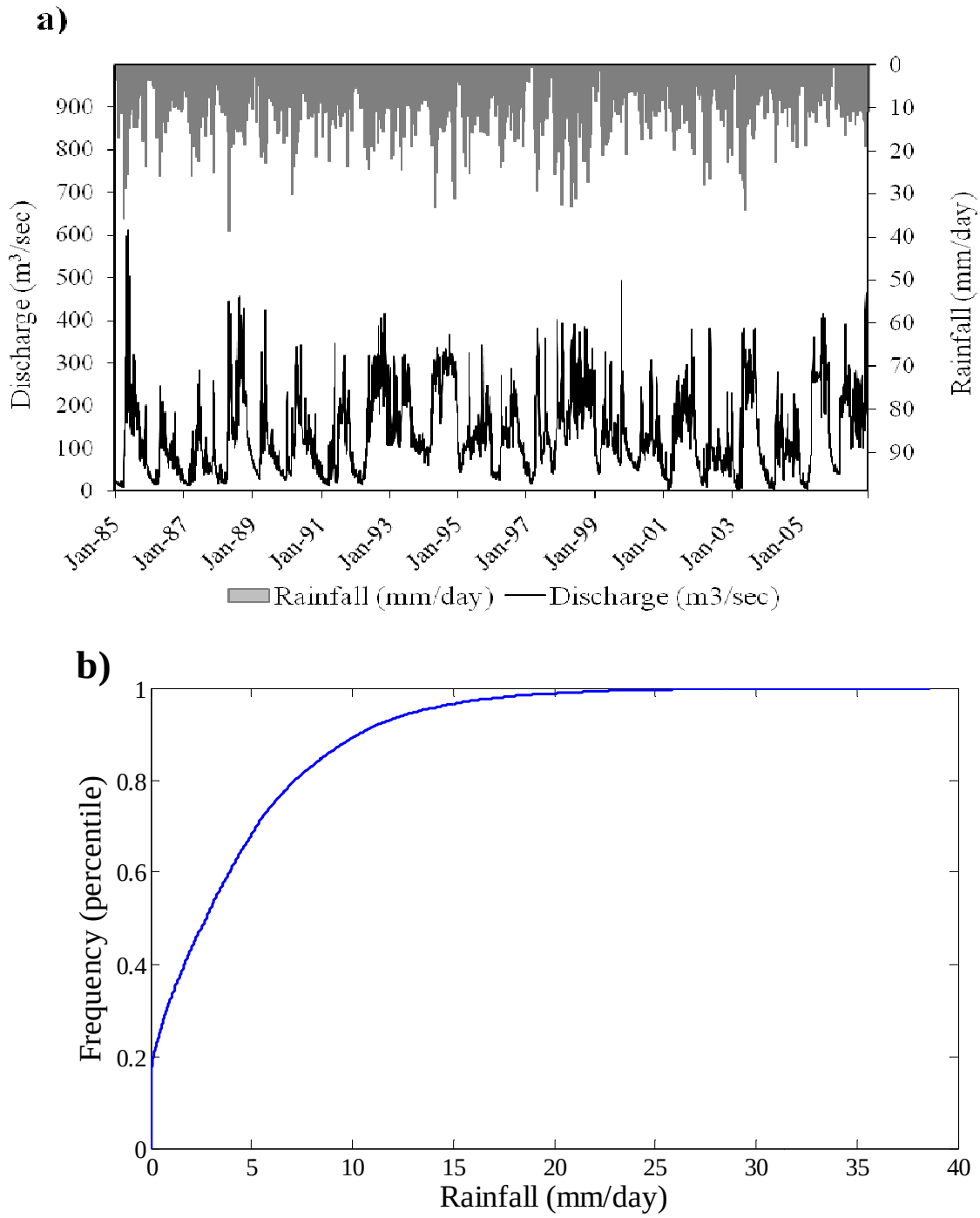

Figure 2.2: Nzoia basin average daily rainfall and discharge time series. b) Cumulative distribution plot of observed basin average rainfall (mm/day) for 1985-2006.

	Decades	Jan	Feb	Mar	Apr	May	Jun	Jul	Aug	Sep	Oct	Nov	Dec	Avg
Rainfall (mm/day)	1985-1994	1.7	2.7	4.5	7.7	7.7	4.5	4.5	5.4	4.1	4.3	4.2	1.6	
	1995-2004	2.20	1.20	4.07	7.23	5.96	4.37	3.93	4.55	4.11	4.65	4.31	2.05	
	Change	0.50	-1.49	-0.41	-0.44	-1.74	-0.13	-0.54	-0.86	0.04	0.40	0.08	0.49	
	% Change	30%	-55%	-9%	-6%	-23%	-3%	-12%	-16%	1%	9%	2%	32%	-4%
Discharge (m^3/sec)	1985-1994	57	51	64	144	22	160	167	182	166	143	131	85	
	1995-2004	83	45	60	129	191	151	154	165	155	141	150	116	
	Change	25	-7	-4	-15	-29	-10	-14	-18	-10	-2	19	31	
	% Change	44%	-13%	-7%	-10%	-13%	-6%	-8%	-10%	-6%	-1%	14%	36%	2%

Table 2.1: Seasonal variation of rainfall and discharge.

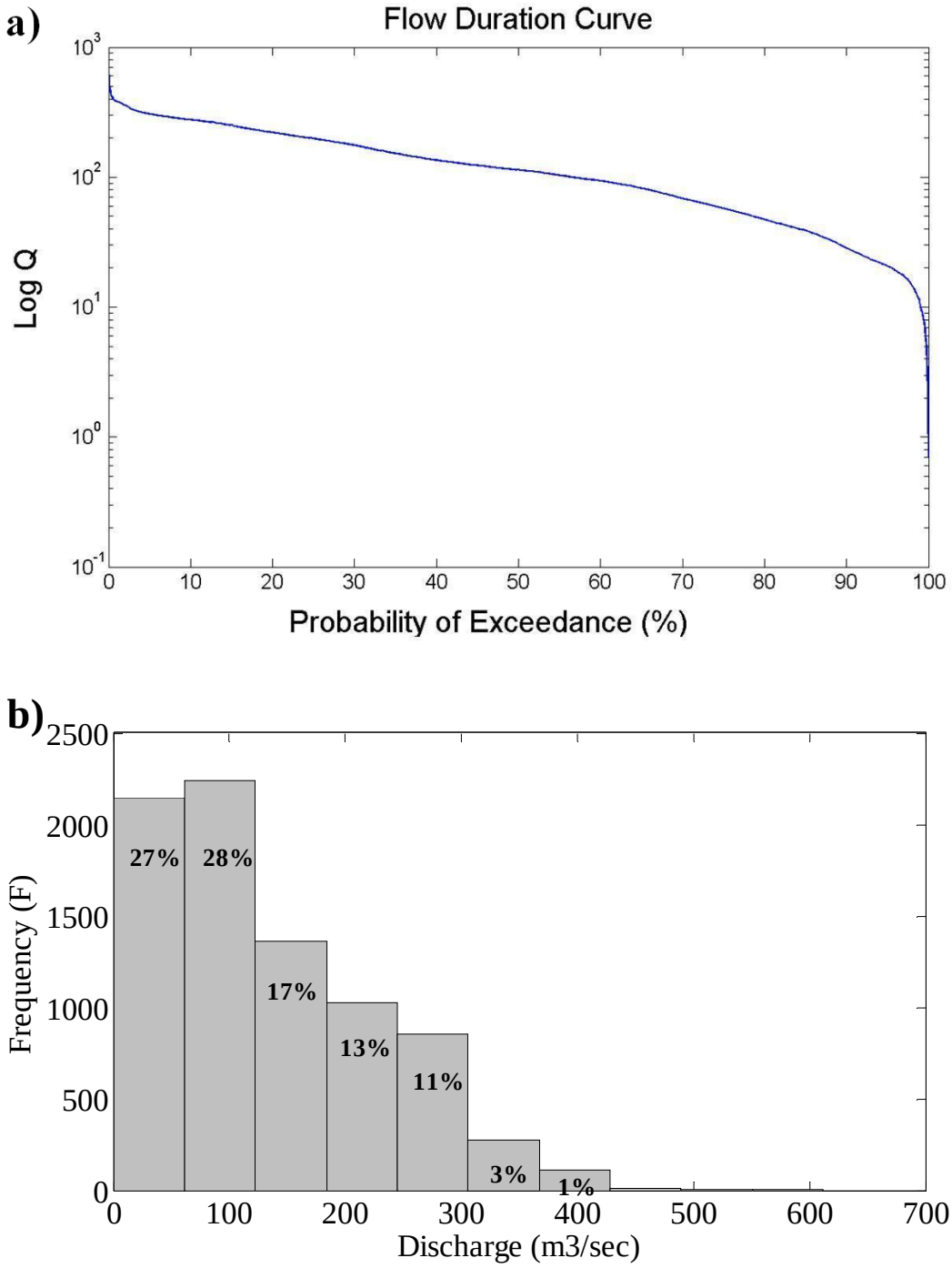

Figure 2.3: Observed daily discharge (m3/sec) for 1985-2006 for Nzoia River a) Flow duration curve b) histogram.

Return periods of rainfall and discharge

The annual peak discharge and precipitation for the given time period are shown in Figure 2.4a, b. The calculated return periods for both the discharge and rainfall are given in Table 2.2. The peak discharges of 1985, 1988, 1999, and 2006 were all above the 5-year flow while 1985 and 1999 recorded discharges of 10-year return periods (Figure 2.4a). In 1985, the recorded peak discharge was of the 100-year return period.

It is observed that the annual peak rainfall in the years 1985, 1988, 1990, 1994, 1998, and 2003 exceeded the 5-year return period values. Similarly, 1994, 1998 and 2003 have the peak rainfall of 10-year. Finally, 1985 and 1988 recorded rainfall of a 20-year return period.

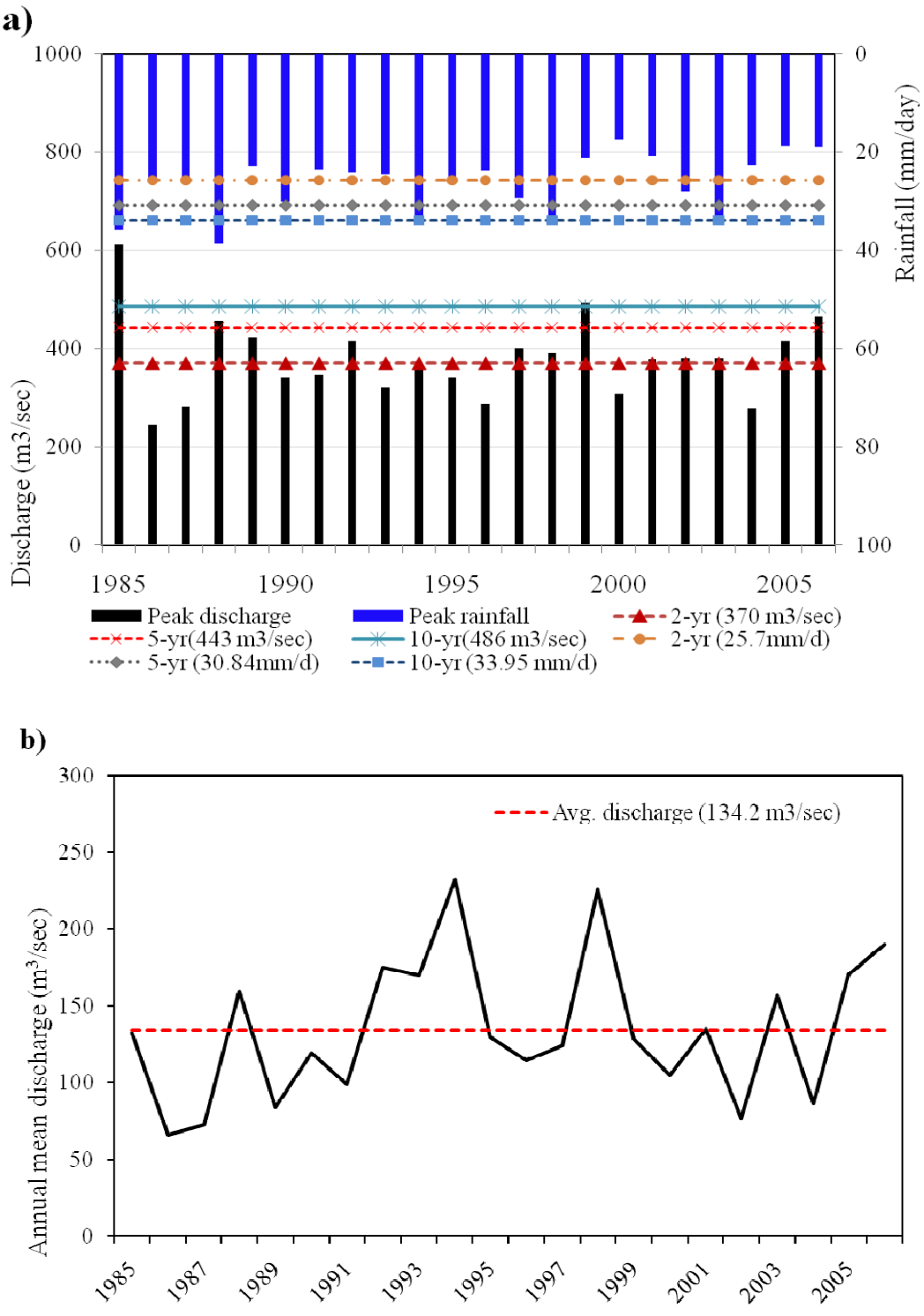

Figure 2.4: Annual peak rainfall and discharge for 1985-2006 with (a) the 2-, 5- and 10-year return period (b) annual mean discharge.

Table 2.2: Discharge and rainfall return periods

Return periods (year)	Discharge (m3/sec)	Rainfall (mm/day)
2	370	26
5	443	31
10	486	34
20	526	37
50	573	40
80	591	41
100	608	43
200	641	45
500	684	48

Annual mean discharge

The discharge time series provide information on the year-to-year variations of both low and peak discharges. Figure 2.4b shows the annual mean discharge for Nzoia River. The lowest annual discharge is 66 m^3/sec in 1986 and the highest is 232 m^3/sec in 1994. The other wet years are 1998 and 2006 and the dry years are 1987 and 2002 (Figure 2.4a). Overall we can observe a slight increase in annual mean discharge. Seasonal cycles included in annual discharge are noticeable with a greater variability of monthly mean stream flow. The maximum monthly discharge is 421 m^3/sec for May 1985. All the wet years of 1994, 1998 and 2006 are marked by high monthly discharges (Figure 2.4b). The dry years of 1986, 1987, and 2002 are not the result of a single dry month but due to continuous low monthly discharges throughout the whole year.

Decadal monthly discharge

The observed data are also analyzed for any change over the past two decades: 1985-1994 (first decade) and 1995-2004 (second decade). Overall there is some decrease (-4.2%) in rainfall in the second decade compared to the first. Similarly there is a marginal increase (+2%) in discharge (Table 2.1). However, there is a more pronounced monthly variation both in rainfall and discharge. A maximum decrease in rainfall is recorded for the month of February (-55%) whereas December witnessed a maximum increase (+32%). Similarly, there is a maximum drop in stream discharge in the months of February and May

(-13%) while a surge of +44% is observed in the month of January (Table 2.1).

2.4 Methodology

The Rainfall-Runoff Models

Quantification of the spatiotemporal distribution of water over the landscape is of critical importance for sustainable water resources management and for mitigating hydrometeorologic natural hazards such as floods and droughts. Rainfall runoff models are practical tools for providing critical information for forecasting these calamities in time. A variety of hydrological models have been developed in the past (see Singh, 1995) for a comprehensive overview with various degrees of hydrological processes represented according to the intended application or availability of data.

Hydrological models have been classified as conceptual or physically-based (Beck, 1987; Refsgaard, 1996; Yilmaz et al., 2010). Conceptual models represent complex, spatially variable, hydrological processes in a watershed using simple, parsimonious mathematical expressions without explicit treatment of the underlying physics or intra-basin heterogeneity (e.g. Bergström, 1995; Burnash, 1995). Spatially distributed, physically-based hydrological models mathematically represent each of the important components of the hydrological cycle based on their physical governing equations (Woolhiser et al., 1990; Refsgaard & Storm, 1995). The potential strengths of distributed hydrological models are: (a) the ability to account for the intra-basin variability of runoff-

producing mechanisms; and (b) the ability to infer model parameter values from geospatial data (e.g. geology, topography, soils, and land cover). A hybrid modelling strategy that maintains a balance between the degree of physical realism and data requirements, so as to provide reliable simulations under a variety of settings, seems to be advantageous.

Coupled Routing and Excess STorage (CREST) model

A semi-distributed hydrologic model, Coupled Routing and Excess STorage (CREST) (Khan et al. 2011a, Wang et al. 2011) is used to simulate the spatiotemporal variation of water fluxes and storages on regular grids. The CREST model is jointly developed by the University of Oklahoma under NASA SERVIR Africa project can simulate the spatial and temporal variation of land surface water fluxes and storages by cell-to-cell simulation. The model accounts for the most important parameters of the water balance component i.e. the infiltration and runoff generation processes.

The main CREST components are briefly described as; 1) data flow module based on cell to cell finite elements; 2) the three different layers within the soil profile that affect the maximum storage available in the soil layers. This representation within cell variability in soil moisture storage capacity (via a spatial probability distribution) and within cell routing can be employed for simulations at different spatiotemporal scales 3) coupling between the runoff generation and routing components via feedback mechanisms. This coupling allows for a

scalability of the hydrological variables, such as soil moisture, and particularly important for simulations at fine spatial resolution.

Rainfall–runoff generation

a) Canopy interception:

Once there is precipitation (P) input to a cell, the rainfall–runoff generation process will be activated. First, a portion of the precipitation is intercepted by the vegetation canopy, and an excess storage reservoir is employed here to simulate this process (Figure 2.5a).

b) Variable infiltration curve:

Next, P_{soil} is separated into two parts: excess rain (R) and infiltration water (I), according to the variable infiltration curve (VIC; also called tension water capacity curve), founded in the Xinanjiang model (Zhao *et al*., 1980; Zhao, 1992), and later employed in the University of Washington VIC model (Liang *et al*., 1996) (Figure 2.5b).

c) Runoff generation

A further partitioning of R into overland excess rain (R_O) and interflow excess rain (R_I) ensues by comparing P_{soil} to the infiltration rate of the first layer (K): where K is closely related to the soil saturated hydraulic conductivity. The partition of overland and interflow excess rain provides quick and slow

hydrograph responses to precipitation.

There are two cell-to-cell routing modules that move water overland as surface runoff and below ground as subsurface interflow (Figure 2.5c, d). These modules run in parallel which enables a computationally efficient and realistic three-dimensional representation of water flux to downstream cells. CREST model framework is illustrated in Figure 2.5, detailed in (Wang et al. 2011) lists the sequential flow of water entering a cell as rainfall, interception by the canopy layer and subsequent redistribution back to the atmosphere via evapotranspiration. The division of rainfall reaching the soil surface into infiltration and surface runoff components, sub-grid routing, routing of overland, channel, and subsurface components downstream, and finally feedbacks between routing and runoff generation components are summarized.

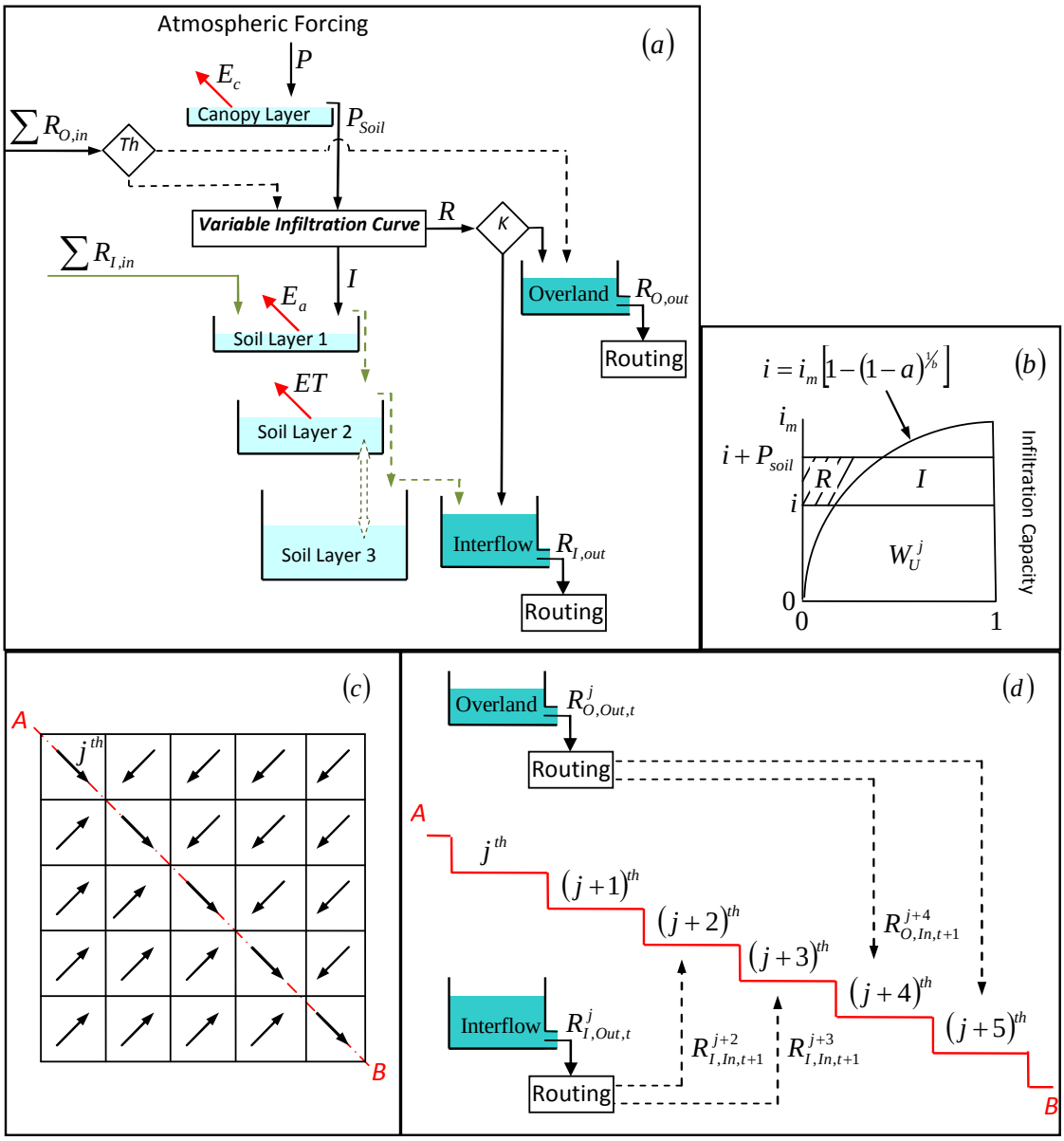

Figure 2.5: Main components of CREST: (a) vertical profile of a cell including rainfall–runoff generation, evapotranspiration, sub-grid cell routing and feedbacks from routing; (b) variable infiltration curve of a cell; (c) plan view of cells and flow directions; and (d) vertical profile along several cells including sub-grid cell routing, downstream routing, and subsurface runoff redistribution from a cell to its downstream cells (Wang et al. 2011).

d) Runoff routing

The typical approach to routing involves determining the depth and momentum of overland water that flows from each cell to a neighbouring cell downstream and continuing this process down to the river network where it is considered open channel flow (Vörösmarty et al., 1989; Liston et al., 1994; Miller et al., 1994; Sausen et al., 1994; Coe 1997; Hagemann and Dümenil 1997). The routing component in CREST is based on a two-layer scheme describing overland runoff and interflow from one cell to the next one downstream, with consideration of open channel flow.

Figure 2.5d illustrates how runoff from interflow, overland flow and channel flow contribute to cells downstream from the *j*th cell after a time step d*T*. The $R_{I,\text{out}}$ moves more slowly in response to a relatively small value of K_X, corresponding to soil saturated hydraulic conductivity, and provides runoff to the nearby (*j*+2)th and (*j*+3)th cells. In contrast, $R_{O,out}$ contributes runoff to the (*j*+4)th and (*j*+5)th cells further downstream due to a larger value of $K_{X.}$ All values for $K_{X,}$ which control the timing of peak flow, can be provided *a priori* using land cover maps, soil surveys and channel cross-sections, but typically must be optimized through calibration.

e) Coupling rainfall–runoff generation and routing

For each cell, the water balance is computed by using equation (1)

$$\frac{\mathrm{dSto}}{\mathrm{d}t} = P - E_a + \sum R_{O,\mathrm{in}} - R_{O,\mathrm{out}} + \sum R_{I,i\mathrm{n}} - R_{I,\mathrm{out}} \qquad (1)$$

where Sto is the total cell water storage, which includes all water stored in the overlying vegetation canopy, the three soil layers, and in the two linear reservoirs (Figure 2.5a). The summations for interflow and overland flow in equation (1) correspond to contributing runoff of multiple upstream cells and from eight possible flow directions, as determined from a DEM-derived flow direction map; see (Figure 2.5c).

In CREST, routed water from a cell impacts the rainfall–runoff generation as well as routing components of downstream cells, thus coupling these processes in the following three ways. First, overland runoff coming from upstream cells is treated the same as adding precipitation directly on the uppermost soil layer, so that P_{soil} calculated from equation (2)

$$\hat{P}_{\mathrm{soil}} = P_{\mathrm{soil}} + \sum R_{O,\mathrm{in}} \qquad (2)$$

where $\hat{P}_{\mathrm{soil}}$ is the adjusted P_{soil} as dictated by the total amount of overland flow from upstream cells. This additional water is available to enter the soil layers from above, as described in Section 2.1.2. Secondly, soil moisture is increased

by lateral interflow coming from upstream cells, so the amount of water available for infiltration in equation (3) is adjusted as:

$$\hat{I} = I + \sum R_{I,\text{in}} \tag{3}$$

where $\hat{I}$ is the adjusted *I* determined by the sum of interflow from upstream cells. Finally, channel runoff coming from upstream cells contributes to the cell's overland reservoir depth, so that S_O in (4) is modified as follows:

$$\hat{S}_O^{t+1} = S_O^t + R_O^t + \sum R_{O,\text{in}} \tag{4}$$

where $\hat{S}_O^{t+1}$ is the adjusted S_O^{t+1}, increased by contributing channel runoff.

These runoff routing-generation feedback mechanisms (i.e. water routed from upper grids could potentially increase runoff generation of the lower grids), via linking the runoff generation and routing modules in CREST, mark it as a distinguishing characteristic from other hydrological models. These feedbacks cause downstream cells to become more readily saturated than upstream cells; a desirable characteristic in excess storage theory is the expansion of the soil saturation area beginning downstream and working its way up (Zhao, 1984). The

CREST approach of module coupling enables realistic fluxes of water both horizontally and vertically through the soil structure and laterally overland. Nevertheless, the actual modelling performance also depends upon the accurate quality of soil information such as depth and types.

In the CREST model the vertical profile of grid cells is subdivided into four excess storage reservoirs representing interception by the vegetation canopy and subsurface water storage in the underlying three soil layers (Figure 2.5a). In addition, two linear reservoirs simulate sub-grid cell routing of overland and subsurface runoff separately. In each cell, a variable infiltration curve (Figure 2.5b) originally proposed by Zhao et al. (1980) is employed to separate precipitation into runoff and infiltration.

Many of the parameters in the CREST model can be estimated based on the availability of field survey data, such as soil surveys, land cover maps, and vegetation coverage. Other parameters are derived directly from a DEM such as flow direction, slope, and drainage area. These physically-based parameters are listed in table 2 along with a suggested source of data to estimate them. There are approximately ten parameters that are much more difficult to estimate from ancillary data and need to be calibrated either manually, automatically (Wang et al. 2011).

Table 2.3: Main physically-based parameters in CREST model

Symbol	Unit	Brief description	Source for estimation
DEM	m	Digital elevation model	Remote sensing
ACC	-	Accumulation grids	Derived from DEM
Dire	-	Flow direction	Derived from DEM
S	degree	Slope between cells	Derived from DEM
d	-	Vegetation coverage	Remote sensing
LAI	m^2 m^2	Leaf area index	Remote sensing
K	mm h^{-1}	Cell mean infiltration rate	Soil survey
I	m	Distance between cells	Derived from DEM

Hydrologic model setup

A moderate resolution CREST model at a 30 arc-second resolution is implemented for the Nzoia basin to retrospectively simulate the main components of water cycles with both in-situ and remote sensing data sets. The model is implemented using digital elevation data to generate flow direction, flow accumulation, and contributing basin area that are required as basic inputs to run the CREST model.

The local drainage direction and accumulation are derived from the Digital Elevation processed from the Model Shuttle Radar Topography Mission (SRTM) (Rabus et al., 2003). The primary forcing datasets enabling the development of a distributed hydrological model using the long term rain gauge and observed streamflow data provided by the local authorities previously discussed in the in-situ data section.

The CREST model is calibrated at the Nzoia basin outlet (Figure 2.1) for the given time period of 1985-1998. A spin up period of one year is assigned to produce reasonably realistic hydrologic states. The model utilizes global optimization approach to capture the parameter interactions. An auto-calibration technique based on the Adaptive Random Search (ARS) method (Brooks, 1958) is used to calibrate the CREST model. The ARS method is considered adaptive in the sense that it uses information gathered during previous iterations to decide how the simulation effort is expended in the current iteration.

Statistical Indices for Model Evaluation

The two most commonly used indicators for the model calibration in order to get the best match of model-simulated streamflow with observations are the Nash-Sutcliffe Coefficient of Efficiency (NSCE) equation 5 (Nash and Sutcliffe, 1970) and relative bias ratio equation 6. Therefore, these are used as objective functions for the automatic calibration. The ideal value for NSCE is 1 and bias is 0%.

$$NSCE = 1 - \frac{\sum \left(Q_{i,o} - Q_{i,s}\right)^2}{\sum \left(Q_{i,o} - \overline{Q_o}\right)^2} \tag{5}$$

$$Bias = \frac{\sum Q_{i,s} - \sum Q_{i,o}}{\sum Q_{i,o}} \times 100\% \tag{6}$$

Where, where, $Q_{i,o}$ is the observed discharge of the i^{th} time step; $Q_{i,s}$ is the simulated discharge of the i^{th} time step; $\overline{Q_o}$ is average of all the observed discharge values.

Indicators of all results from CREST auto-calibration form a normal distribution with near zero Bias as mathematical expectation. The optimized parameter combination with NSCE=0.873 and Bias =-0.228% is found as final result by the ARS method.

Model Calibration and Verification

CREST is calibrated using daily observed discharge data for the period between 1985 and 1999. A one-year period (1984) is used for warming up the model states. CREST calibration, performed using the ARS method described in Sec. 2.4, resulted in good performance with NSCE=0.87 and bias =-0.23% (Figure 2.6a).

The performance of CREST in discharge simulation at the drainage outlet is validated. The validation of the hydrological model is performed for the period 1999–2004. The simulation quality during the validation period is comparable, even with a decrease in model efficiency. One reason for the noise in the simulation might be due to the increase in human activities in the catchment area during the recent years. With this optimized parameter combination and model status at the last day from calibration (Dec. 31, 1998), discharge from 1999 to 2004 is simulated and compared to observations (Figure 2.6b). The error metrics with NSCE of 0.65 and 1.04% bias for the validation period (Figure 2.6b) indicates that the CREST model can reproduce observed discharge in the Nzoia basin with acceptable skill.

The simulation results for Nzoia using TRMM 3B42 V6 as precipitation forcing. It can be seen that from 1999 and 2003, the model simulated daily discharge with a NSCE of 0.48 and bias of -4.57% (Figure 2.6c). The model for the validation period captures peak and low flows and there is acceptable

agreement between simulation and observation at different flow conditions throughout the simulation period.

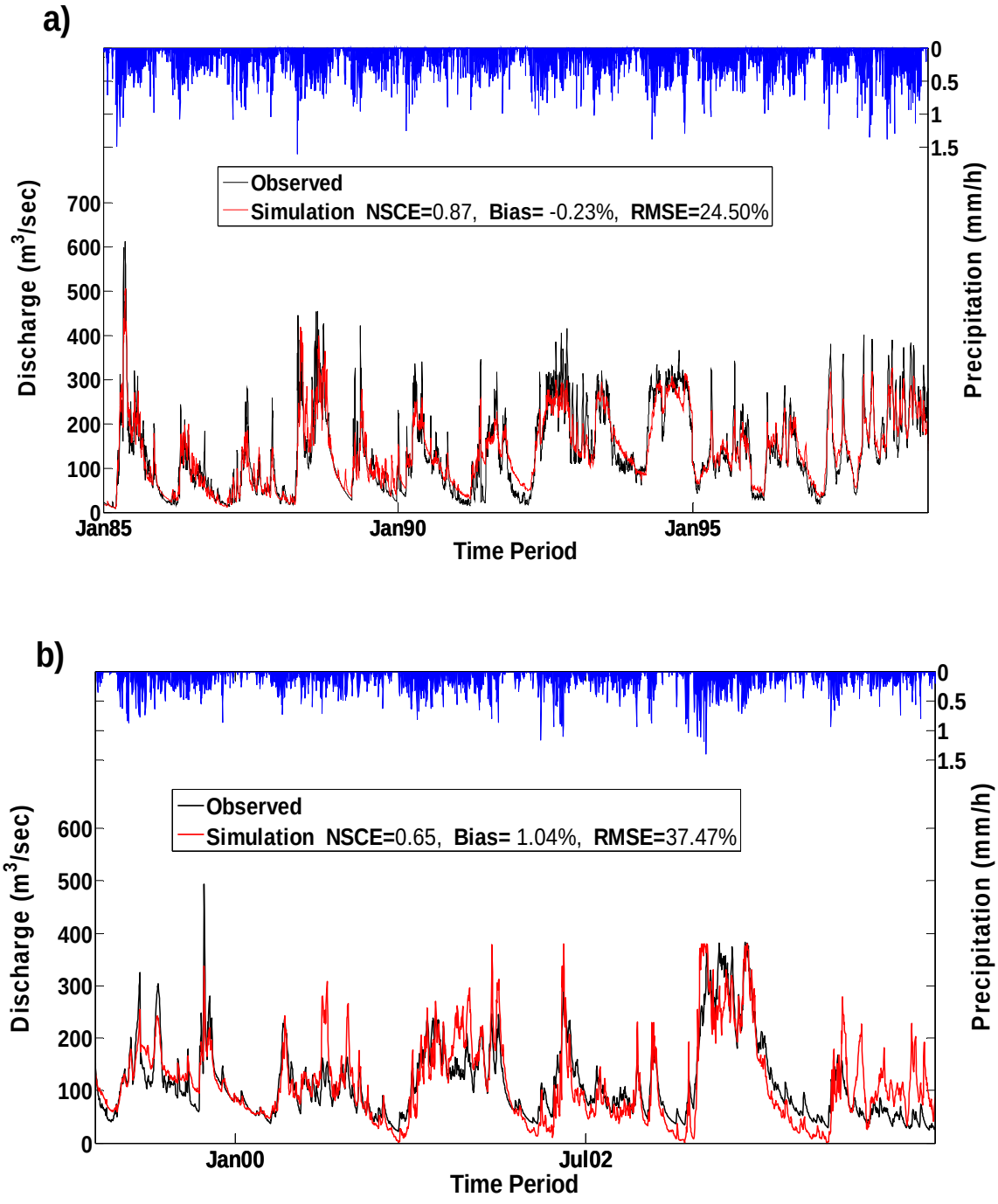

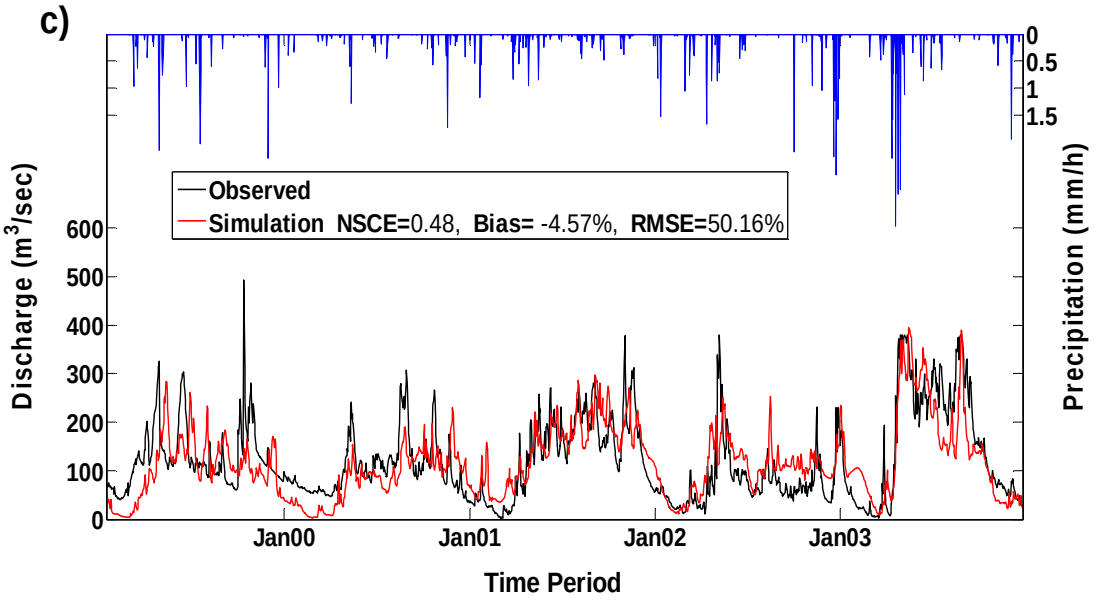

Figure 2.6: Precipitation observed and simulated runoffs for a) calibration period (1985-1998), b) validation period (1999-2004), c) validation with the TRMM 3B42 V6 from (1999-2003).

2.5 Hydrologic model reconstruction results

Basin-based water balance modeling studies are important in both hydrology and climate research since they provide information on the hydrological cycle and the amount of renewable water available for ecosystems at various land-atmosphere interaction scales ranging, in general, from daily, seasonal, annual, to decadal. Water balance for watersheds, lakes or over a unit land surface area is normally expressed

$$P - R - ET = dS/dt \quad (7)$$

Where P is Precipitation, R surface runoff, ET is evapotranspiration and dS/dt change in storage (Thornthwaite, 1948;Vörösmarty et al., 1989;Willmott et al., 1985). In the equation (7), precipitation is the important climate variable for accurate water budget estimation and measured directly on a regular basis in gauged basins. CREST model simulates the spatio-temporal variation of water fluxes and storages on a regular grid with the grid cell resolution being user-defined. The model can output many variables as a raster grid for any time period.

The hydrologic variables were generated from CREST model retrospective simulation from 1999 to 2003 using TRMM 3B42 V6. These four years were selected to minimize the model run time. Since simulation of the model involves

thousands of iterations, model run time in particular is a critical factor to complete a simulation. Water balance basin average calculations were made at daily and long-term mean monthly scale and are discussed hereunder.

Precipitation

Satellite precipitation TMPA 3B42 V6 product is used as a forcing to characterize the hydrologic variables at the study basin. As expected, 3B42 V6 captured the seasonality of precipitation over the Nzoia basin. The monthly distribution of 3B42 V6 precipitation data also shows two rainy seasons that are comparable with the observed precipitation shown in Figure 2.7. The TMPA product showed fairly good agreement throughout the year; similar results are reported in Li et al 2009. The 3B42 V6 estimates fall under the ±1 std dev of monthly mean values throughout the year (Figure 2.7). Figure 2.8 shows the spatial distribution of rainfall over the catchment.

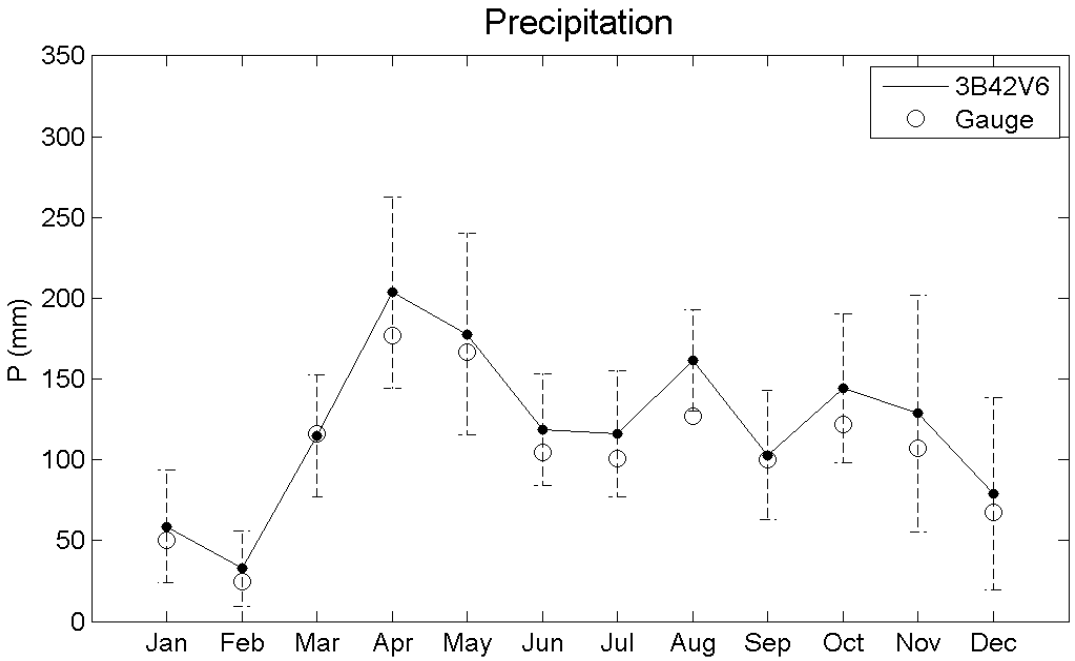

Figure 2.7: Monthly model versus observed Precipitation (P), for annual cycle from 1996 to 2006. Error bars showing the ±1 std dev of monthly mean values.

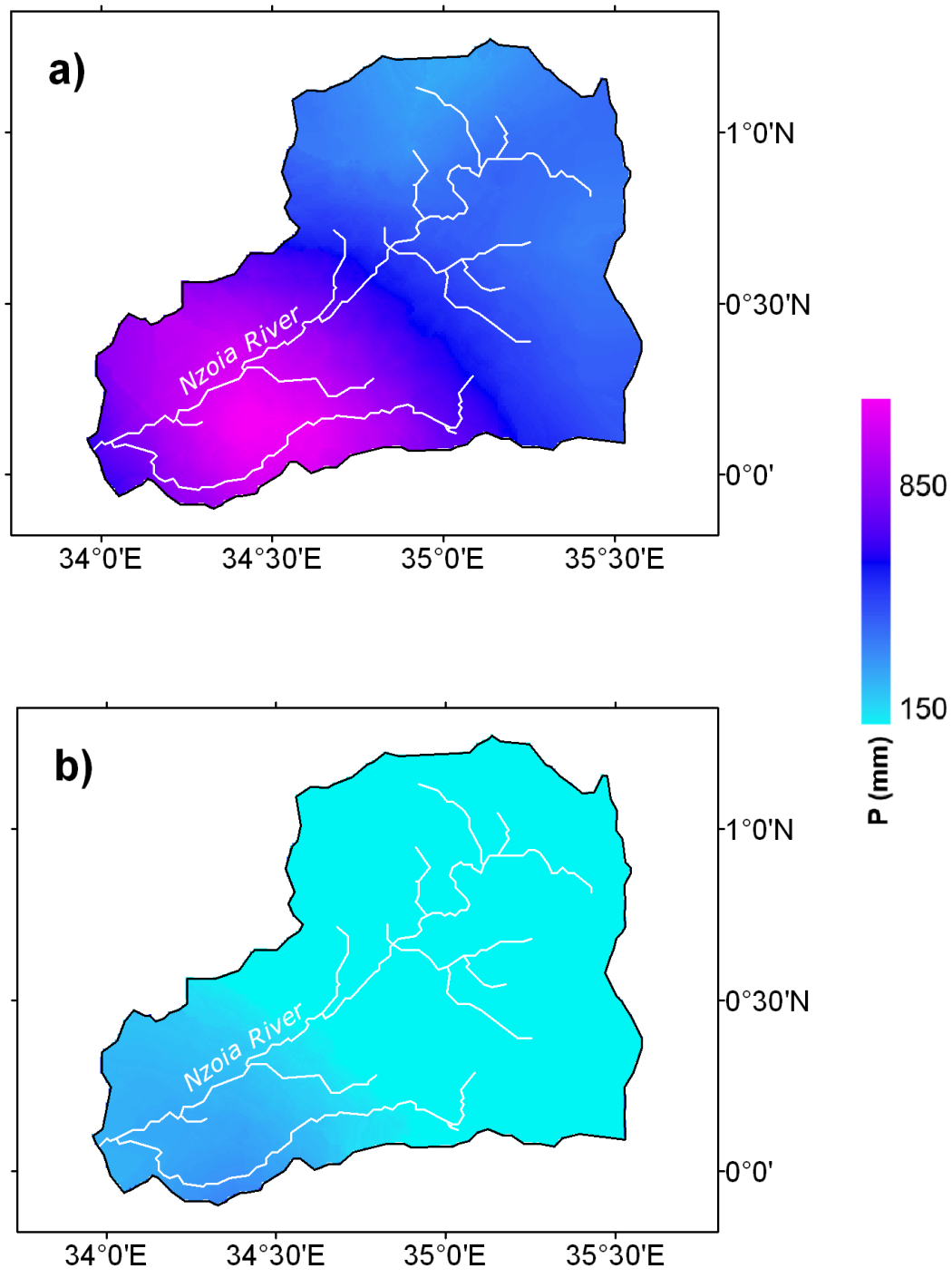

Figure 2.8: Spatially distributed precipitation (P) (a) wet season MAMJ (from March to June), (b) dry season NDJF (from Nov to Feb)

Runoff

The basin average monthly analysis shows that the model produces nearly the same basin-wide runoff. Model runoff is compared to the river discharge gauged at the catchment outlets of the basin. The runoff estimates are expressed in mm/month, to allow inspection of the relative contribution of the catchment. The overall comparison of runoff estimates are reasonably well matched in magnitude and time evolution (Figure 2.9). The model slightly underestimates R for the months of June, July, August and September. Model underestimation can be attributed to the accuracy of the TMPA V6 data. The model underestimates runoff for the validation period (Figure 2.6c). Spatially distributed runoff averaged over study period (1996-2006) during wet and dry season is illustrated in Figure 2.10.

Several articles evaluated satellite precipitation products by comparing time series of observed river streamflow with simulated streamflow using rainfall–runoff models over Africa (Hughes, 2006; Nicholson, 2005; Li et al. 2009) and other ungauged or poorly gauged regions (Su et al 2008; Collischonn et al., 2008). These studies showed that TMPA V6 underestimate the rainfall values that lead to under prediction by the hydrologic model. The observed values still fall under the ±1 standard deviation (std dev) of monthly mean values. It is to be noted that there is fluctuation of observed streamflow which is an indication of water management practices on the Nzoia River, also depicted in figure 2.9.

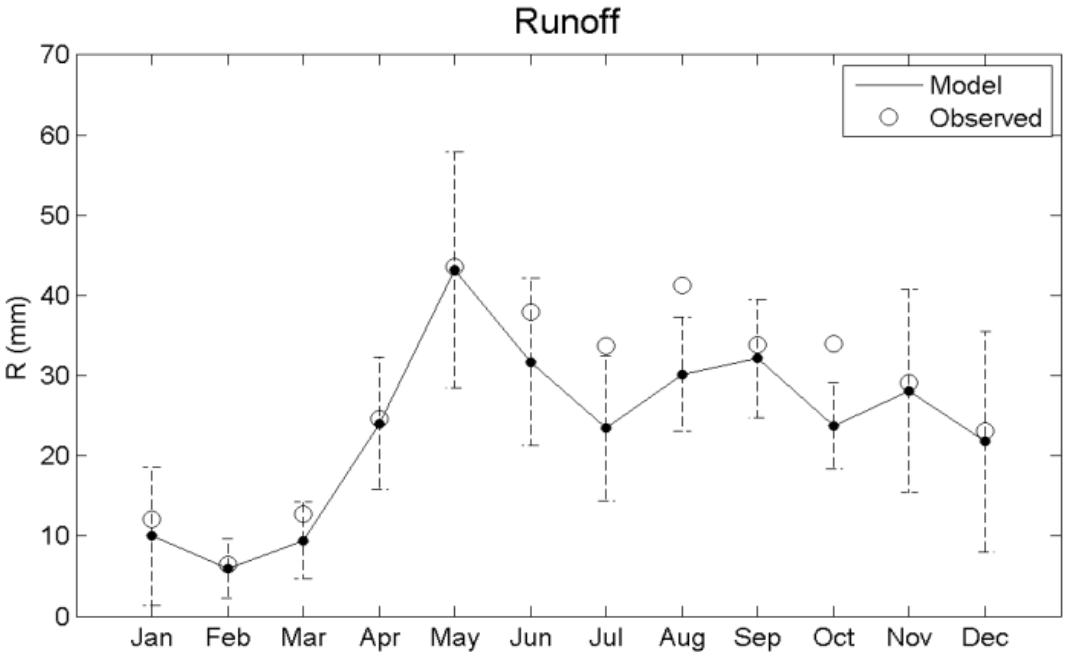

Figure 2.9: Monthly model versus observed Runoff (R) for mean annual cycle from 1996 to 2006. Error bars showing the ±1 std dev of monthly mean values.

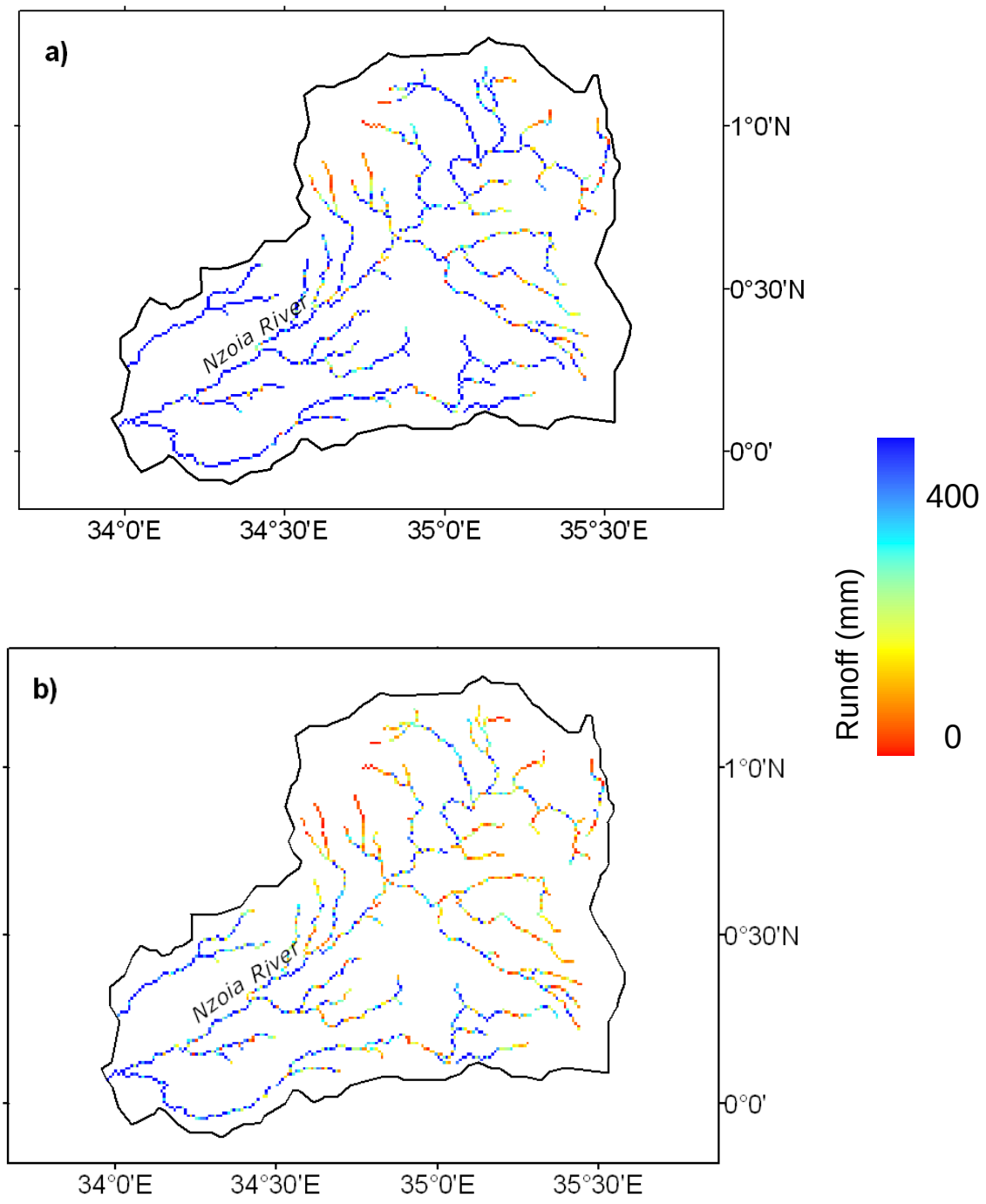

Figure 2.10: Spatially distributed average runoff in (a) wet season MAMJ (from March to June), (b) dry season NDJF (from November to Feb).

Evapotranspiration

Estimation of evapotranspiration, a key hydrologic variable provides better understating of the relationships between water balance and climate. In arid and semi-arid biomes, around 90% or more of the annual precipitation can be evapotranspired, and thus ET determines the freshwater recharge and discharge from aquifers in these environments (Wilcox et al., 2003). Moreover, it is projected that climate change will influence the global water cycle and intensify ET globally (Huntington, 2006; Meehl et al., 2007) consequently impacting the scarce water resources. Therefore, estimation of average monthly and annual evapotranspiration is important.

Figure 2.11 shows the simulated time series of evapotranspiration for the time period. Generally in the drier months, evapotranspiration equals rainfall amounts. The evapotranspiration, however, does not vary as much as rainfall does in a given year.

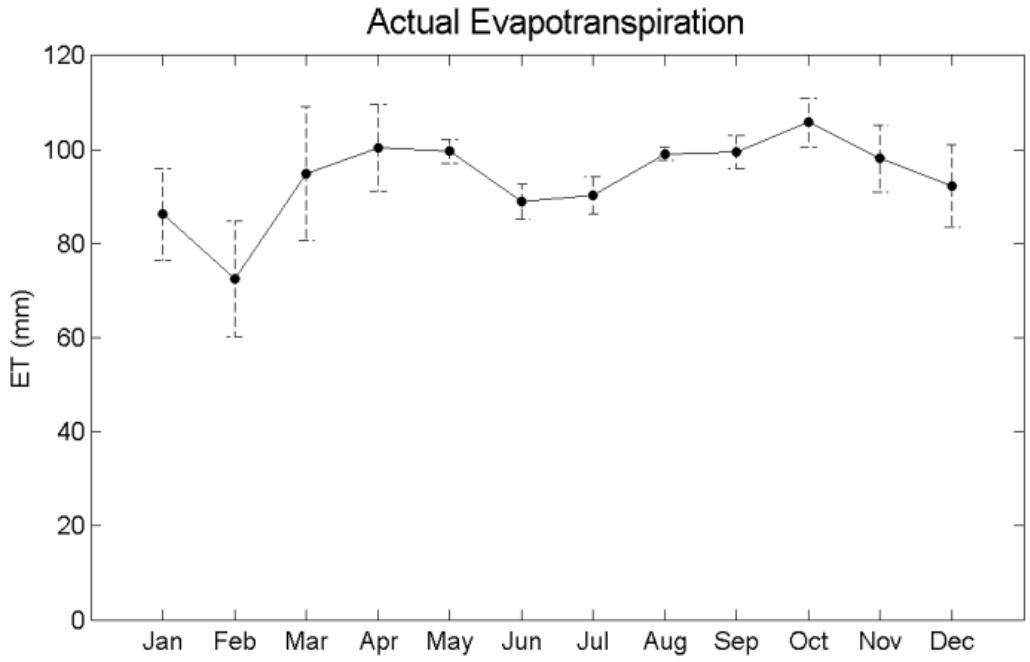

Figure 2.11: Monthly model Evapotranspiration (ET) form mean annual cycle from 1996 to 2006. Error bars showing the ±1 std dev of monthly mean values.

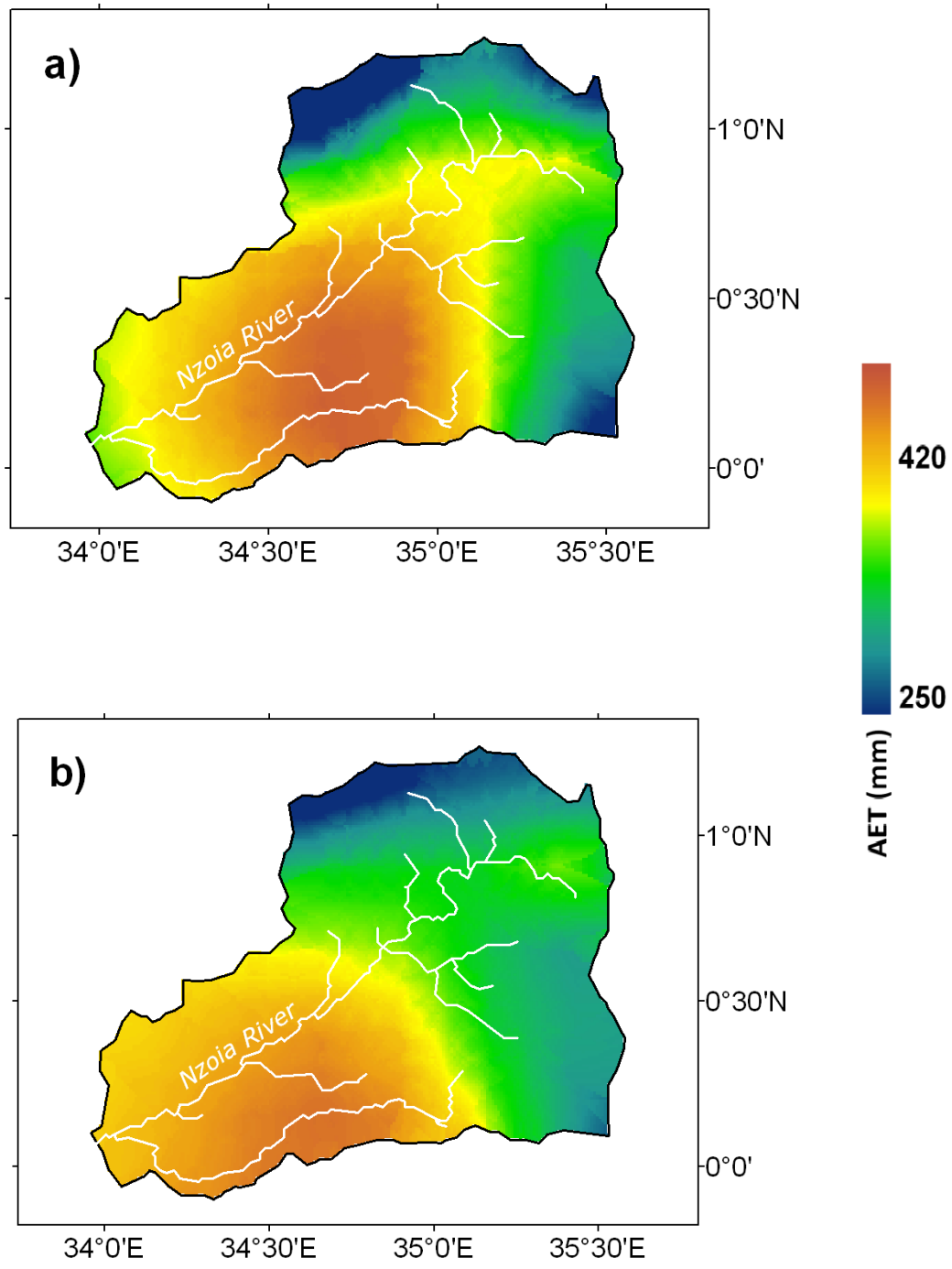

Figure 2.12: Spatially distributed evapotranspiration (AET) during (a) wet season MAMJ (from March to June), (b) dry season NDJF (from Nov to Feb).

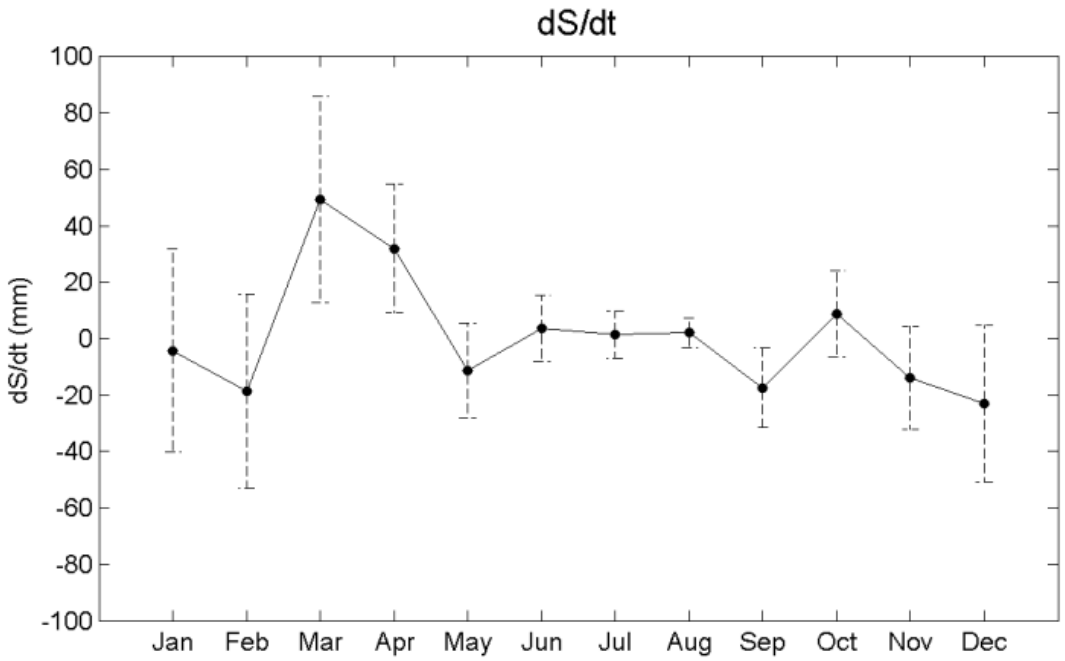

Figure 2.13: Monthly model change in storage for mean annual cycle from 1996 to 2006. Error bars showing the ±1 std dev of monthly mean values.

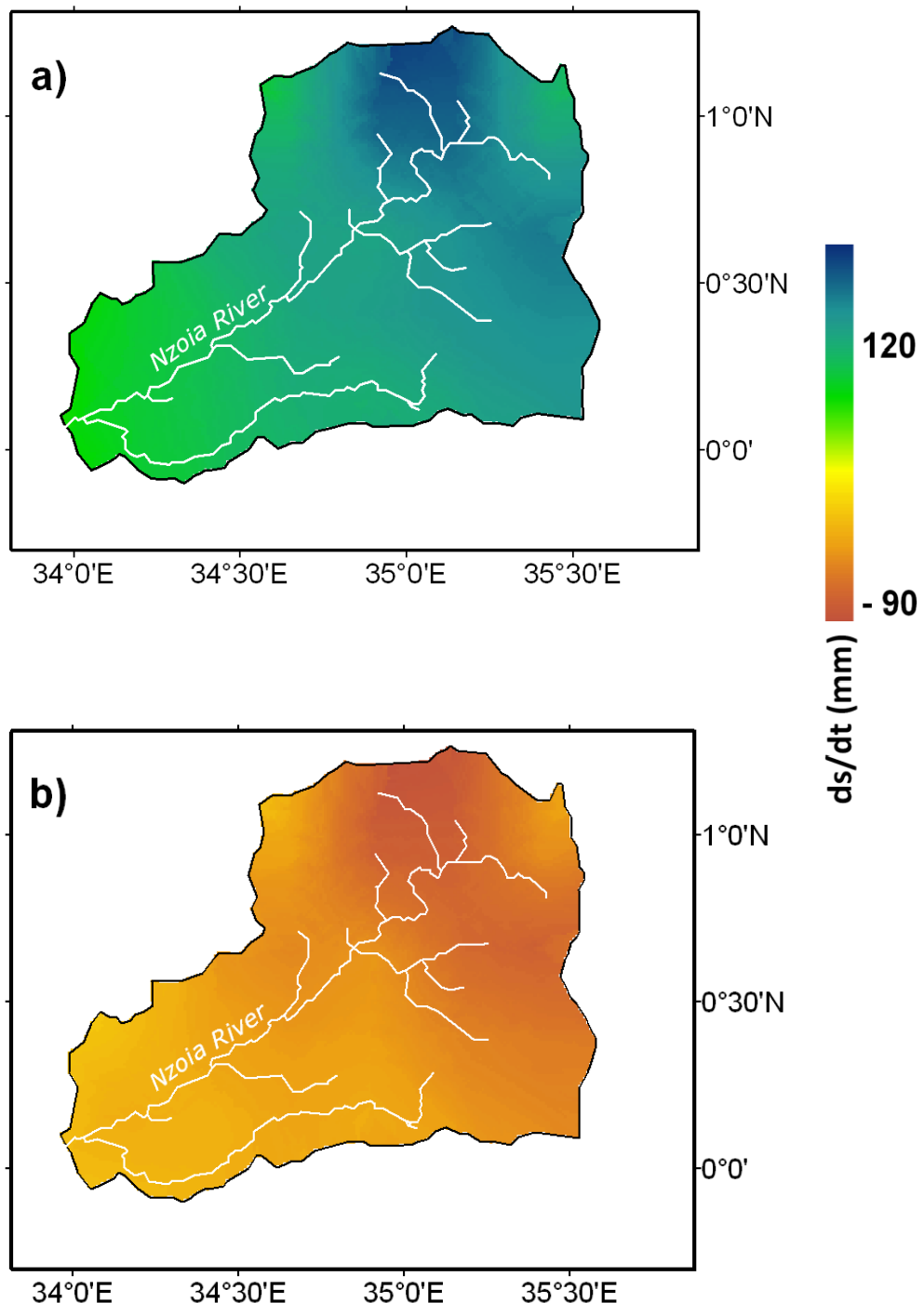

Figure 2.14: Spatially distributed change in storage (dS/dt) during (a) wet season MAMJ (from March to June), (b) dry season NDJF (from Nov to Feb).

2.6 Summary and Conclusion

In this study, we used observed data from 1985-2006, for the hydroclimatology of Nzoia basin by studying 1) rainfall and stream discharge patterns, 2) return periods of rainfall and discharge, 3) annual mean discharge and decadal monthly variation of both rainfall and discharge. In addition, a semi-distributed hydrologic model driven by satellite remote sensing data is used to study the water balance of the sub catchment. Runoff and precipitation observation have been used to evaluate the hydrologic model results.

The observed record at Nzoia showed that for the 1985-2006 time period the basin received quite consistently 2-, 5- and 10-years rainfall in totality for the past 21 years (1985-2006). The second decade (1995- 2004) however, received less 5-year and 10-year equivalent rainfalls compared to the first decade (1985-1994). The discharge data showed that the 2-years returned period equivalent discharge is observed more frequently in the second decade than in the first decade. There is only a marginal increase in annual mean discharge for the last 21 years. The 2-, 5- and 10- years peak discharges (table 3), for the entire study period shows that more years since the mid 1990s have high peak discharges even with relatively less precipitation. This might have been the effect of changing land-use and land cover types or increased channelization of the Nzoia basin over time.

Githui (2008) revealed that the land use land cover changes during 1973-

2001 have been significant and have contributed to a considerable increase in runoff. The agricultural area has increased from about 39.6 to 64.3% while forest area has decreased from 12.3 to 7.0%. Generally runoff was highest from agricultural lands while runoff from shrubland was greater than that from grasslands.

The discharge data for the study period showed that the basin is dry and arid with no sustained base flow. The short spell of high discharge shows the rain caused flooding in the basin. With a decrease in rainfall, the primary input flux into the Nzoia basin, the water budget situation might deteriorate over the coming years. Noticeable variations in monthly average rainfall and discharge were observed for the two decades (1985-1994 and 1995-2004). The rainfall fluctuated from as low as 55% (in February) to as high as 32% (in December) in drier months. Similarly, there are decreases in February and May monthly average discharge by 13% while January saw a surge of 44%. But overall, there is only a very slight increase (2%) in annual mean discharge suggesting an insignificant imbalance in water budget in the basin during the study period.

The study utilizes quasi-global satellite precipitation and other remote sensing data products. This helps to understand the utility of the remotely sensed data for hydroclimatology studies at a sub-catchment with sparse ground observations. Simulation of the key hydrological processes and their interconnection with climate and basin characteristics is a critical step in

estimating catchment water balance. Therefore, a semi-distributed hydrologic model (CREST) is implemented to simulate hydrological states and flux variables such as runoff, ET, precipitation and soil moisture at a spatial resolution of 30 arc seconds at 3 hourly time steps. The CREST model is forced by satellite-based precipitation and evapotranspiration estimates, rain gauge observations, and other remote sensing products. Observations on runoff and precipitation have been used to evaluate the model results at the sub-catchment level. TMPA 3B42 V6 showed good agreement with gauge observations (Figure 2.7).

Spatial distribution of CREST modeling results for precipitation (P), runoff (R), evapotranspiration (ET), and dS/dt (Figure 2. 8, 2.10, 2.12, and 2.14.) In general, the model reproduces P, ET, and dS/dt fairly well. Considerable agreement is observed between the monthly model runoff estimates and gauge observations reported for the Nzoia River (Figure 2.9). Runoff values respond to precipitation events occurring across the catchment during the wet season from March to early June. The hydrologic model reasonably captured the soil moisture storage variability (Figure 2.13).

An important advantage of spatially distributed hydrologic model, such as CREST model, is that it not only provides estimates of hydrological variables at the basin outlet, but also at any location as represented by a cell or grid within the given basin. These spatially distributed model inputs, states, and outputs, are useful for visualizing the hydrologic behavior of a basin. These results reveal that

relatively high flows were being experienced near the basin outlet from previous rainfall, with a new flood peak responding to the rainfall in the upper part of the basin.

Comparison of the model outputs such as evapotranspiration and soil moisture estimates against field measurements can help evaluate the model performance. The model developed from this study can be applied to poorly gauged catchments using satellite forcing data and also be used to investigate the catchment scale water balance. Implementing the CREST model resulted in spatiotemporally distributed hydrological variables that can be utilized in addressing issues pertaining to sustainability of the resources within the catchment.

References

Alsdorf, D., D. Lettenmaier & C. Vörösmarty (2003) The need for global, satellite-based observations of terrestrial surface waters. *Eos Trans. AGU,* 84, 275–276.

Alsdorf, D., E. Rodríguez & D. Lettenmaier (2007) Measuring surface water from space. *Reviews of Geophysics,* 45.

Barton, I. J. & J. M. Bathols (1989) Monitoring floods with AVHRR. *Remote Sensing of Environment,* 30, 89-94.

Beck, M. B. (1987) Water quality modeling: a review of the analysis of uncertainty. Water Resour. Res. 23, 1393–1442.

Bergström, S. (1995) The HBV model. In: Computer Models of Watershed Hydrology (V. Singh, ed.), 443–476. Highlands Ranch, CO: Water Resources Publications.

Birkett, C. M., L. A. K. Mertes, T. Dunne, M. H. Costa & M. J. Jasinski (2002) Surface water dynamics in the Amazon Basin: Application of satellite radar altimetry. *Journal of Geophysical Research-Atmospheres,* 107.

Blasco, F., M. F. Bellan & M. U. Chaudhury (1992) Estimating the extent of floods in Bangladesh using SPOT data. *Remote Sensing of Environment,* 39, 167-178.

Brakenridge, G., E. Anderson, S. Nghiem, S. Caquard & T. Shabaneh. 2003a. Flood warnings, flood disaster assessments, and flood hazard reduction: the roles of orbital remote sensing. In *30th International Symposium on Remote Sensing of Environment,*. Honolulu, HI: Pasadena, CA: Jet Propulsion Laboratory, National Aeronautics and Space Administration, 2003.

Brakenridge, G., H. Carlos & E. Anderson. 2003b. Satellite gaging reaches: A strategy for MODIS-based river monitoring. 479–485.

Brakenridge, G. R., S. V. Nghiem, E. Anderson & R. Mic (2007) Orbital microwave measurement of river discharge and ice status. *Water Resources Research,* 43.

Brakenridge, R. 2006. MODIS-based flood detection, mapping and measurement: The potential for operational hydrological applications. In *Transboundary Floods: Reducing Risks Through Flood Management*, 1-12. Springer Verlag.

Brooks, S. H. (1958) A discussion of random methods for seeking maxima. *Operations Research,* 6, 244-251.

Burnash, R. J. C. (1995) The NWS river forecast system—catchment modeling. In: Computer Models of Watershed Hydrology (V. Singh, ed.), 311–366. Highlands Ranch, CO: Water Resources Publications.

Coe, M. T. (1997) Simulating continental surface waters: an application to Holocene Northern Africa. J. Climate 10, 1680–1689.

Di Baldassarre, G., G. Schumann & P. D. Bates (2009) A technique for the calibration of hydraulic models using uncertain satellite observations of flood extent. *Journal of Hydrology,* 367, 276-282.

France, M. & P. Hedges. 1986. Hydrological Comparison of Landsat TM, Landsat MSS and Black & White Aerial Photography.

Friedl, M. A., D. K. McIver, J. C. F. Hodges, X. Y. Zhang, D. Muchoney, A. H. Strahler, C. E. Woodcock, S. Gopal, A. Schneider, A. Cooper, A. Baccini, F. Gao & C. Schaaf (2002) Global land cover mapping from MODIS: algorithms and early results. *Remote Sensing of Environment,* 83, 287-302.

Fujisada, H., F. Sakuma, A. Ono & M. Kudoh (1998) Design and preflight performance of ASTER instrument protoflight model. *IEEE Transactions on Geoscience and Remote Sensing,* 36, 1152-1160.

Gale, S. J. & S. Bainbridge (1990) The floods in eastern Australia. *Nature,* 345,

767-767.

Hagemann, S. & Dümenil, L. (1998) A parameterization of the lateral waterflow for the global scale. Climate Dynamics 14, 17–31.

Horritt, M. S. (2000) Calibration of a two-dimensional finite element flood flow model using satellite radar imagery. *Water Resources Research,* 36, 3279-3291.

Horritt, M. S. & P. D. Bates (2002) Evaluation of 1D and 2D numerical models for predicting river flood inundation. *Journal of Hydrology,* 268, 87-99.

Horritt, M. S., G. Di Baldassarre, P. D. Bates & A. Brath (2007) Comparing the performance of a 2-D finite element and a 2-D finite volume model of floodplain inundation using airborne SAR imagery. *Hydrological Processes,* 21, 2745-2759.

Huffman, G. J., R. F. Adler, D. T. Bolvin, G. J. Gu, E. J. Nelkin, K. P. Bowman, Y. Hong, E. F. Stocker & D. B. Wolff (2007) The TRMM multisatellite precipitation analysis (TMPA): Quasi-global, multiyear, combined-sensor precipitation estimates at fine scales. *Journal of Hydrometeorology,* 8, 38-55.

Liang, X., Lettenmaier, D. P. & Wood, E. F. (1996) One-dimensional statistical dynamic representation of subgrid spatial variability of precipitation in the two-layer variable infiltration capacity model. *Journal of Geophysical Research*. 101(D16), 21,403–21,422.

Li, L., Hong, Y., Wang, J., Adler, R., Policelli, F.S., Habib, S., Irwn, D., Korme, T., Okello, L., 2008, Evaluation of the Real-time TRMM-based Multi-satellite Precipitation Analysis for anOperational Flood Prediction System in Nzoia Basin, Lake Victoria, Africa, *Journal of Natural Hazards* doi 10.1007/s11069-008-9324-5.

Liston, G. E., Sud, Y. C. & Wood, E. F. (1994) Evaluating GCM land surface hydrology parameterizations by computing river discharges using a runoff routing model. J. Appl. Met. 33, 394–405.

Jensen, J. 2005. *Introductory digital image processing: a remote sensing perspective*. Prentice Hall PTR Upper Saddle River, NJ, USA.

Jensen, J. R., M. E. Hodgson, E. Christensen, H. E. Mackey, L. R. Tinney & R. Sharitz (1986) Remote-sensing inland wetlands - A multispectral approach. *Photogrammetric Engineering and Remote Sensing,* 52, 87-100.

Jonkman, S. N. (2005) Global perspectives on loss of human life caused by floods. *Natural Hazards,* 34, 151-175.

Lang, R. L., G. F. Shao, B. C. Pijanowski & R. L. Farnsworth (2008) Optimizing unsupervised classifications of remotely sensed imagery with a data-assisted labeling approach. *Computers & Geosciences,* 34, 1877-1885.

Lehner, B., K. Verdin & A. Jarvis (2008) New global hydrography derived from spaceborne elevation data. *Eos,* 89.

Marcus, W. & M. Fonstad (2008) Optical remote mapping of rivers at sub-meter resolutions and watershed extents. *Earth Surface Processes and Landforms,* 33, 4-24.

McCarthy, J. 2001. *Climate change 2001: impacts, adaptation, and vulnerability: contribution of Working Group II to the third assessment report of the Intergovernmental Panel on Climate Change*. Cambridge University Press.

Miller, J., Russell, G. & Caliri, G. (1994) Continental scale river flow in climate models. J. Climate 7, 914–928.

Nash, J. & J. Sutcliffe (1970) River flow forecasting through conceptual models part I--A discussion of principles. *Journal of hydrology,* 10, 282-290.

Puech, C. & D. Raclot (2002) Using geographical information systems and aerial photographs to determine water levels during floods. *Hydrological Processes,* 16, 1593-1602.

Rabus, B., M. Eineder, A. Roth & R. Bamler (2003) The shuttle radar topography mission - a new class of digital elevation models acquired by spaceborne radar. *Isprs Journal of Photogrammetry and Remote Sensing,* 57, 241-262.

Rasid, H. & M. Pramanik (1993) Areal extent of the 1988 flood in Bangladesh: How much did the satellite imagery show? *Natural Hazards,* 8, 189-200.

Refsgaard, J. C. & Storm, B. (1995) MIKE SHE. In: Computer Models of Watershed Hydrology (V. Singh, ed.), 809–846. Highlands Ranch, CO: Water Resources Publications.

Refsgaard, J. C. (1996) Terminology, modelling, protocol and classification of hydrological model codes. In: Distributed Hydrological Modelling (M. B. Abbott & J. C. Refsgaard, eds), 17–39. Amsterdam: Kluwer Academic Publishers, Water Science and Technology Library.

Sandholt, I., L. Nyborg, B. Fog, M. Lô, O. Bocoum & K. Rasmussen (2003) Remote sensing techniques for flood monitoring in the Senegal River Valley. *Geografisk Tidsskrift, Danish Journal of Geography,* 103, 71.

Sausen, R., Schubert, S. & Dumenil, L. (1994) A model of river runoff for use in coupled atmosphere–ocean models. J. Hydrol. 155, 337–352.

Schumann, G., P. Bates, M. Horritt, P. Matgen & F. Pappenberger (2009) Progress in integration of remote sensing–derived flood extent and stage data and hydraulic models. *Reviews of Geophysics,* 47.

Schumann, G., R. Hostache, C. Puech, L. Hoffmann, P. Matgen, F. Pappenberger & L. Pfister (2007) High-resolution 3-D flood information from radar imagery for flood hazard management. *IEEE Transactions on Geoscience and Remote Sensing,* 45, 1715-1725.

Singh, V. P. (ed.) (1995) Computer Models of Watershed Hydrology. Highlands Ranch, CO: *Water Resources* Publications.

Smith, L. C. (1997) Satellite remote sensing of river inundation area, stage, and

discharge: A review. *Hydrological Processes,* 11, 1427-1439.

Stancalie, G., A. Diamandi, C. Corbus & S. Catana (2004) Application of EO data in flood fore-casting for the Crisuri Basin, Romania. *Flood Risk Management: Hazards, Vulnerability and Mitigation Measures*, 101.

Swenson, S. & J. Wahr (2009) Monitoring the water balance of Lake Victoria, East Africa, from space. *Journal of Hydrology,* 370, 163-176.

Vörösmarty, C. J., Moore, B., Grace, A., Gildea, M., Melillo, J., Peterson, B., Rastetter, E. & Steudler, P. (1989) Continental-scale model of water balance and fluvial transport: an application to South America. Global Biogeochem. Cycles 3, 241–265.

Wang, Y. (2004) Using Landsat 7 TM data acquired days after a flood event to delineate the maximum flood extent on a coastal floodplain. *International Journal of Remote Sensing,* 25, 959-974.

Wang, Y., J. D. Colby & K. A. Mulcahy (2002) An efficient method for mapping flood extent in a coastal floodplain using Landsat TM and DEM data. *International Journal of Remote Sensing,* 23, 3681-3696.

Watson, J. P. (1991) A visual interpretation of a LANDSAT mosaic of the Okavango-delta and surrounding area. *Remote Sensing of Environment,* 35, 1-9.

Wilcox, B., Seyfried, M., and Breshears, D.: The water balance on rangelands, Encyclopedia of water science, 791–794, 2003.

Woolhiser, D. A., Smith, R. E. & Goodrich, D. C. (1990) KINEROS, Kinematic Runoff and Erosion Model: Documentation and User Manual. US Dept of Agriculture – Agric. Research Service, USDA-ARS no. 77.

Xiao, Q. & W. Chen (1987) Songhua River ood monitoring with meteorological satellite imagery. *Remote Sensing Information*, 37–41.

Yamaguchi, Y., A. B. Kahle, H. Tsu, T. Kawakami & M. Pniel (1998) Overview of Advanced Spaceborne Thermal Emission and Reflection Radiometer (ASTER). *IEEE Transactions on Geoscience and Remote Sensing,* 36, 1062-1071.

Yong, B., L. Ren, Y. Hong, J. Wang, W. Wang, and X. Chen (2010) Hydrologic Evaluation of TRMM Standard Precipitation Products in Basins Beyond its Inclined Latitude Band: a Case Study in Laohahe Basin, China, *Water Resour. Res*, doi:10.1029/2009WR008965

Zhao Renjun, Zhang Yilin, Fang Leren, Liu Xinren & Zhang Quansheng (1980) The Xinanjiang Model. In: Hydrological Forecasting (Proc. Oxford Symp., April 1980), 351–356. Wallingford: IAHS Press, IAHS Publ. 129.

Zhao, R. J. (1992) The Xianjiang model applied in China. J. Hydrol. 135(3), 371–381.

CHAPTER 3 : MULTISPECTRAL REMOTE SENSING FOR FLOOD DETECTION

Abstract

Implementation of a flood prediction system can potentially help mitigate flood induced hazards. Such a system typically requires implementation and calibration of a hydrologic model using in-situ observations (e.g. rain gauges and stream gauges). Recently, satellite remote sensing data has emerged as a viable alternative or supplement to the in-situ observations due to its availability over vast ungauged regions. The focus of this study is to integrate the best available satellite products within a semi-distributed hydrologic model to characterize the spatial extent of flooding over sparsely-gauged or ungauged basins. A satellite remote sensing based approach is proposed to calibrate a hydrologic model, simulate the spatial extent of flooding, and evaluate the probability of detecting inundated areas.

A raster-based semi-distributed hydrologic model, CREST, is implemented for the Nzoia basin, a sub-basin of Lake Victoria in Africa. MODIS Terra and ASTER-based raster flood inundation maps were produced over the region and used to benchmark the hydrologic model simulations of inundated areas. The analysis showed the value of integrating satellite data such as precipitation, land cover type, topography and other data products along with space based flood

inundation extents as inputs for the hydrologic model. It is concluded that the quantification of flooding spatial extent through optical sensors can help to evaluate hydrologic models and hence potentially improve hydrologic prediction and flood management strategies in ungauged catchments.

3.1 Introduction

Floods are among the most recurring and devastating natural hazards, impacting human lives and causing severe economic damage throughout the world. It is understood that flood risks will not subside in the future and with the onset of climate change flood intensity and frequency will threaten many regions of the world (Jonkman 2005, McCarthy 2001). The current trend and future scenarios of flood risks demand accurate spatial and temporal information on the flood hazards and risks.

Techniques utilizing satellite remote sensing data can provide objective information that may help to detect and monitor the spatio-temporal evolution of floods (Brakenridge et al. 2003a, Brakenridge, Carlos and Anderson 2003b, Smith 1997). For example, orbital sensors, such as NASA's Moderate-Resolution Imaging Spectroradiometer (MODIS), provide necessary data to help detecting floods in regions where no other means are available for flood monitoring with good accuracy (Brakenridge et al. 2007, Brakenridge 2006). Such data, after certain processing are capably of provide timely information on flood extents with global coverage and frequent observations

To date, satellite observations have become practical tools for development of cost-effective methods for hydrologic prediction in poorly or even ungauged basins around the globe, regardless of the political boundaries. It has been demonstrated that orbital remote sensing can be used for river inundation

mapping and has the potential to remotely measure runoff (Birkett et al. 2002, Brakenridge 2006).

The application of satellite imagery for flood mapping began with the use of Landsat Thematic Mapper (TM) and Multi-Spectral Scanner (MSS), the Satellite Pour l'Observation de la Terre (SPOT) (Blasco, Bellan and Chaudhury 1992, France and Hedges 1986, Jensen et al. 1986, Watson 1991), the Advanced Very High Resolution Radiometer (AVHRR) (Barton and Bathols 1989, Gale and Bainbridge 1990, Rasid and Pramanik 1993, Sandholt et al. 2003, Xiao and Chen 1987), Advanced Spaceborne Thermal Emission and Reflection Radiometer (ASTER), Moderate-Resolution Imaging Spectroradiometer (MODIS) and Landsat-7 sensors (Brakenridge et al. 2003a, Brakenridge et al. 2003b, Stancalie et al. 2004, Wang 2004, Wang, Colby and Mulcahy 2002). For a comprehensive review on extraction of flood extent and surface water level from various satellite sensors please refer to Smith; Watson (Puech and Raclot 2002, Smith 1997, Alsdorf, Lettenmaier and Vörösmarty 2003, Alsdorf, Rodríguez and Lettenmaier 2007a, Marcus and Fonstad 2008, Schumann et al. 2009).

Satellite remote sensing data have emerged as viable alternative or supplement to in situ observations due to their availability over vast ungauged regions. Microwave satellite data can be effectively used for flood monitoring through the cloud cover but its spatial resolution is relatively coarse for flood mapping at around 10-km grid scale, such as Advance Microwave Scanning

Radiometer for the Earth Observing System (AMSR-E) microwave data.

Satellite radar imagery has proved invaluable in mapping flood extent (Horritt 2000, Horritt and Bates 2002, Schumann et al. 2007). For example, flood extent maps derived from Synthetic Aperture Radar (SAR) sensors have been used to validate hydraulic models (Di Baldassarre, Schumann and Bates 2009, Horritt et al. 2007). However, limitations of the SAR include inability to detect flooding in urban areas, inaccurate image calibration that leads to geometric and radiometric distortions, difficulties for data processing, and more prohibitively, low temporal resolution of the current radar satellites with a revisit time of 35 days (Schumann et al. 2007).

Other sensors such as the Advanced Synthetic Aperture Radar (ASAR) instrument onboard ENVISAT with a spatial resolution of (150-1000m) and a revisit time few days can be effective for flood detection (Di Baldassarre et al. 2009, Schumann et al. 2009, Schumann et al. 2007). Contrary to the space-borne microwave data, visible/infrared sensors aboard on NASA MODIS Terra satellite can detect floods globally with relatively high spatial (30m ASTER, 250m MODIS) and temporal (daily if clear sky) resolution. For the past decade, noticeable efforts have been made to investigate the potential to use flood inundation extent derived from optical sensors as a tool to validate the performance of hydrologic models in sparsely or unguaged basins (Brakenridge et al. 2007, Brakenridge 2006).

The objective of the chapter is to investigate the utility of flood spatial extent information obtained from orbital sensors to calibrate and evaluate hydrologic models in an effort to potentially improve hydrologic prediction and flood management strategies in ungauged catchments. The goal of this exercise was to assemble a reasonable (rather than definitive) approach to act as a test-bed to investigate how the improved satellite based flood inundation extent can be used to calibrate hydrologic model. The chapter is organized as follows: the study area, data and the hydrological model. The methodology section outlines the methods for space based flood inundation mapping and for hydrologic model based flood extent mapping. Results section provides a comparison between the two methods and validates the model performance using MODIS/ASTER-derived flood inundation maps, followed by final concluding remarks in the last section.

3.2 Study Area and Data

Nzoia Basin

The rainy season that onsets from October through early December brings devastating floods in Uganda, Kenya, Tanzania and other countries in East Africa almost every year. This region, surrounding Lake Victoria, is heavily populated with around thirty million people (Figure 3.1). During December 2006, the United Nations Office for the Coordination of Humanitarian Affairs estimated that 1.8 million people had been affected by the flooding in Kenya, Ethiopia and Somalia.

Repeated flooding affects many lives particularly in the Lake Victoria

region. With an area of 68,600 km2, Lake Victoria is the second largest freshwater lake in the world (Swenson and Wahr 2009). Nzoia, a sub-basin of the Lake Victoria, is chosen as the study area because of its regional importance as it is a flood-prone basin and also one of the major tributaries to Lake Victoria. The Nzoia River basin covers approximately 12,900 km2 with elevation ranging between 1,100 to 3,000 m. Annual average rain within the region is 1,500 mm . Table 1 lists recent flooding events investigated in this study.

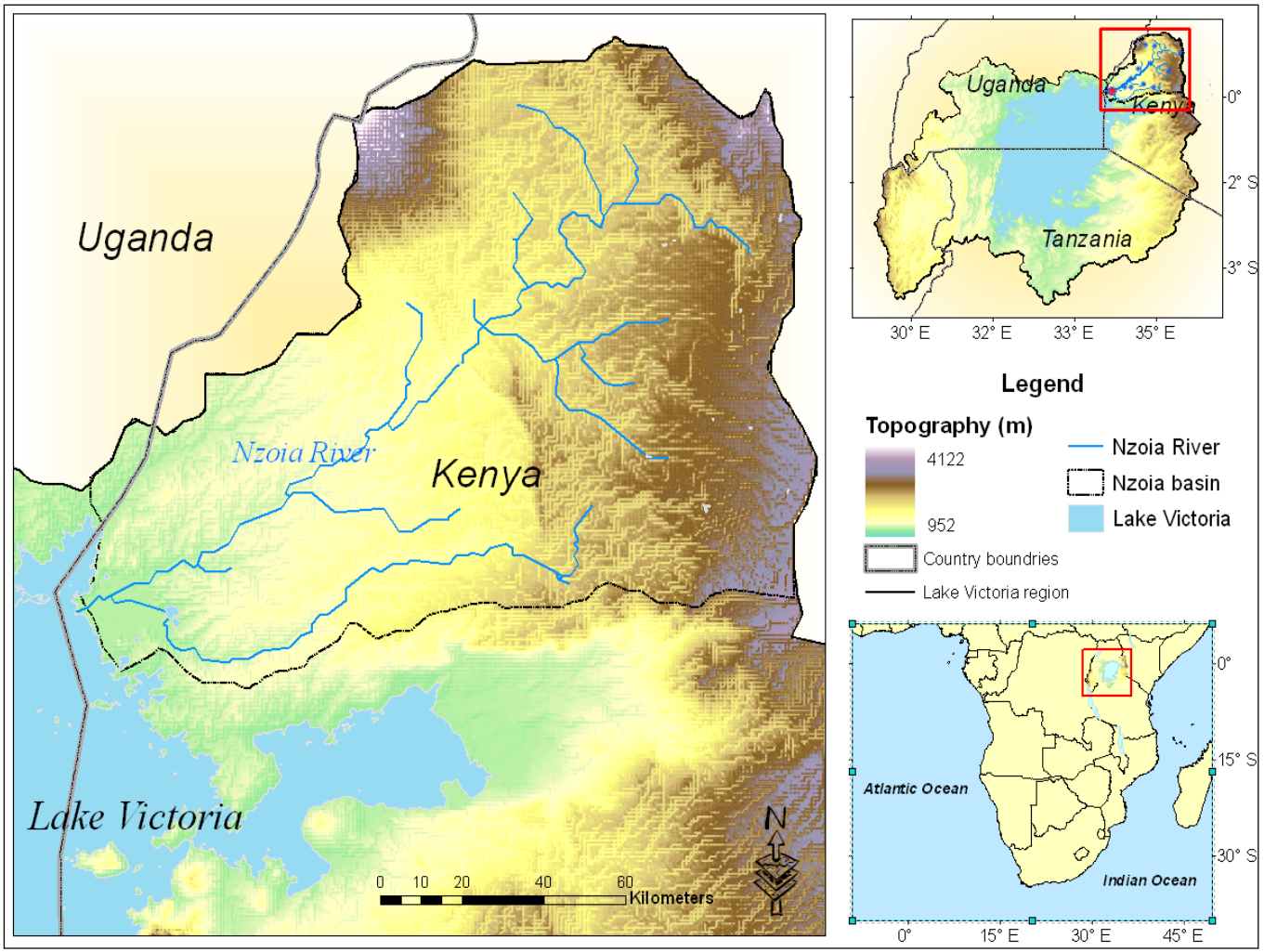

Figure 3.1 Map showing Nzoia river basin in Lake Victoria region, East Africa

Table 3.1: Selected flood events, location, flooded areas/river; verified with the (Dartmouth Flood Observatory) DFO flood inventory. Numbers in parenthesis are the Julian days of the corresponding year.

Events	Images retrieved (DOY)	Countries effected	Rivers flooded
1.	2006/12/04 (338)	Kenya	Ewaso Nyiro, Uaso Nyiro, Tana river and tributaries. Ramisi. Lak Dera, Lak Bor, Lagahar. Ndarugu. Sosiani. Ramisi. Nzoia. Ongoche, Kuja, Migori, Ongohe.
		Uganda	River Ssezibwa
		Tanzania	Wembere, Mwanza
2.	2007/08/15 (227) 2007/08/22 (234) 2007/08/24 (236)	Kenya	Nzoia, Sabwani, Malakisi, Malaba Kirik, Moroto, Aswa, Ora, Ssezibwa,
		Uganda	Dopeth. Muzizi. Nyangoma
		Tanzania	Wembere, Mwanza
3.	2008/11/12 (317)	Kenya	Western Kenya, Nzoia River

3.3 Methodology

This study presents a methodology based entirely on satellite remote sensing data (including topography, land cover, precipitation, and flood inundation extent) to calibrate a hydrologic model, simulate the spatial extent of flooding, and evaluate the probability of detecting inundated areas. MODIS and ASTER-based raster flood inundation maps were derived to benchmark the hydrologic model to simulate the spatial extent of flooding and associated hazards.

The methodology contains three major components(Khan et al. 2011b) (Figure 3.2). First, the data from MODIS and ASTER sensors were archived and processed to derive flood inundation maps for the selected events (Table 3.1). Second, a grid-based semi-distributed hydrologic model is implemented and further calibrated using the satellite derived flood inundation maps in the study area. Finally, the performance of hydrologic prediction in Nzoia basin is evaluated by comparing the simulated flood inundation extents with those derived from MODIS and ASTER imagery. A similar technique described below is used by the Dartmouth Flood Observatory (http://www.dartmouth.edu/~floods/) to generate flood maps

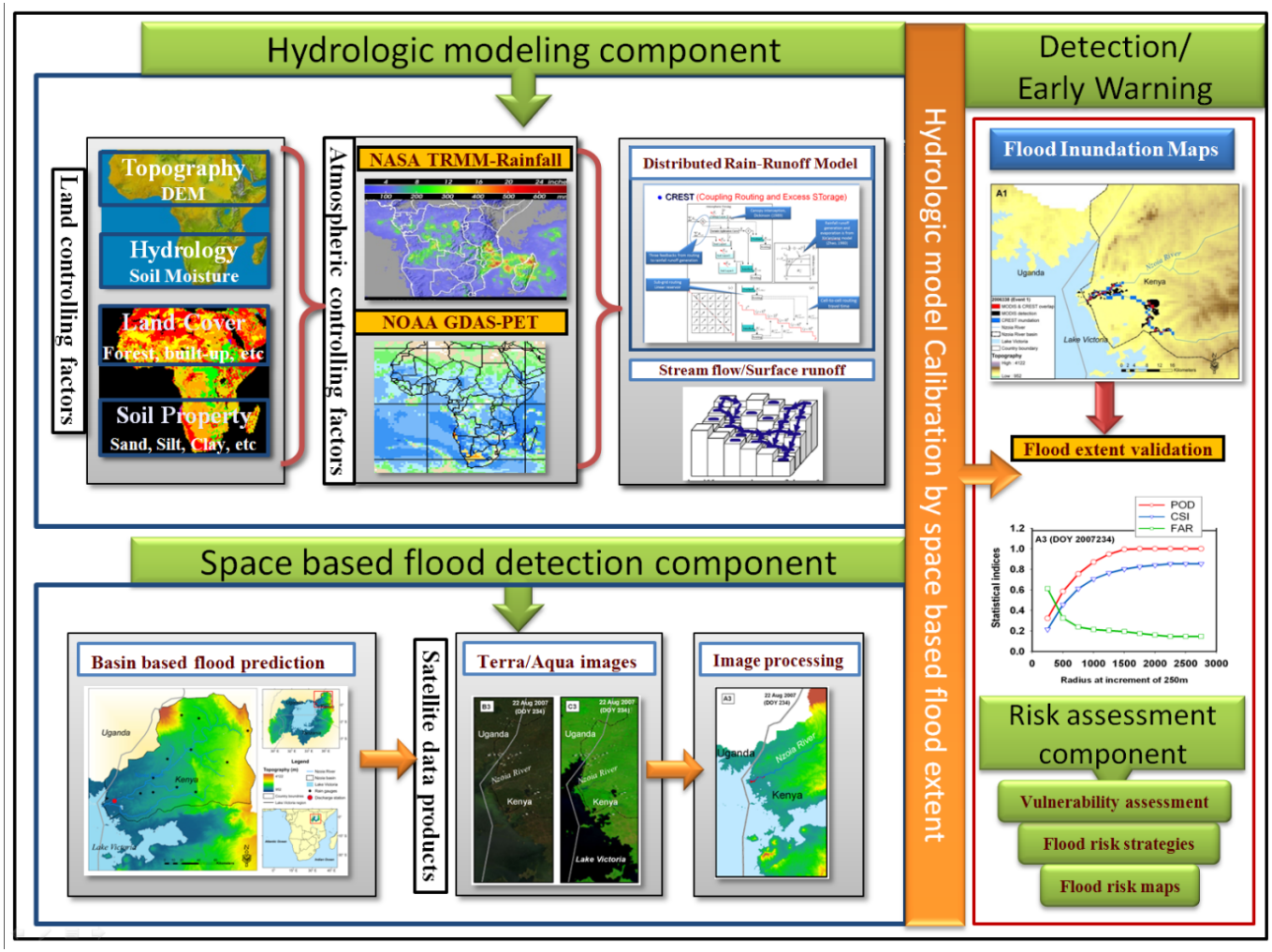

Figure 3.2 Schematic of the satellite remote sensing and hydrological modeling based flood monitoring system.

Satellite based flood inundation mapping

In this study we used Moderate Resolution Imaging Spectroradiometer (MODIS) and Advanced Spaceborne Thermal Emission and Reflection Radiometer (ASTER) for flood inundation mapping. MODIS instruments onboard NASA's Terra and Aqua satellites offer a unique combination of near-global daily coverage with acceptable spatial resolution. These capabilities are being utilized for flood monitoring at regional and global scale. (Brakenridge et al. 2003a, Brakenridge et al. 2003b) demonstrated that MODIS data can be used to distinguish between flooded and non-flooded areas with suitable spatial resolution. This can be very crucial in regions where no other means flood monitoring are available. NASA's Goddard Space Flight Center (GSFC), through the Rapid Response System, processes and displays images in near real time—within 2 to 4 hours of retrieval. MODIS Rapid Response data are available from Terra and Aqua in near real time at: http://rapidfire.sci.gsfc.nasa.gov/. This system, initially developed for fire hazard detection and monitoring, can be utilized for flood detection throughout the globe. Several spectral bands at spatial resolutions of approximately 250 and 500 m are appropriate for accurate discrimination of water from land. Excluding the effects of cloud cover, there is also global coverage on a near-daily basis.

Another sensor used in this study is ASTER, an imaging instrument flying on Terra satellite that launched in December 1999 as part of NASA's Earth

Observing System (EOS). ASTER is a cooperative effort between NASA, Japan's Ministry of Economy, Trade and Industry (METI) and Japan's Earth Remote Sensing Data Analysis Center (ERSDAC). ASTER is an advanced multispectral imager with high spatial, spectral, and radiometric resolution. The ASTER instrument covers a wide spectral region, from visible to thermal infrared with 14 spectral bands. It has total of 14 bands in Visible to Near-Infrared (VNIR), Short Wave-Infrared (SWIR) and Thermal-Infrared (TIR) wavelengths. The ground resolutions of the VNIR, SWIR and TIR images are 15, 30 and 90 m, respectively (Fujisada et al. 1998, Yamaguchi et al. 1998). Data from this sensor can be acquired on demand from Land Processes Distributed Active Archive Center (LP DAAC) at the USGS EROS Data Center, with the standard Hierarchical Data Format (http://LPDAAC.usgs.gov).

There are several methods for identifying flooded vs. non flooded areas using optical remote sensing imagery (e.g. (Jensen 2005, Jensen et al. 1986)). The first step is to identify spectral classes within the imagery. One of the widely used clustering algorithm used for this task is the Iterative Self-Organizing Data Analysis Technique Algorithm (ISODATA), which uses the Euclidean distance in the feature space to assign every pixel to a cluster through a number of iterations (Jensen 2005). ISODATA begins with either arbitrary cluster means or means of an existing signature set, and each time the clustering repeats, the means of these clusters are shifted. The new cluster means are used for the next iteration.

To perform ISODATA, the analyst selects the number of spectral classes (NSC), a convergence threshold (CT), and number of iterations for the algorithm, which introduces considerable subjectivity into the classification process (Lang et al. 2008). This process of flood water classification is performed using the ENVI™ software. In this study, the strategies for MODIS and ASTER based inundation extent extractions are described in detail. The method for the flood detection and mapping using satellite imagery included the following steps:

1) Terra MODIS near real time subsets covering the region of Lake Victoria were retrieved from NASA website http://rapidfire.sci.gsfc.nasa.gov/subsets

2) Color composite images were downloaded for image processing. The false composite of MODIS band 1, 2 and 7 (Red, Near Infrared, and Short-wave infrared) has a resolution of 250m. The true color composite of MODIS band 1, 3 and 4 is used for visual interpretation.

3) False color composite images were subset to the region of interest and ISODATA classification is performed (20 classes and 3 iterations)

4) All the water classes were combined into one water class.

5) The raster type images were exported as Geographical Information System (GIS) compatible format for further processing.

6) The images obtained in Step 5 were overlaid on the true color image to remove the cloud contamination/shadows that were falsely classified as water.

7) The final product overlaid in GIS under a reference water layer (SRTM based water bodies) is used to identify the current flooded areas.

Hydrological model setup and implementation

A semi-distributed hydrologic model, Coupled Routing and Excess STorage (CREST), developed by (Wang et al. 2011).is used to generate modeled flood areal extents for comparison with the satellite based flood inundation maps. The model accounts for the most important parameters of the water balance component i.e. the infiltration and runoff generation processes. The main CREST model components are briefly described as ; 1) data flow module based on cell to cell finite elements ; 2) the three different layer within the soil profile that affect the maximum storage available in the soil layers. This representation of within cell variability in soil moisture storage capacity (via a spatial probability distribution) and within cell routing can be employed for simulations at different spatiotemporal scales 3) coupling between the runoff generation and routing components via feedback mechanisms. This coupling allows for a scalability of the hydrological variables, such as soil moisture, and particularly important for simulations at fine spatial resolution.

CREST model simulates the spatio-temporal variation of water fluxes and storages on a regular grid with the grid cell resolution being user-defined. The scalability of model simulations is accomplished through sub-grid scale representation of soil moisture variability (through spatial probability distributions)

and physical process representation. CREST model can also simulate inundation extent in an effort to obtain spatial and temporal variation of floodwater within grid-based domain. For more information of the CREST model (Wang et al. 2011).

In CREST model, parameters related to topography, soil properties and topography are directly estimated form the land surface controlling data based shown in the framework (Figure 3.2). To apply the CREST model over Nzoia basin on 1km spatial resolution, local drainage direction and accumulation is established using the 30 arc seconds resolution SRTM DEM from HydroSHEDS data. The precipitation forcing data is TRMM-based Multi-satellite Precipitation Analysis 3B42 Real-Time (TMPA 3B42RT) products (Huffman et al. 2007b). The subscript 'RT' refers to real time, which in reality refers to a pseudo real time where data is available to the user via the internet with a 8- 16 hour latency for the end user. The key remote sensing datasets enabling the development of a hydrological model in Nzoia basin includes the following:

1) The digital elevation data from SRTM (Rabus et al. 2003) ; http://www2.jpl.nasa.gov/srtm/), SRTM-derived hydrological parameter files of HydroSHEDS (Lehner, Verdin and Jarvis 2008).

2) The rainfall data is from the TRMM-based Multi-satellite Precipitation Analysis 3B42 Real-Time (TMPA 3B42RT) operating in near-real time (Huffman et al. 2007b) The data is available on the TRMM web site

(http://trmm.gsfc.nasa.gov) at 0.25º×0.25º spatial and 3h temporal scales within 50º N–S latitude band.

3) Soil parameters are provided by the FAO (2003) (http://www.fao.org/AG/agl/agll/dsmw.html),

4) MODIS land classification map is used as a surrogate for land use/cover, with 17 classes of land cover according to the International Geosphere–Biosphere Programme classification (Friedl et al. 2002).

5) Global daily Potential Evapotranspiration (PET) data is obtained from the Famine Early Warning Systems Network (FEWS NET: http://earlywarning.usgs.gov/Global/index.php).

Model Calibration and Validation

CREST model is calibrated using available daily observed discharge data for the period between 1998 and 2004 (Figure 3.3). A one-year period (1998) is used for warming up the model states. The model utilizes global optimization approach to capture the parameter interactions. An auto-calibration technique based on Adaptive Random Search (ARS) method by Brooks (Brooks 1958) is used to calibrate the CREST model. The ARS method is considered adaptive in the sense that it uses information gathered during previous iterations to decide how simulation effort is expended in the current iteration.

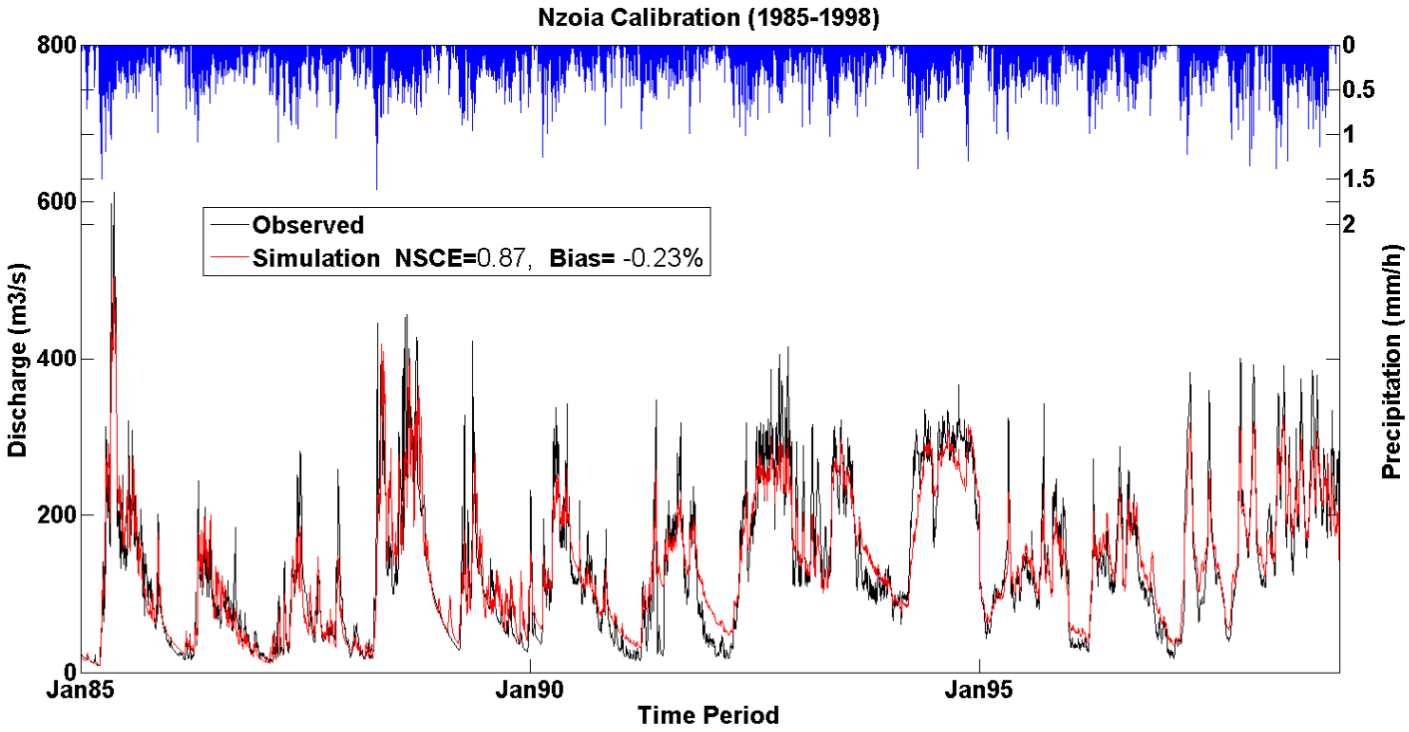

Figure 3.3: Nzoia basin precipitation observed and simulated runoffs during calibration period (1985-1998).

Flood inundation module

The CREST model flood inundation component uses one of the model outputs, the grid to gird total free water, to simulate the flood extents. A predefined total free water depth threshold approximately 70 mm is employed to determine flood inundated extents. This value is not fixed but changes with the calibration of satellite-based flood inundation images that are used during auto-calibration process. For more information about CREST model inputs and outputs, please refer to (Wang et al. 2011).

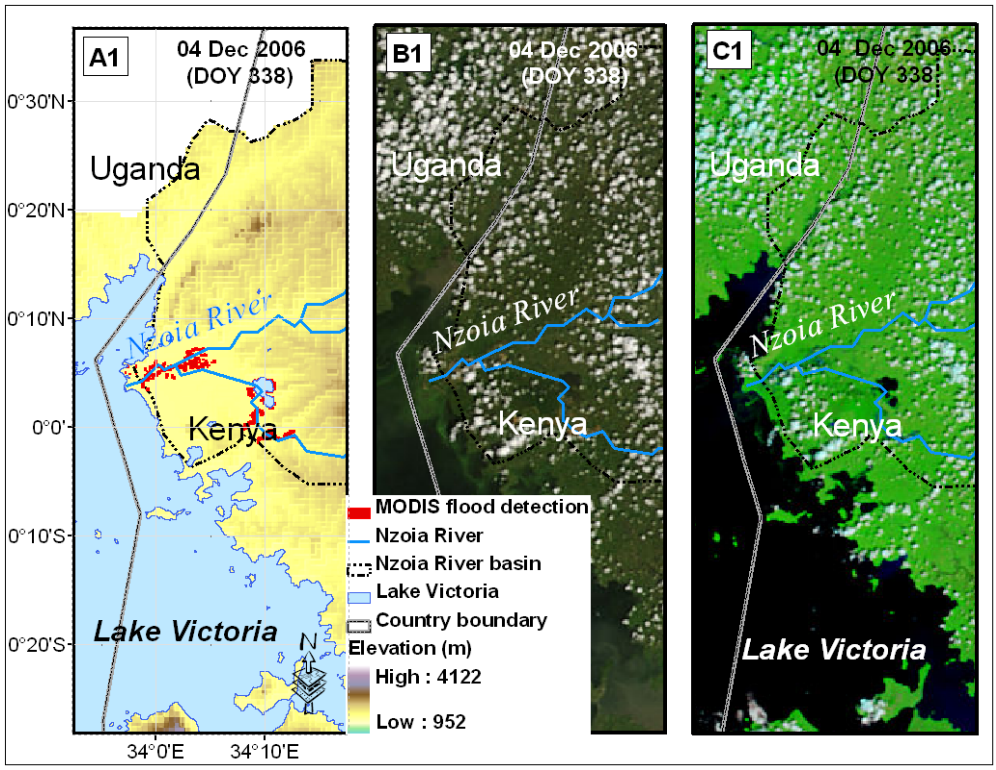

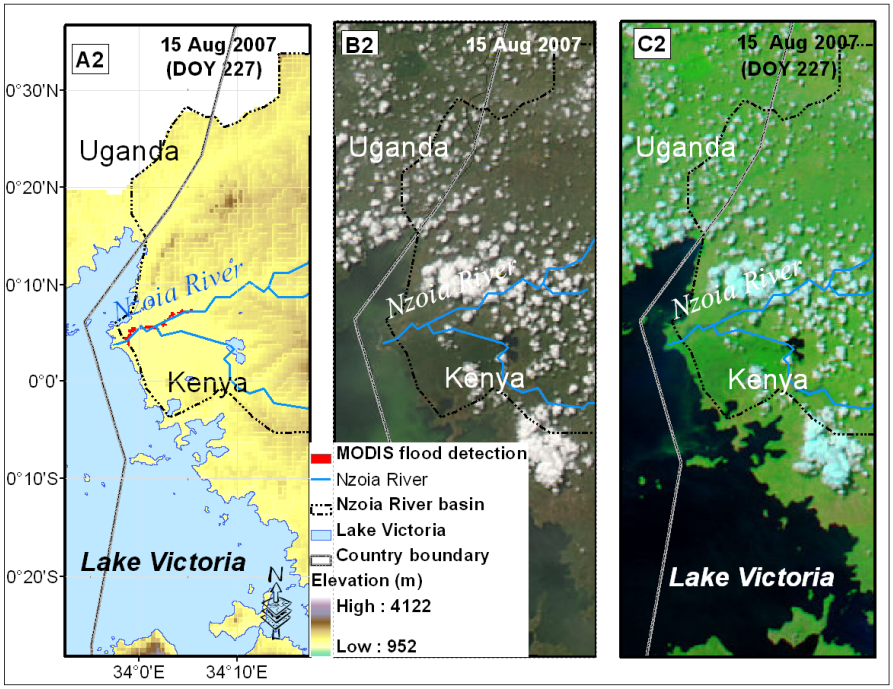
A2
15 Aug 2007
(DOY 227)
B2
15 Aug 2007
C2
15 Aug 2007
(DOY 227)
0°30'N
0°20'N
0°10'N
0°0'
0°10'S
0°20'S
34°0'E
34°10'E
Uganda
Kenya
Nzoia River
Lake Victoria
MODIS flood detection
Nzoia River
Nzoia River basin
Lake Victoria
Country boundary
Elevation (m)
High : 4122
Low : 952
N

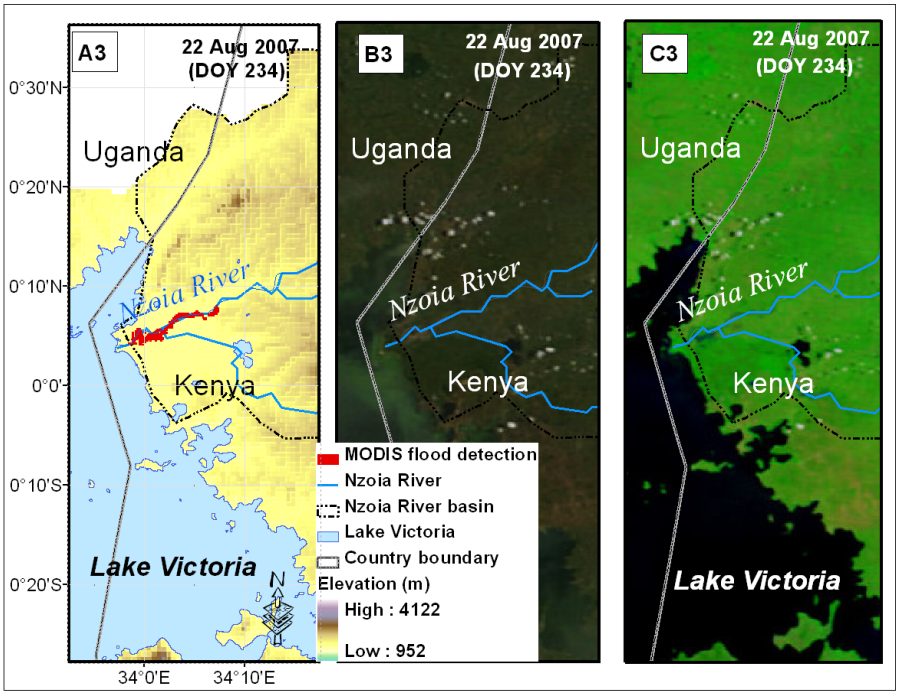
A3
22 Aug 2007
(DOY 234)
B3
22 Aug 2007
(DOY 234)
C3
22 Aug 2007
(DOY 234)
0°30'N
0°20'N
0°10'N
0°0'
0°10'S
0°20'S
34°0'E
34°10'E
Uganda
Kenya
Nzoia River
Lake Victoria
MODIS flood detection
Nzoia River
Nzoia River basin
Lake Victoria
Country boundary
Elevation (m)
High : 4122
Low : 952
N

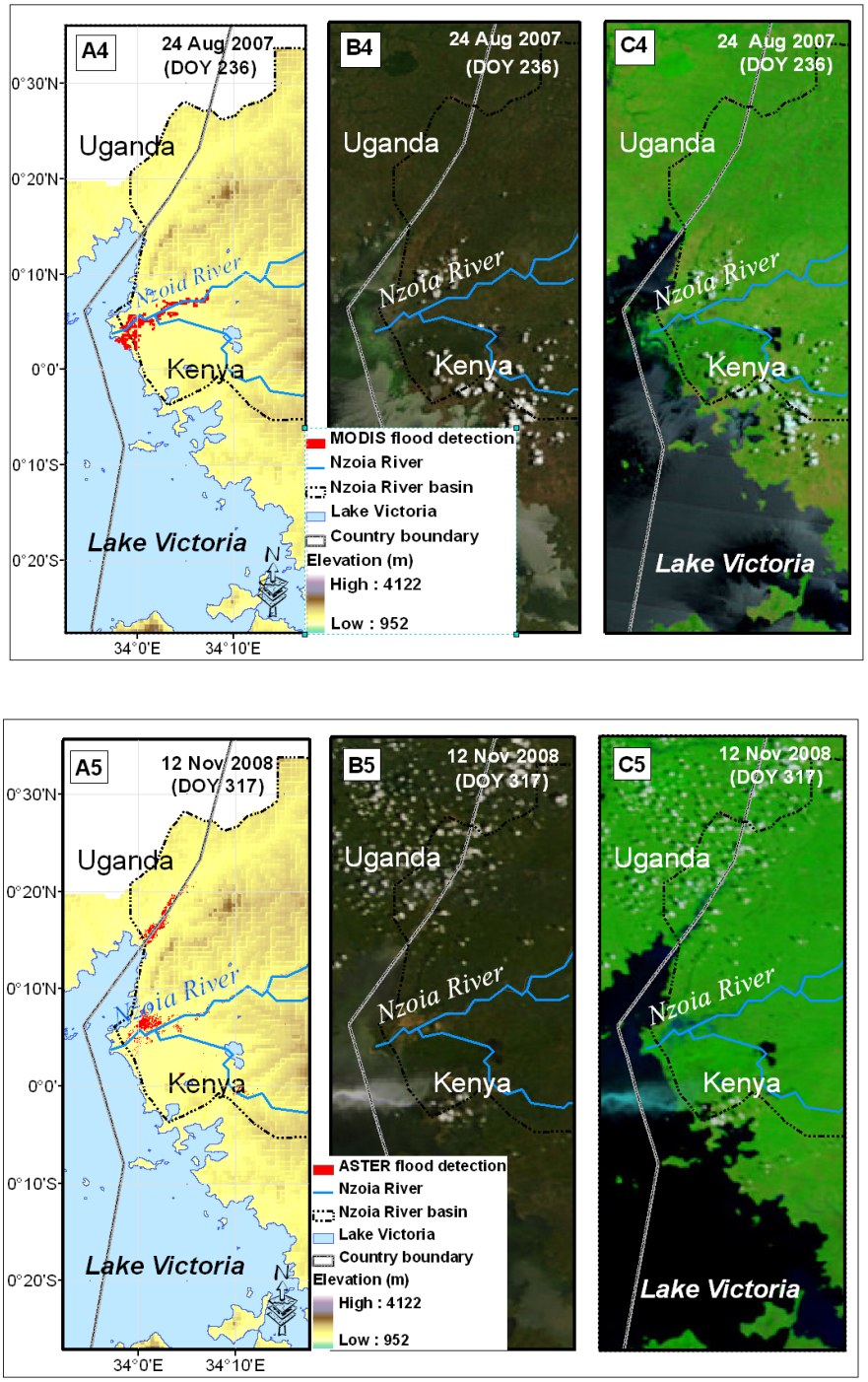

Figure 3.4: A1-A4, MODIS based inundation maps for 04 Dec 2006, 15, 22, 24 August 2007 and A5 ASTER map for 12 Nov 2008 respectively. B1-B5; MODIS true color composite of band 1, 3 and 4. C1-C5 MODIS false color (7, 2, 1 band)

Flood inundation evaluation indices

Finally, CREST model simulated inundation spatial extents were compared to the flood inundation maps, derived from satellite imagery. Several categorical verification statistics, which measure the correspondence between the estimated and observed occurrence of events, were used in this study; Probability of Detection (POD), False Alarm Ratio (FAR), and Critical Success Index (CSI)., POD measures the fraction of observed events that were correctly diagnosed, and is also called the ‘‘hit rate’’ (Table 2). FAR gives the fraction of diagnosed events that were actually nonevents. CSI gives the overall fraction of correctly diagnosed events by CREST model. Perfect values for these scores are POD= 1, FAR= 0, and CSI= 1.

$$\mathbf{POD} = \frac{\mathbf{Hits}}{\mathbf{Hits} + \mathbf{Misses}}$$

$$\mathbf{FAR} = \frac{\mathbf{False\ alarms}}{\mathbf{Hits} + \mathbf{False\ alarms}}$$

$$\mathbf{CSI} = \frac{\mathbf{Hits}}{\mathbf{Hits} + \mathbf{Misses} + \mathbf{False\ alarms}}$$

CREST model is calibrated using MODIS based flood extent maps for different events listed in Table 2 for which gauged streamflow aobservation are

not available. As pointed out earlier the purpose of this exercise is to investigate the possibility to calibrate the hydrological model through satellite remote sensing datasets. Calibration period includes two cloud free MODIS images available in 2006 and 2007.Then we validate the calibration by comparing with other flood extent imagery. The objective function selected to guide the calibration process is the Critical Success Index CSI between satellite-based inundation maps and CREST-modeled flood extents. The calibration terminates when improvements in CSI within the last three iterations are less than 0.001. The approach can have far reaching implication in unguaged basins where no other means are available to calibrate hydrological model.

3.4 Results and Analysis

In this section we present the application of the two alternative methods for inundation mapping, namely CREST model based and satellite-based methods described in Section III, to generate the flood inundation maps for three different flood events in the study area (see Figure 3.4 and Table 3.1). The comparison of CREST-simulated flood extent with satellite-based observations will provide an evaluation of the model performance in simulation of spatio-temporal evolution of the flood inundation extent.

Unsupervised classification is an automatic and objective process that generates precise flooding maps. However, flood inundation mapping from the binary flood classification from optical sensors can be influenced by cloud and

vegetation cover. These lead to under detection or over detection due to the influence of riparian vegetation and the natural variability of the water surface respectively. Comparison between the CREST model and satellite based flood inundation extent for the three events listed in table 1 are discussed below:

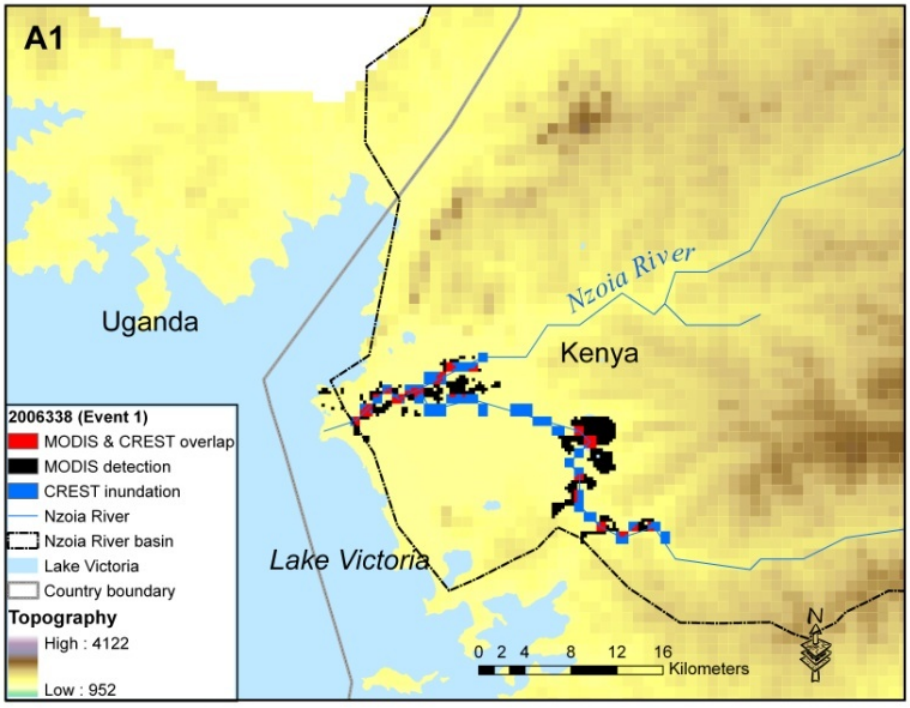

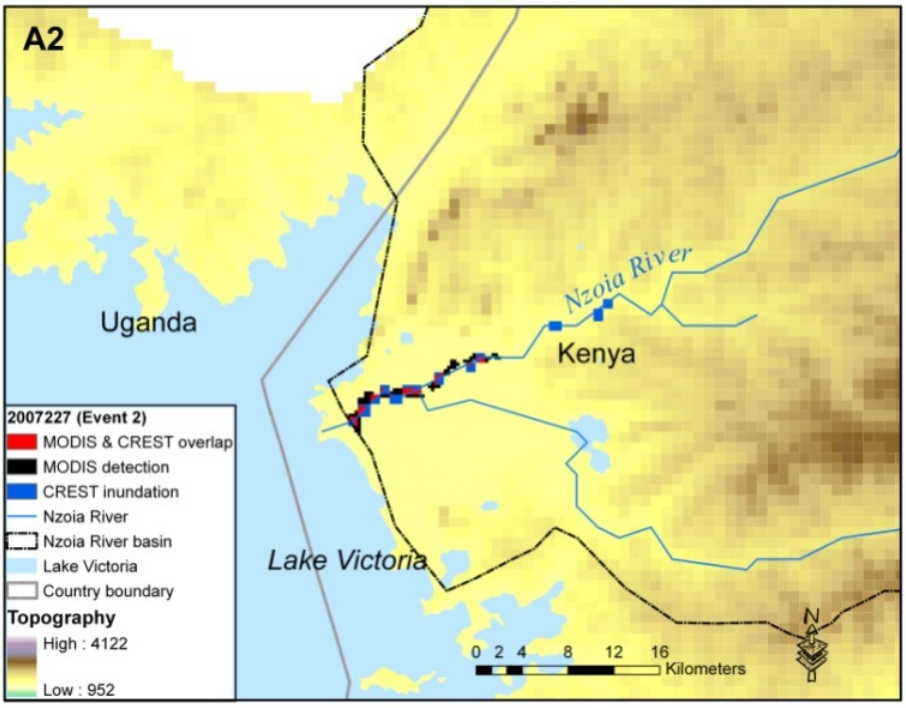
A2
Uganda
Nzoia River
Kenya
Lake Victoria
2007227 (Event 2)
MODIS & CREST overlap
MODIS detection
CREST inundation
Nzoia River
Nzoia River basin
Lake Victoria
Country boundary
Topography
High : 4122
Low : 952
0 2 4 8 12 16
Kilometers
N

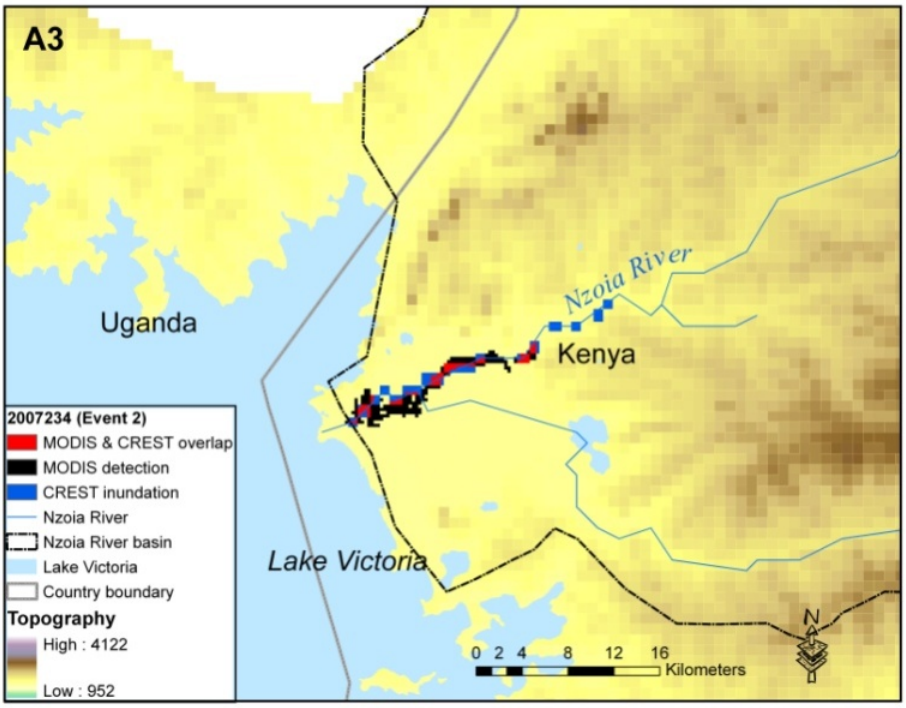
A3
Uganda
Nzoia River
Kenya
Lake Victoria
2007234 (Event 2)
MODIS & CREST overlap
MODIS detection
CREST inundation
Nzoia River
Nzoia River basin
Lake Victoria
Country boundary
Topography
High : 4122
Low : 952
0 2 4 8 12 16
Kilometers
N

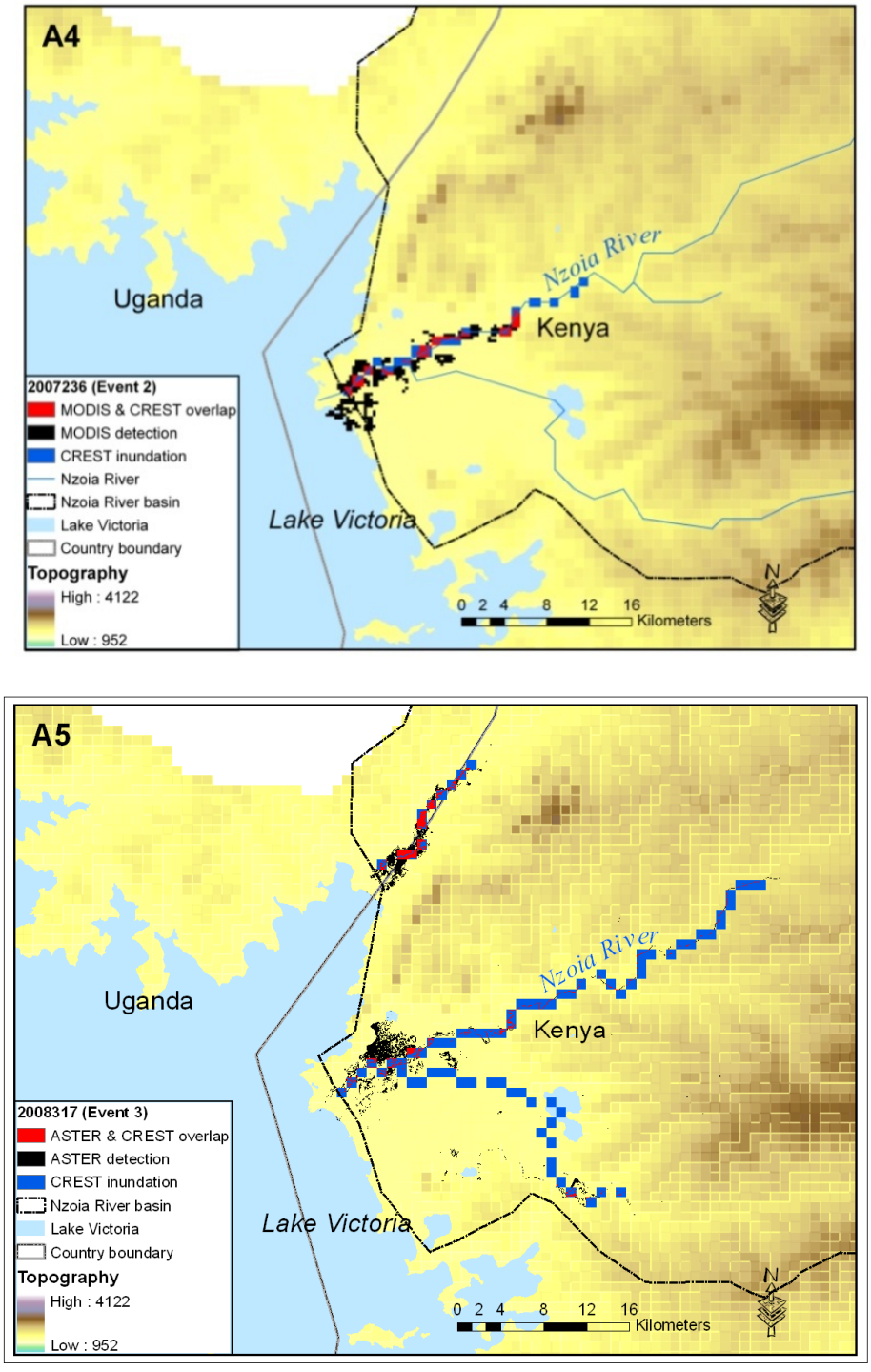

Figure 3.5: Comparison of satellite-based and CREST simulated flood inundation extents. First legend entry is the year and the Julian day of the flood event, followed by the event identification number (in Table 3.1).

Evaluation of the CREST-simulated inundation extent during Event 1

Figure 3.4 B1 and C1 illustrate true color composite and false color composite (bands 7, 2, 1) MODIS scenes respectively. After MODIS data acquisition for 04 December false color composite, the flood extent is extracted using the ISODATA classification (Figure 3.4 A1). The December event is also simulated using the hydrologic model. Inter comparison between the satellite based flood detection and CREST flood inundation map (Figure 3.5 A1). The regular river channel and water bodies are shown as light-blue, MODIS detections are in black and CREST in blue color. The overlapping flooded areas from MODIS and CREST are shown in red. Further examination of flood extents from the CREST and MODIS indicates that the spatial patterns of the flood extent are similar as illustrated in Figure 3.5 A1. To quantify this similarity, a spatial correlation is introduced and analyzed on a pixel-by-pixel basis. If a pixel is classified in the same category (regular river channel and water bodies, flooded area), on both inundation maps, the pixel is recoded as 1 (hits), otherwise non flooded areas as 0 (misses).

Figure 3.6 A1 shows the statistical comparison between the flood extents derived from MODIS and CREST for December 2006 event. POD shows an increase from 0.23 at a radius of 250 m to 0.75 at a radius of 1000 m and increased to 0.98 at a radius of 2000 m. Figure 3.6 A1 also illustrates that within 250 m radius, FAR could be as high as 0.7. However, with the increase of radius

to 1000m, FAR is reduced to low 0.18. The CSI is improved from 0.14 within 250 m to 0.64 with increase of radius to 1000m. With further increase in radius to 2000 m CSI is improved to 0.92. Thus, the two maps shows spatial agreement of 92% at a radius of 2000 m in Figure 3.6 A1.

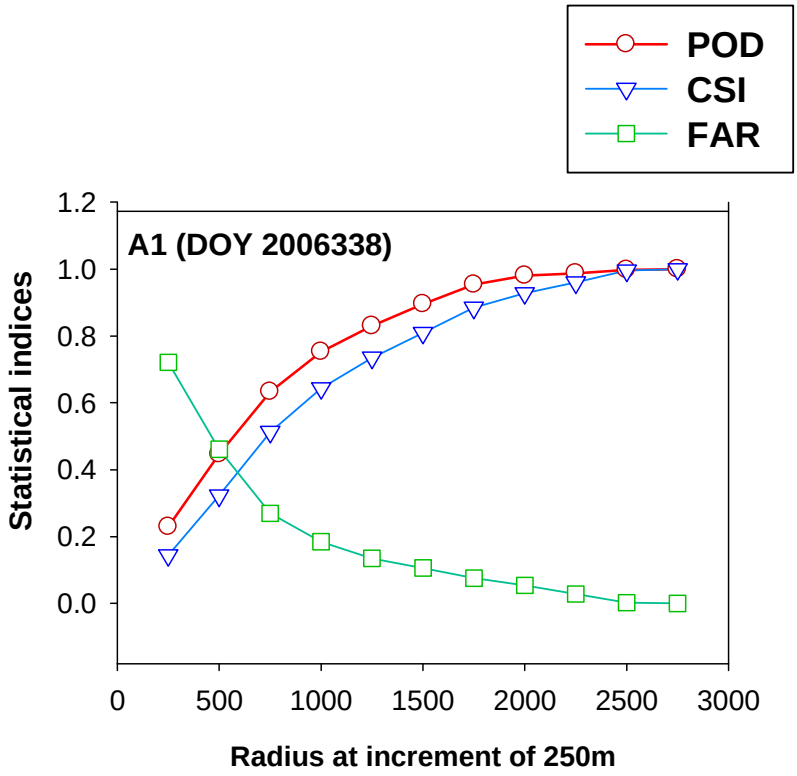

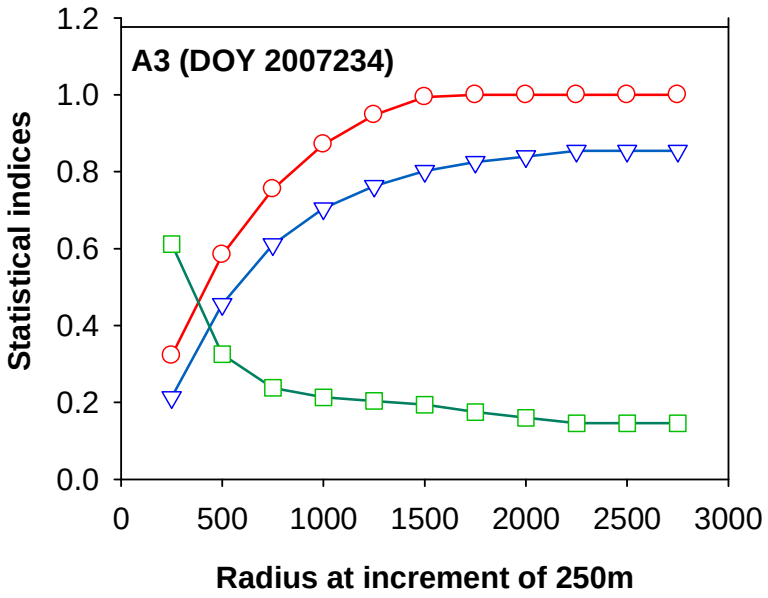

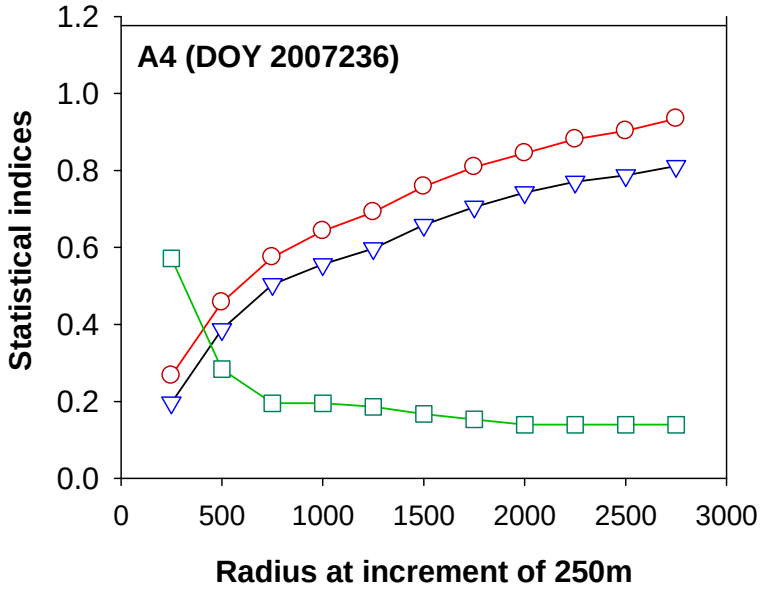

Figure 3.6: Comparison between estimated accuracy of products relative to the inundation area derived from MODIS (A1-A4) and CREST model.

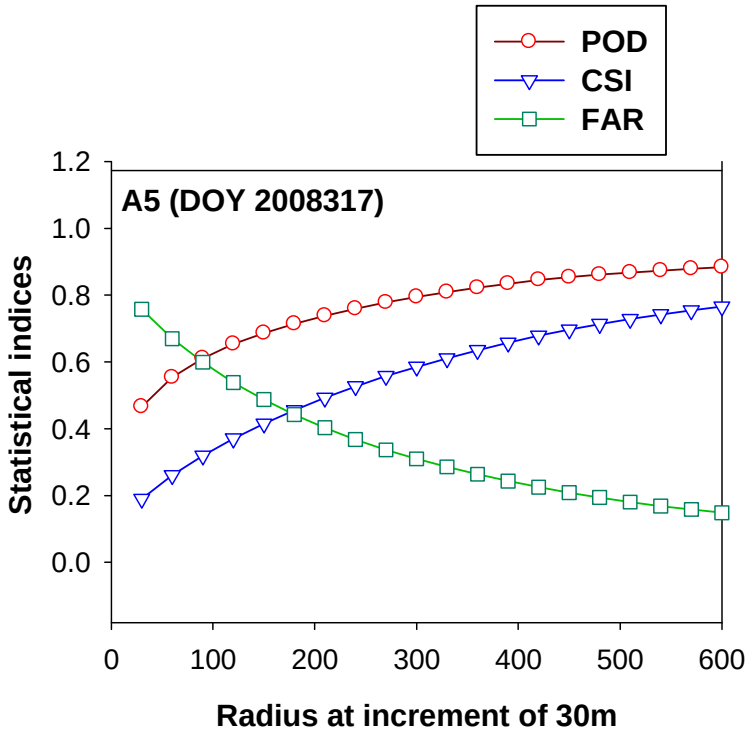

Figure 3.7: Comparison between estimated accuracy of products relative to the inundation area derived from ASTER and CREST model.

Evaluation of the CREST-simulated inundation extent during Event 2

A well-documented flood event that occurred during August 2007, with an estimated return period of 10 years, is used to validate CREST model performance. Figure 3.4 B2, B3, B4 and C2, C3, C4 show the true color composite and false color composite (bands 7,2,1) MODIS scenes respectively. MODIS-based flood extent maps shown in Figure 3 A2, A3 and A4 are derived from the false color composite scenes for 15 22 and 24 August 2007 respectively.

The statistical comparison between the CREST and MODIS flood inundation extent for these events are presented in Figure 3.6 A2, A3 and A4. Figure 3.6 A2 reveals that on the 15th August 2007 POD is increased from 0.37 to 0.93 with an increase of radius from 250m to 1000m. Similarly, FAR and CSI have showed improvements with increase in radius for other days of this event (Figure 3.6 A3 and A4).

Evaluation of the CREST-simulated inundation extent during Event 3

For the November 2008 event the ASTER image with higher spatial resolution are shown in Figure 3.7 A5. The POD of CREST shows an increase from 0.46 at a radius of 30m to 0.88 at a radius of 600m. Figure 3.7 A5 also illustrates that within 30 m radius, FAR could be as high as 0.75. However, with the increase of radius to 600m, FAR substantially reduced to as low as 0.15. The CSI is improved from 0.19 at 30 m to more than 0.76 at a radius of 600m.

3.5 Conclusion and Future Work

The feasibility to setup hydrological model using satellite-based flood inundation extents, instead of a conventional flood modeling techniques in data scarce environment is evaluated. The proposed approach implements a semi-distributed hydrologic model with remote sensing data and further calibrates the hydrologic model through satellite-based flood inundation maps. Utilizing the public domain datasets available through satellite sensors and their integration with the hydrologic models has the potential to improve simulation and prediction of the spatial extent of floods.

The broader impact of such technique is to provide a cost-effective tool to progressively build capacity for flood disaster prediction and risk reductions in poorly- or un-gauged basins located in many under developed countries in Africa or South Asia. Operationally implementing this strategy in those areas will provide flood managers and international aid organizations a realistic decision-support tool in order to better assess emerging flood impacts. This study demonstrated the applicability of distributed hydrological model calibration using satellite-derived flood inundation maps from MODIS and ASTER images in gauged basins.

The recent release of ASTER Global Digital Elevation Model (GDEM) with a resolution of 30m and higher temporal resolution (less than current TRMM 3-hour resolution) of satellite-based precipitation products can help to implement

hydrological models at higher resolutions. Thus, further research on how to utilize spatially distributed observations, such as higher resolution imagery and other sensors, such as microwave sensors, should be studied in various geographical locations for the evaluation and calibration of distributed hydrologic models. Further flood mapping accuracy is also expected to continuously improve the ISODATA clustering classifications. The case study of Nzoia basin illustrate that regions with scarce ground based observations, remote sensing data can be used to implement evaluate hydrologic models with certain accuracy. However, it noted that with the integration of different data sets i.e. satellite remote sensing products, ground based observations as well as the catchment information can improve the flood monitoring and management.

References

Adhikari, P., Y. Hong, K. R. Douglas, D. B. Kirschbaum, J. Gourley, R. Adler & G. Robert Brakenridge (2010) A digitized global flood inventory (1998–2008): compilation and preliminary results. *Natural Hazards***,** 1-18.

Alsdorf, D., D. Lettenmaier & C. Vörösmarty (2003) The need for global, satellite-based observations of terrestrial surface waters. *Eos Trans. AGU,* 84**,** 275–276.

Alsdorf, D., E. Rodríguez & D. Lettenmaier (2007a) Measuring surface water from space. *Reviews of Geophysics,* 45.

--- (2007b) Measuring surface water from space. *Reviews of Geophysics,* 45.

Artan, G., H. Gadain, J. Smith, K. Asante, C. Bandaragoda & J. Verdin (2007) Adequacy of satellite derived rainfall data for stream flow modeling. *Natural Hazards,* 43**,** 167-185.

Barton, I. J. & J. M. Bathols (1989) Monitoring floods with AVHRR. *Remote Sensing of Environment,* 30**,** 89-94.

Birkett, C. M., L. A. K. Mertes, T. Dunne, M. H. Costa & M. J. Jasinski (2002) Surface water dynamics in the Amazon Basin: Application of satellite radar altimetry. *Journal of Geophysical Research-Atmospheres,* 107.

Blasco, F., M. F. Bellan & M. U. Chaudhury (1992) Estimating the extent of floods in Bangladesh using SPOT data. *Remote Sensing of Environment,* 39**,** 167-178.

Brakenridge, G., E. Anderson, S. Nghiem, S. Caquard & T. Shabaneh. 2003a. Flood warnings, flood disaster assessments, and flood hazard reduction: the roles of orbital remote sensing. In *30th International Symposium on Remote Sensing of Environment,*. Honolulu, HI: Pasadena, CA: Jet Propulsion Laboratory, National Aeronautics and Space Administration, 2003.

Brakenridge, G., H. Carlos & E. Anderson. 2003b. Satellite gaging reaches: A strategy for MODIS-based river monitoring. 479–485.

Brakenridge, G. R., S. V. Nghiem, E. Anderson & R. Mic (2007) Orbital microwave measurement of river discharge and ice status. *Water Resources Research,* 43.

Brakenridge, R. 2006. MODIS-based flood detection, mapping and measurement: The potential for operational hydrological applications. In *Transboundary Floods: Reducing Risks Through Flood Management*, 1-12. Springer Verlag.

Brooks, S. H. (1958) A discussion of random methods for seeking maxima. *Operations Research,* 6**,** 244-251.

Calmant, S. & F. Seyler (2006) Continental surface waters from satellite altimetry. *Comptes Rendus Geosciences,* 338**,** 1113-1122.

Carpenter, T. M., J. A. Sperfslage, K. P. Georgakakos, T. Sweeney & D. L. Fread (1999) National threshold runoff estimation utilizing GIS in support of operational flash flood warning systems. *Journal of Hydrology,* 224**,** 21-44.

De Groeve, T. (2010) Flood monitoring and mapping using passive microwave remote sensing in Namibia. *Geomatics, Natural Hazards and Risk,* 1**,** 19 - 35.

Di Baldassarre, G., G. Schumann & P. D. Bates (2009) A technique for the calibration of hydraulic models using uncertain satellite observations of flood extent. *Journal of Hydrology,* 367**,** 276-282.

Entekhabi, D., E. Njoku, P. O'Neill, K. Kellogg, W. Crow, W. Edelstein, J. Entin, S. Goodman, T. Jackson & J. Johnson (2010) The Soil Moisture Active Passive (SMAP) Mission. *Proceedings of the IEEE,* 98**,** 704-716.

France, M. & P. Hedges. 1986. Hydrological Comparison of Landsat TM, Landsat MSS and Black & White Aerial Photography.

Friedl, M. A., D. K. McIver, J. C. F. Hodges, X. Y. Zhang, D. Muchoney, A. H. Strahler, C. E. Woodcock, S. Gopal, A. Schneider, A. Cooper, A. Baccini, F. Gao & C. Schaaf (2002) Global land cover mapping from MODIS: algorithms and early results. *Remote Sensing of Environment,* 83**,** 287-302.

Fujisada, H., F. Sakuma, A. Ono & M. Kudoh (1998) Design and preflight performance of ASTER instrument protoflight model. *IEEE Transactions on Geoscience and Remote Sensing,* 36**,** 1152-1160.

Gale, S. J. & S. Bainbridge (1990) The floods in eastern Australia. *Nature,* 345**,** 767-767.

Harris, A. & F. Hossain (2008) Investigating the optimal configuration of conceptual hydrologic models for satellite-rainfall-based flood prediction. *Geoscience and Remote Sensing Letters, IEEE,* 5**,** 532-536.

Hong, Y., R. Adler, F. Hossain, S. Curtis & G. Huffman (2007) A first approach to global runoff simulation using satellite rainfall estimation. *Water Resources Research,* 43**,** W08502.

Horritt, M. S. (2000) Calibration of a two-dimensional finite element flood flow model using satellite radar imagery. *Water Resources Research,* 36**,** 3279-3291.

Horritt, M. S. & P. D. Bates (2002) Evaluation of 1D and 2D numerical models for predicting river flood inundation. *Journal of Hydrology,* 268**,** 87-99.

Horritt, M. S., G. Di Baldassarre, P. D. Bates & A. Brath (2007) Comparing the performance of a 2-D finite element and a 2-D finite volume model of floodplain inundation using airborne SAR imagery. *Hydrological Processes,* 21**,** 2745-2759.

Huffman, G., D. Bolvin, E. Nelkin, D. Wolff, R. Adler, G. Gu, Y. Hong, K. Bowman & E. Stocker (2007a) The TRMM Multisatellite Precipitation Analysis (TMPA): Quasi-global, multiyear, combined-sensor precipitation estimates at fine scales. *Journal of Hydrometeorology,* 8**,** 38-55.

Huffman, G. J., R. F. Adler, D. T. Bolvin, G. J. Gu, E. J. Nelkin, K. P. Bowman, Y. Hong, E. F. Stocker & D. B. Wolff (2007b) The TRMM multisatellite precipitation analysis (TMPA): Quasi-global, multiyear, combined-sensor precipitation estimates at fine scales. *Journal of Hydrometeorology,* 8**,** 38-55.

Jensen, J. 2005. *Introductory digital image processing: a remote sensing perspective*. Prentice Hall PTR Upper Saddle River, NJ, USA.

Jensen, J. R., M. E. Hodgson, E. Christensen, H. E. Mackey, L. R. Tinney & R. Sharitz (1986) Remote-sensing inland wetlands - A multispectral approach. *Photogrammetric Engineering and Remote Sensing,* 52**,** 87-100.

Jonkman, S. N. (2005) Global perspectives on loss of human life caused by floods. *Natural Hazards,* 34**,** 151-175.

Khan, S. I., P. Adhikari, Y. Hong, H. Vergara, R. F Adler, F. Policelli, D. Irwin, T. Korme & L. Okello (2011a) Hydroclimatology of Lake Victoria region using hydrologic model and satellite remote sensing data. *Hydrol. Earth Syst. Sci.,* 15**,** 107-117.

Khan, S. I., Y. Hong, J. Wang, K. K. Yilmaz, J. J. Gourley, R. F. Adler, G. R. Brakenridge, F. Policelli, S. Habib & D. Irwin (2011b) Satellite Remote Sensing and Hydrologic Modeling for Flood Inundation Mapping in Lake Victoria Basin: Implications for Hydrologic Prediction in Ungauged Basins. *Geoscience and Remote Sensing, IEEE Transactions on,* 49**,** 85-95.

Kugler, Z. & T. De Groeve. 2007. The Global Flood Detection System. Office for Official Publications of the European Communities.

Lang, R. L., G. F. Shao, B. C. Pijanowski & R. L. Farnsworth (2008) Optimizing unsupervised classifications of remotely sensed imagery with a data-assisted labeling approach. *Computers & Geosciences,* 34**,** 1877-1885.

Lehner, B., K. Verdin & A. Jarvis (2008) New global hydrography derived from spaceborne elevation data. *Eos,* 89.

Marcus, W. & M. Fonstad (2008) Optical remote mapping of rivers at sub-meter resolutions and watershed extents. *Earth Surface Processes and Landforms,* 33**,** 4-24.

McCarthy, J. 2001. *Climate change 2001: impacts, adaptation, and vulnerability: contribution of Working Group II to the third assessment report of the Intergovernmental Panel on Climate Change*. Cambridge University Press.

Nash, J. E. & J. V. Sutcliffe (1970) River flow forecasting through conceptual models part I -- A discussion of principles. *Journal of Hydrology,* 10**,** 282-290.

Pelling, M., A. Maskrev, P. Ruiz & L. Hall (2004) Reducing disaster risk: a challenge for development. *UNDP global report. New York: United Nations Development Program*.

Pronzato, L., E. Walter, A. Venot & J. Lebruchec (1984) A general-purpose global optimizer: Implimentation and applications. *Mathematics and Computers in Simulation,* 26**,** 412-422.

Puech, C. & D. Raclot (2002) Using geographical information systems and aerial photographs to determine water levels during floods. *Hydrological Processes,* 16**,** 1593-1602.

Rabus, B., M. Eineder, A. Roth & R. Bamler (2003) The shuttle radar topography mission - a new class of digital elevation models acquired by spaceborne radar. *Isprs Journal of Photogrammetry and Remote Sensing,* 57**,** 241-262.

Rasid, H. & M. Pramanik (1993) Areal extent of the 1988 flood in Bangladesh: How much did the satellite imagery show? *Natural Hazards,* 8**,** 189-200.

Reed, S., J. Schaake & Z. Zhang (2007) A distributed hydrologic model and threshold frequency-based method for flash flood forecasting at ungauged locations. *Journal of Hydrology,* 337**,** 402-420.

Sandholt, I., L. Nyborg, B. Fog, M. Lô, O. Bocoum & K. Rasmussen (2003)

Remote sensing techniques for flood monitoring in the Senegal River Valley. *Geografisk Tidsskrift, Danish Journal of Geography,* 103**,** 71.

Schumann, G., P. Bates, M. Horritt, P. Matgen & F. Pappenberger (2009) Progress in integration of remote sensing–derived flood extent and stage data and hydraulic models. *Reviews of Geophysics,* 47.

Schumann, G., R. Hostache, C. Puech, L. Hoffmann, P. Matgen, F. Pappenberger & L. Pfister (2007) High-resolution 3-D flood information from radar imagery for flood hazard management. *IEEE Transactions on Geoscience and Remote Sensing,* 45**,** 1715-1725.

Shiklomanov, A., R. Lammers & C. Vorosmarty (2002) Widespread decline in hydrological monitoring threatens pan-Arctic research. *EOS Transactions,* 83**,** 13.

Sivapalan, M. (2003a) Prediction in ungauged basins: a grand challenge for theoretical hydrology. *Hydrological Processes,* 17**,** 3163-3170.

Sivapalan, M., K. Takeuchi, S. Franks, V. Gupta, H. Karambiri, V. Lakshmi, X. Liang, J. McDonnell, E. Mendiondo & P. O CONNELL (2003b) IAHS Decade on Predictions in Ungauged Basins (PUB), 2003–2012: Shaping an exciting future for the hydrological sciences/La décennie de l'AISH sur les prévisions en bassins non jaugés (PBNJ), 2003–2012: émergence d'un futur passionnant pour les sciences hydrologiques. *Hydrological Sciences Journal,* 48**,** 857-880.

Smith, E., G. Asrar, Y. Furuhama, A. Ginati, A. Mugnai, K. Nakamura, R. Adler, M.-D. Chou, M. Desbois, J. Durning, J. Entin, F. Einaudi, R. Ferraro, R. Guzzi, P. Houser, P. Hwang, T. Iguchi, P. Joe, R. Kakar, J. Kaye, M. Kojima, C. Kummerow, K.-S. Kuo, D. Lettenmaier, V. Levizzani, N. Lu, A. Mehta, C. Morales, P. Morel, T. Nakazawa, S. Neeck, K. i. Okamoto, R. Oki, G. Raju, J. Shepherd, J. Simpson, B. Sohn, E. Stocker, W.-K. Tao, J. Testud, G. Tripoli, E. Wood, S. Yang & W. Zhang. 2007. International Global Precipitation Measurement (GPM) Program and Mission: An Overview. In *Measuring Precipitation From Space,* eds. V. Levizzani, P. Bauer & F. J. Turk, 611-653. Springer Netherlands.

Smith, L. C. (1997) Satellite remote sensing of river inundation area, stage, and

discharge: A review. *Hydrological Processes,* 11**,** 1427-1439.

Stancalie, G., A. Diamandi, C. Corbus & S. Catana (2004) Application of EO data in flood fore-casting for the Crisuri Basin, Romania. *Flood Risk Management: Hazards, Vulnerability and Mitigation Measures***,** 101.

Stokstad, E. (1999) HYDROLOGY: Scarcity of Rain, Stream Gages Threatens Forecasts. *Science,* 285**,** 1199.

Su, F., Y. Hong & D. Lettenmaier (2008) Evaluation of TRMM multisatellite precipitation analysis (TMPA) and its utility in hydrologic prediction in the La Plata basin. *Journal of Hydrometeorology,* 9**,** 622-640.

Swenson, S. & J. Wahr (2009) Monitoring the water balance of Lake Victoria, East Africa, from space. *Journal of Hydrology,* 370**,** 163-176.

Wang, J., H. Yang, L. Li, J. J. Gourley, K. Sadiq I, K. K. Yilmaz, R. F. Adler, F. S. Policelli, S. Habib & D. Irwn (2011) The coupled routing and excess storage (CREST) distributed hydrological model. *Hydrological Sciences Journal,* 56**,** 84-98.

Wang, Y. (2004) Using Landsat 7 TM data acquired days after a flood event to delineate the maximum flood extent on a coastal floodplain. *International Journal of Remote Sensing,* 25**,** 959-974.

Wang, Y., J. D. Colby & K. A. Mulcahy (2002) An efficient method for mapping flood extent in a coastal floodplain using Landsat TM and DEM data. *International Journal of Remote Sensing,* 23**,** 3681-3696.

Watson, J. P. (1991) A visual interpretation of a LANDSAT mosaic of the Okavango-delta and surrounding area. *Remote Sensing of Environment,* 35**,** 1-9.

Xiao, Q. & W. Chen (1987) Songhua River ood monitoring with meteorological satellite imagery. *Remote Sensing Information***,** 37–41.

Yamaguchi, Y., A. B. Kahle, H. Tsu, T. Kawakami & M. Pniel (1998) Overview of Advanced Spaceborne Thermal Emission and Reflection Radiometer (ASTER). *IEEE Transactions on Geoscience and Remote Sensing,* 36**,** 1062-1071.

Yilmaz, K., R. Adler, Y. Tian, Y. Hong & H. Pierce (2010) Evaluation of a satellite-based global flood monitoring system. *International Journal of Remote Sensing,* 31**,** 3763-3782.

CHAPTER 4 : MICROWAVE SENSORS FOR FLOOD PREDICTION IN UNGUAGED BASIN (PUB)

Abstract

Operational flood forecasting is contingent on the availability of precipitation and river discharge, to benchmark hydrologic models and therefore, a challenge in data poor regions around the world. Lately, near real-time precipitation from Tropical Rainfall Measuring Mission (TRMM) has proved its tangible value for flood detection and monitoring, but not for forecasting. In this study, an unconventional flood monitoring framework is proposed by using TRMM precipitation forcing and more importantly, river discharge proxy from the Advanced Microwave Scanning Radiometer (AMSR-E) to benchmark a distributed hydrologic model in Okavango basin, Southern Africa. The AMSR-E passive microwave sensor based discharge signal, highly correlated with in-situ data at temporal correlation coefficient (CC) of 0.9, and is used from 2002 to 2007 to calibrate the hydrologic model.

The model simulated flows are converted to flood frequencies. Flood frequency analysis of continuous runoff data from model is used to estimate flood magnitude and return periods in frequency domain. Model performance was improved with a Nash–Sutcliffe Efficiency of 0.90 and CC of 0.80 respectively. It is concluded that satellite data from microwave sensors can be used to calibrated

hydrologic model in data poor environment. Given the globally availability of satellite-based precipitation and river discharges, this proof of concept study can have substantial implications on flood monitoring and forecasting in ungaged basins throughout the globe.

4.1 Introduction

Globally the sparse in-situ hydrometeorological networks are the main source for quantitative water resource management. Over the past half-century hydrologic analysis such as flood and drought risk assessments are dependent on these in-situ data. Hydrologic or land surface models are driven by streamflow and rainfall observations to predict hydrologic extremes. Therefore, adequate ground based observations on hydrologic variable plays a critical role in water resources planning and management. Unluckily, most areas of the Earth's surface lack in situ observations that intricate quantification of the water budget. Many nations are ungauged or sparsely gauged, and in some countries existing measurement networks are declining. (Calmant and Seyler 2006, Shiklomanov, Lammers and Vorosmarty 2002, Sivapalan 2003a, Stokstad 1999). Evidently, the lack or inadequate gauged observations challenges the implementation of hydrologic models for early warning and decision-making systems.

To address the limited data availability issue in ungauged regions, research efforts such as the Predictions in Ungauged Basins (PUB) initiative was launched in 2003 by the International Association of Hydrological Sciences. One of the PUB science questions is to integrate remote sensing data into hydrologic models (Sivapalan et al. 2003b). More recently, several efforts have been directed to use the widely available satellite remote sensing data to complement in-situ hydrologic data over vast ungauged regions. Various studies proposed the optimal use of satellite precipitation and other remote sensing data products for

flood forecasting (Harris and Hossain 2008, Hong et al. 2007, Yilmaz et al. 2010, Artan et al. 2007, Su, Hong and Lettenmaier 2008, Khan et al. 2011b). The advantage of these datasets is the global availability over regions where ground networks are nonexistent. In addition to satellite precipitation, efforts are underway to monitor change in river discharge remotely from space.

At present, unlike precipitation, river discharge cannot be estimated directly from the satellite sensors. Observable hydraulic variables such as water level, height, width, sinuosity and area are used to estimate river runoff. Recently, passive microwave sensors have been used to measured change in surface water flow as the bankfull river discharge. (Brakenridge et al. 2007) have globally detected floods using Advanced Microwave Scanning Radiometer (AMSR-E) brightness temperature at 36GHz H-polarization. This technique relates change in brightness temperature to the change in moisture in wet and dry pixel detected by the sensor. River flooding is detected using the emission model, polarization ratio and dielectric properties of different soil textures from wet and adjoining dry areas. This technique is used for flood detection and mapping but not for flood forecasting.

In this chapter, a novel framework is developed by integrating microwave satellite remote sensing and hydrologic modeling for flood early warning in data poor regions. The impetus is to use the AMSR-E brightness temperature based surface water change signal to calibrate a hydrologic model. This discharge is

the ratio of brightness temperatures of a wet pixel and dry pixel, refered to measurement (M) and calibration (C) area (Brakenridge et al. 2007), a proxy for river water surface change. This M/C ratio is operationally being used at global scale for flood detection by Dartmouth Flood Observatory, River Watch (Figure 4.1) and the Joint Research Centre (JRC) of the European Commission. (De Groeve 2010, Kugler and De Groeve 2007). It is proposed to employ this microwave sensor based discharge signal (M/C ratio) to calibrate a distributed hydrologic model for flood forecasting in ungauged basins.

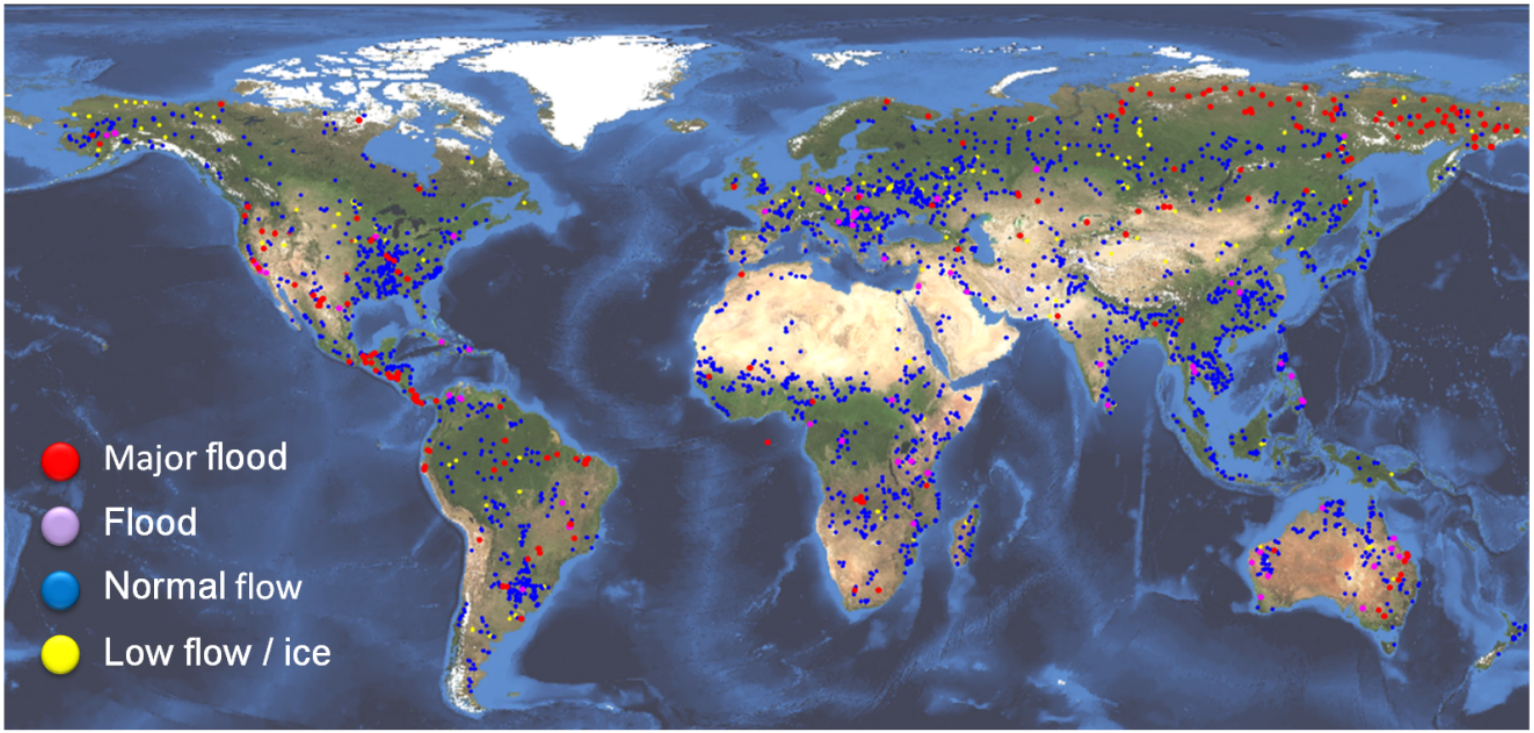

Figure 4.1: River Watch; satellite-based flood detection at more than 2500 selected river measurement sites. Flood detection for January 11, 2011. Source: Modified from http://floodobservatory.colorado.edu/.

4.2 Data and methods

An unconventional approach is developed by utilizing the passive microwave sensor based discharge signal instead of river runoff to calibrate a hydrologic model. A semi-distributed hydrologic model Coupled Excess Routing and Storage (CREST) (Wang et al. 2011, Khan et al. 2011b) computes the runoff generation and flow routing processes with a simple and robust structure. The model runs on a user specified time step and comprise of soil moisture storage and a flow routing routine. A breif summary of the model components are outlined here ; 1) data flow module based on cell to cell finite elements; 2) the three different layers within the soil profile that affect the maximum storage available in the soil layers. This representation within cell variability in soil moisture storage capacity and within cell routing can be employed for simulations at different spatiotemporal scales 3) coupling between the runoff generation and routing components via feedback mechanisms.

The key forcing datasets for CREST model are the satellite precipitation product from the TRMM Multi Satellite Precipitation Analysis (TMPA) (Huffman et al. 2007a) and the evapotranspiration from the Famine Early Warning Systems Network (FEWS NET), (http://earlywarning.usgs.gov/fews/global/index.php). Digital Elevation processed from the Shuttle Radar Topography Mission (SRTM) (Rabus et al., 2003) is used to generate flow direction, flow accumulation, and contributing basin area.

CREST model is calibrated using an auto-calibration technique based on the Adaptive Random Search (ARS) method (Pronzato et al. 1984, Brooks 1958). The model is implemented in the upper part of Okavango basin in Southern Africa (Figure 4.2), is representative for many poorly and ungauged basin throughout the world. Okavango River flows through Angola, Namibia and Botswana, with the main runoff generation part from Angola. River discharge and stage data are used from Rundu telemetry station located on the main Okavango River (Figure 4.2).

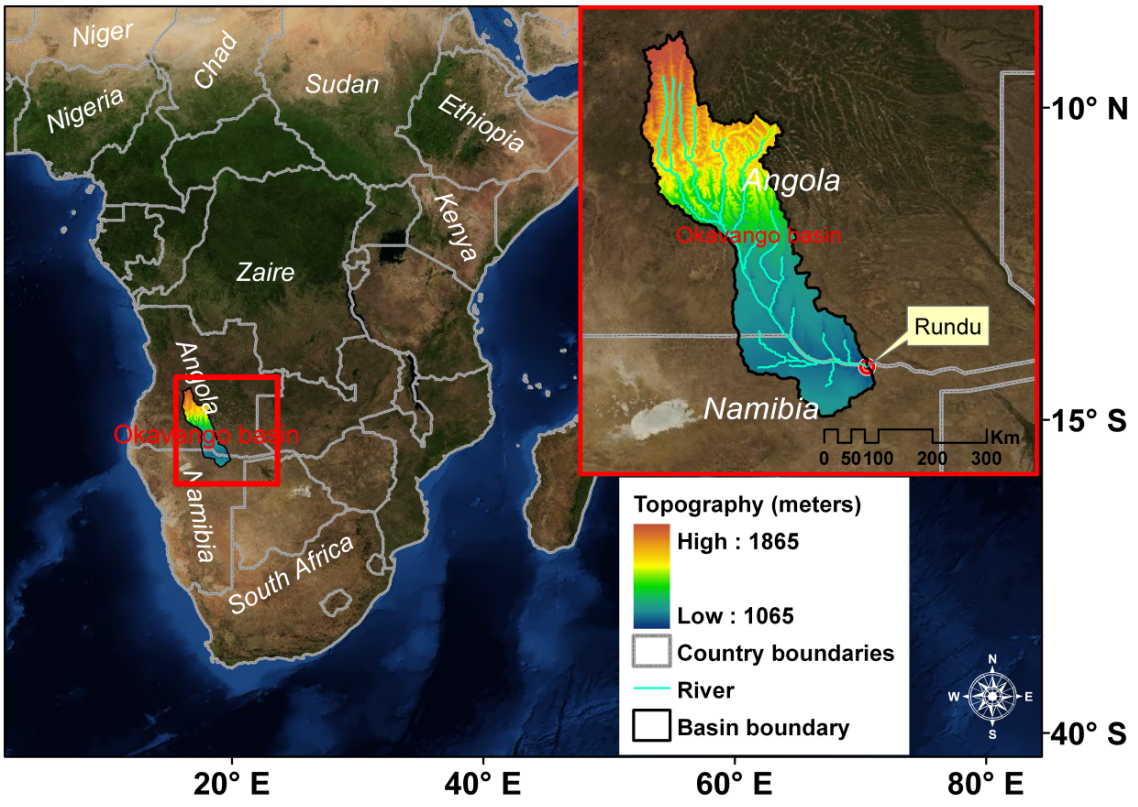

Figure 4.2: Upper Okavango basin with Okavango River spanning Angola and Namibia. Location of gauging station at Rundu, Namibia.

4.3 Satellite based flood frequency approach

Satellite based surface water change signal is supplemented with the sparse gauge runoff observations to calibrate hydrologic model. The attractive feature of this technique is the continuous accounting for flood forecasting can make difference in data poor environment. This technique will reduce the dependency on gauged runoff and precipitation data to calibrate hydrologic models. Moreover, typically models are calibrated at point location in the watershed, in contrast the geo-spatio-temporal passive microwave data allows to implement this strategy throughout the river reach.

The satellite-based discharge signal correlated closely with a correlation coefficient (CC) of 0.9, with the observed runoff over the period from 2002 to 2007 at Rundu in Namibia. The satellite based discharge signal (M/C ratio) were able to capture high flow peaks per year, however discharge estimates are not very accurate during the low flows (Figure 4. 3). For comparison purpose CREST model is calibrated with gauge runoff from 2002 to 2005. The correspondence between observed and simulated flows were evaluated using the Nash–Sutcliffe Efficiency (NSE) (Nash and Sutcliffe 1970) and CC.

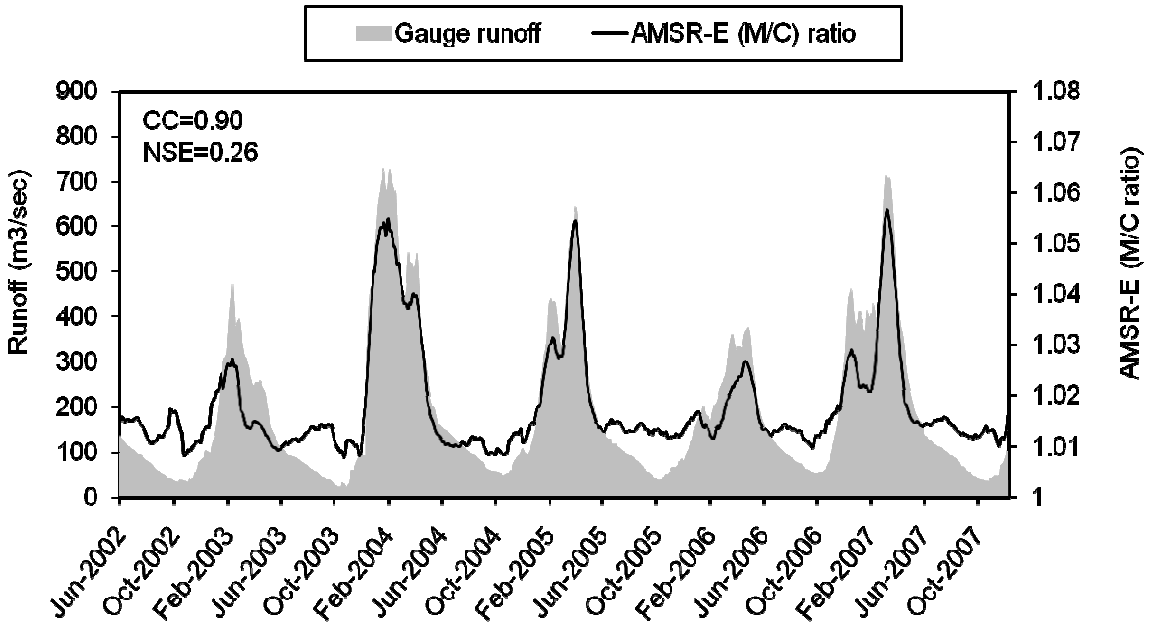

Figure 4.3: Time series of AMSR-E sensor based discharge signal (M/C ratio) in (black line) and gauged runoff in (shaded area).

Evaluation indices CREST simulation performance is assessed using three commonly-used statistical indices. First, for statistical goodness of fit of simulated flows, we utilized the Nash-Sutcliffe coefficient of efficiency described earlier in Chapter II. Second, the Pearson Correlation Coefficient (CC), equation (8) is used to assess the agreement between simulated and observed discharge as follows:

$$\mathrm{CC} = \frac{\sum\left(Q_{i,o} - \overline{Q_o}\right)\left(Q_{i,s} - \overline{Q_s}\right)}{\sqrt{\sum\left(Q_{i,o} - \overline{Q_o}\right)^2 \sum\left(Q_{i,s} - \overline{Q_s}\right)^2}} \tag{8}$$

Where, where, $Q_{i,o}$ is the observed discharge of the i^{th} time step. $Q_{i,s}$ is the simulated discharge of the i^{th} time step. $\overline{Q_o}$ is average of all the observed discharge values. $\overline{Q_S}$ is the average of all daily simulated discharge values.

The hydrologic model performed acceptable for the high flows than low flows, with a NSE of 0.63 and 0.84 CC (Figure 4.4a). The simulated low flows are biased relative to the observed data. However, the focus of this study is on high peak flows, therefore, CREST model is calibrated within frequency domain to forecast the high flows regimes.

This flood frequency based approach requires the conversion of model

simulated and observed flows to daily exceedance frequencies. Streamflow and satellite based discharge signal (M/C ratio) are converted to frequencies by computing the daily exceedance frequency (or probability) based on the period-of-data flow exceedance curve (or flow duration curve). In this way, frequencies associated to simulated streamflow from CREST can be compared to those computed from M/C ratio for calibrating model parameters.

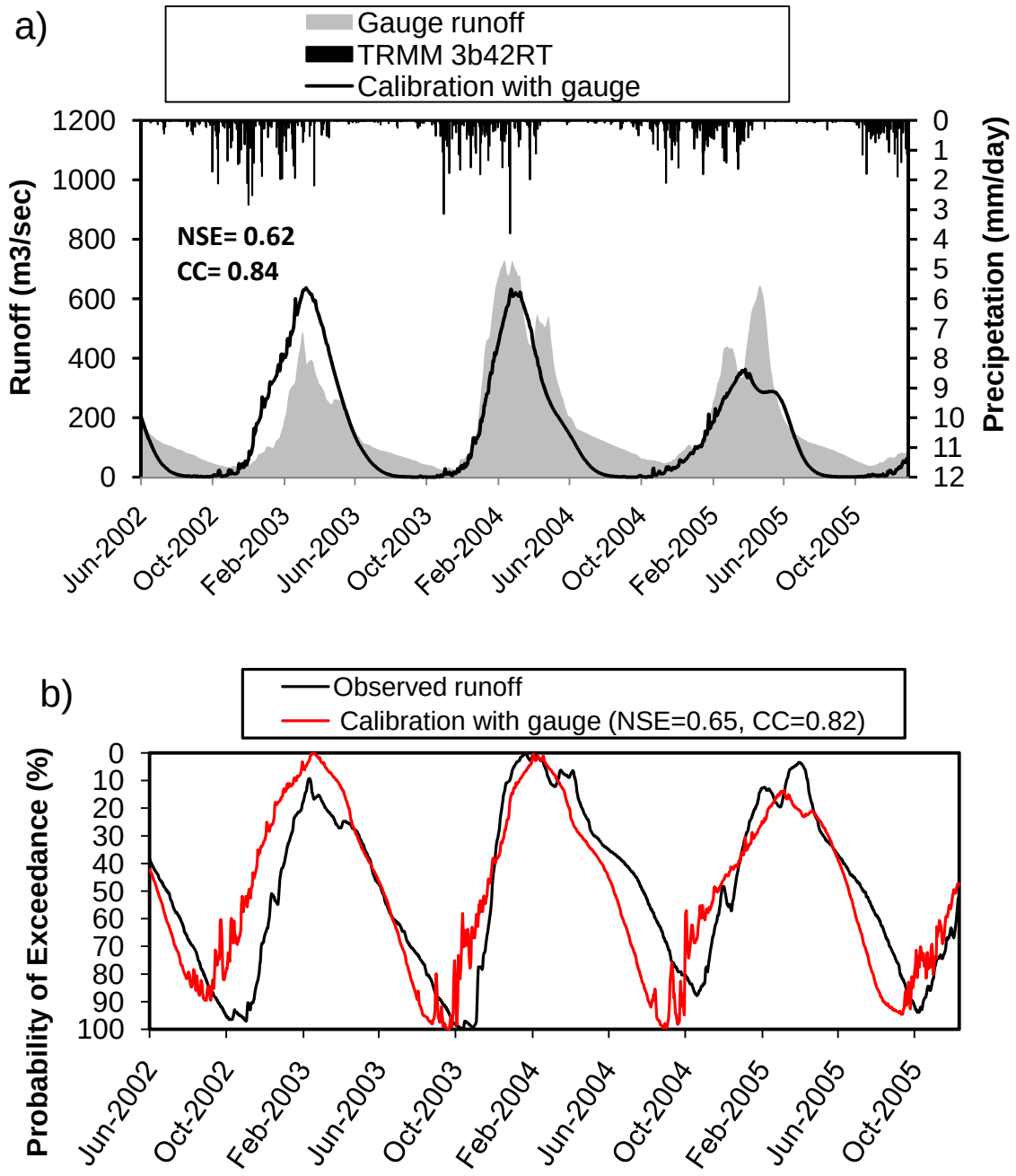

Figure 4.4: a) Hydrograph showing CREST simulation with gauge (solid line), gauge observations (shaded area) and TRMM precipitation (inverted bars). b) CREST simulation with gauge (dashed line) and observed runoff (solid line) in frequency domain.

To implement the approach, CREST model simulated flows are converted to flood frequencies. Flood frequency analysis of continuous runoff data from model is used to estimate flood magnitude and return periods. The application of distributed hydrologic model for flood frequency analysis can improve the accuracy of flood forecast in ungauged basins. (Reed, Schaake and Zhang 2007, Carpenter et al. 1999). The satellite based discharge signal were used to calibrate and validate the CREST model in frequency domain over the period from 2002-2007.

Results reported in Figure 4.5a in frequency domain shows, a good agreement between the satellite based discharge signal and the observed flood peaks. CREST model calibrated with M/C ratio showed skill in ranking events with NSE of 0.90 and 0.80 CC. The hydrologic model calibration accurately tracked the high flows. The exceedance level indicates that the model can predicts forthcoming flooding in the forecasts. It follows that there is also close agreement between the frequency distributions fitted to the observed and simulated peaks, suggesting that the corresponding parameter sets are useful for the simulation of flood frequency characteristic. Model simulations for the validation period also produced reliable results for the flooding events (Figure 4.4b). Figure 4.4c illustrates further the threshold frequency corresponding to a 2-6 years return period and therefore can have significant added value for an operational flood forecasting system.

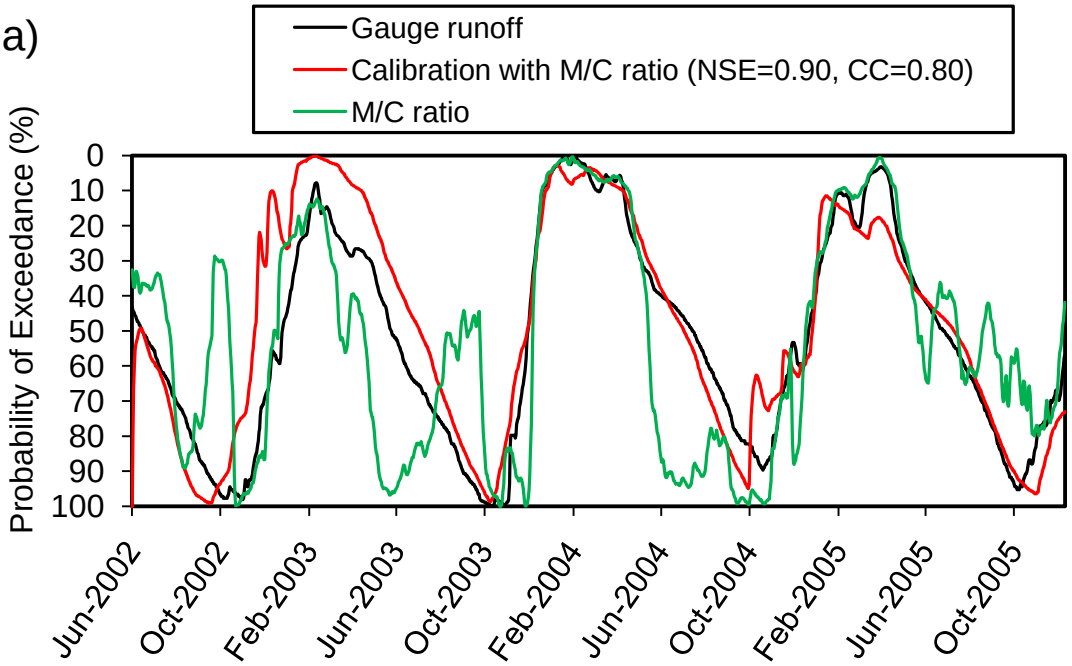
a)
Gauge runoff
Calibration with M/C ratio (NSE=0.90, CC=0.80)
M/C ratio
Probability of Exceedance (%)
0
10
20
30
40
50
60
70
80
90
100
Jun-2002
Oct-2002
Feb-2003
Jun-2003
Oct-2003
Feb-2004
Jun-2004
Oct-2004
Feb-2005
Jun-2005
Oct-2005

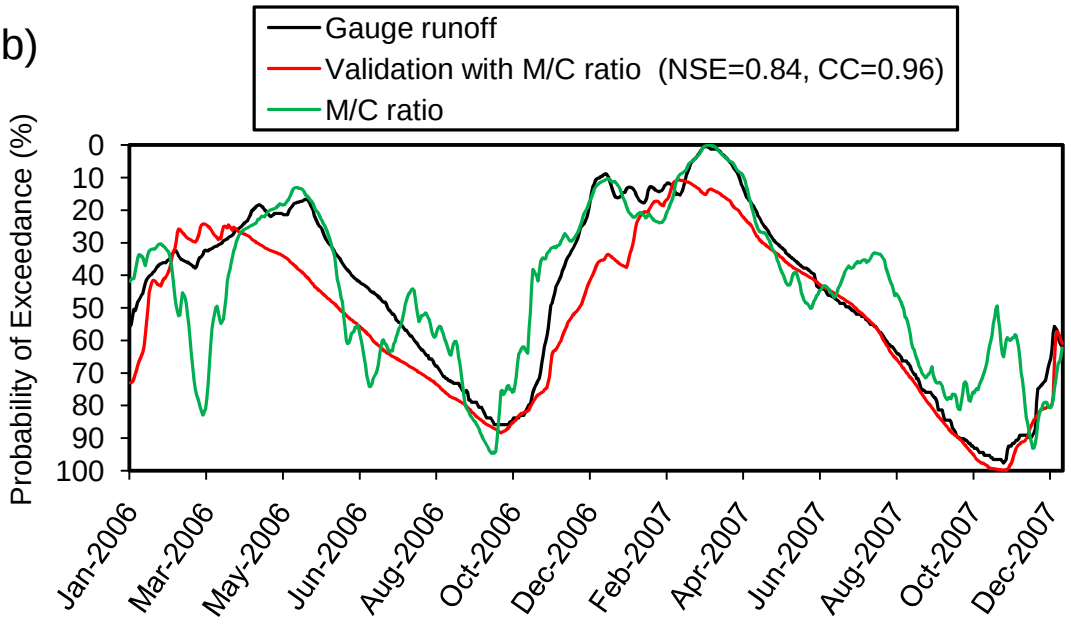
b)
Gauge runoff
Validation with M/C ratio (NSE=0.84, CC=0.96)
M/C ratio
Probability of Exceedance (%)
0
10
20
30
40
50
60
70
80
90
100
Jan-2006
Mar-2006
May-2006
Jun-2006
Aug-2006
Oct-2006
Dec-2006
Feb-2007
Apr-2007
Jun-2007
Aug-2007
Oct-2007
Dec-2007

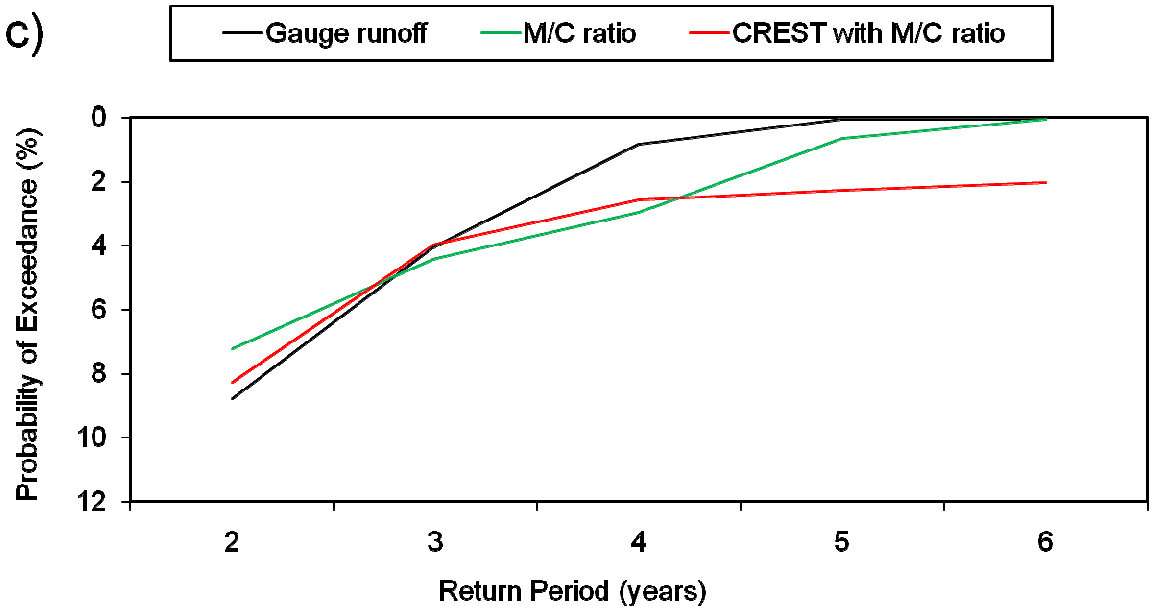

Figure 4.5: Exceedance probabilities; a) CREST simulation with M/C ratio (red line) and observed runoff (black line) and M/C ratio (green line) for calibration period (2002-2005). b) Model simulations for validation period (2006-2007) c) return period.

4.4 Discussion

One way of risk analysis is to look at impacts from previous hazardous events. The physical exposure can be obtained by modeling the area extent affected by one event. The frequency is computed by counting the number of events for the given area divided by the number of years of observation (in order to achieve an average frequency per year). Using the area affected, the number of exposed population can be extracted using a Geographical Information System (GIS), the population affected multiplied by the frequency provides the physical exposure.

The study results herein suggest that the calibrated hydrologic model provides acceptable hydrograph simulations and also provide acceptable estimates of the frequency characteristics of the flood peaks. Additionally, the globally available information with a relatively high resolution in both space and time can be useful in regions with limited or no data. The methodology presented here should provide enough lead time for flood warnings and mitigations measures. This information may be applicable to other catchments using appropriate choices of rainfall runoff models.

This proof of concept study has demonstrated the efficacy of satellite remote sensing data for flood forecasting in poorly and ungauged basins. In particular, a semi-distributed rainfall-runoff model calibrated with unconventional data can implicitly simulate the varying runoff response for a given rainfall event.

Contrary to the traditional data types that represent point measurements, passive microwave based flood evolution at the pixel level. This spatially continuous and daily data can be used to implement distributed hydrological models. This approach utilized the passive microwave sensor based discharge signal to calibrate hydrologic model parameters can provide enhanced streamflow forecasts in ungauged basins.

4.5 Advances in Remote Sensing Hydrology

In the next coming decades natural hazards mitigation, global change research, weather forecasting and decision-making will rely on earth observing satellites. Therefore, in this section a brief description on some of the future satellite mission is provided. Sensors aboard these satellites will offer hydrologic and other environmental observations. Some of the main satellite missions and the hydrologic applications are discussed briefly.

The Global Precipitation Measurement (GPM) Mission

The Global Precipitation Measurement (GPM) mission is an international initiative and a follow on to the TRMM. The two main sensors on the GPM Core are the, the GPM Microwave Imager (GMI), and the Dual frequency Precipitation Radar (DPR). The GMI will be a conical-scan, nine channel passive microwave radiometer. The configuration of this instrument provides a broad measurement swath (850 km), and like the TMI, maintains a constant earth incidence angle of

52.8° and a constant footprint size for each measurement channel regardless of scan position. The Dual-frequency Precipitation Radar (DPR) will provide high resolution (approximately 4-km), high precision measurements of rainfall, rainfall processes, and cloud dynamics (Smith et al. 2007). GPM mission promises new possibilities for flood forecast with the advent of precipitation products with higher quality and spatio-temporal resolution down to hour and 4-km respectively.

Soil Moisture, Active and Passive (SMAP) Mission

Spatially distributed soil moisture measurements and freeze/thaw states are needed to improve our understanding of regional and global water cycles. Soil Moisture Active and Passive (SMAP) mission (Entekhabi et al. 2010) is one of four first-tier missions recommended by the NRC Earth Science Decadal Survey Report. SMAP will provide global views of Earth's soil moisture and surface freeze/thaw state, introducing a new era in hydrologic applications and providing unprecedented capabilities to investigate the cycling of water, energy and carbon over global land surfaces.

The main goal of SMAP is to provide estimates of soil moisture in the top 5 cm of soil with an accuracy of 0.04 cm3/cm3 volumetric soil moisture, at 10 km resolution, with 3-day average intervals over the global land area. (Entekhabi et al. 2010, Das, Entekhabi and Njoku In press). Moreover, these estimates are also helpful in understanding terrestrial ecosystems, and the processes that interlink the water, energy, and carbon cycles.

Soil moisture and freeze/thaw information provided by SMAP will lead to improved weather forecasts, flood and drought forecasts, and predictions of agricultural productivity and climate change. This mission will contribute to the goals of the Carbon Cycle and Ecosystems, Weather, and Climate Variability and Change Earth Science focus areas as well as to hydrological science.

Surface Water and Ocean Topography (SWOT) Mission

Surface Water and Ocean Topography (SWOT) is one of the recommended mission during the decadal survey committee for launch during 2020. It will provide observations on lake and river water levels for inland water dynamics (Alsdorf, Rodríguez and Lettenmaier 2007). The core technology in SWOT mission is the wide swath Ka-band and C-band radar radar interferometer (KaRIN), which would achieve spatial resolution on the order of tens of meters The mission will measure water surface elevations, water surface slope, and the areal extent of lakes, wetlands, reservoirs, floodplains, and rivers at global scale. Many of the limitations of current generation altimeters with respect to the size of surface water bodies measured and revisit times will be relaxed by the planned SWOT mission (Alsdorf and Lettenmaier, 2003; Alsdorf et al., 2007). The planned SWOT satellite mission is designed to infer river discharges from remotely sensed river hydrologic characteristics. SWOT will provide highly accurate river surface slope estimates, in addition to information about water surface elevations and inundated areas for rivers with widths greater than about

100 m (Alsdorf, Lettenmaier and Vörösmarty 2003). Exploratory results for this strategy using synthetic data have been encouraging (Lee et al., 2008). Earth scientists and other researchers are optimistic about the SWOT missions and its application in hydrologic science and water resource management throughout the globe.

References

Alsdorf, D., D. Lettenmaier & C. Vörösmarty (2003) The need for global, satellite-based observations of terrestrial surface waters. *Eos Trans*. AGU, 84, 275–276.

Alsdorf, D., E. Rodríguez & D. Lettenmaier (2007) Measuring surface water from space. *Reviews of Geophysics,* 45.

Artan, G., H. Gadain, J. Smith, K. Asante, C. Bandaragoda & J. Verdin (2007) Adequacy of satellite derived rainfall data for stream flow modeling. *Natural Hazards*, 43, 167-185.

Barton, I. J. & J. M. Bathols (1989) Monitoring floods with AVHRR. Remote Sensing of Environment, 30, 89-94.

Birkett, C. M., L. A. K. Mertes, T. Dunne, M. H. Costa & M. J. Jasinski (2002) Surface water dynamics in the Amazon Basin: Application of satellite radar altimetry. *Journal of Geophysical Research-Atmospheres*, 107.

Blasco, F., M. F. Bellan & M. U. Chaudhury (1992) Estimating the extent of floods in Bangladesh using SPOT data. *Remote Sensing of Environment*, 39, 167-178.

Brakenridge, G., E. Anderson, S. Nghiem, S. Caquard & T. Shabaneh. 2003a. Flood warnings, flood disaster assessments, and flood hazard reduction: the roles of orbital remote sensing. In 30th International Symposium on Remote Sensing of Environment,. Honolulu, HI: Pasadena, CA: Jet Propulsion Laboratory, National Aeronautics and Space Administration, 2003.

Brakenridge, G., H. Carlos & E. Anderson. 2003b. Satellite gaging reaches: A strategy for MODIS-based river monitoring. 479–485.

Brakenridge, G. R., S. V. Nghiem, E. Anderson & R. Mic (2007) Orbital microwave measurement of river discharge and ice status. *Water Resources Research,* 43.

Brakenridge, R. 2006. MODIS-based flood detection, mapping and measurement: The potential for operational hydrological applications. In Transboundary Floods: Reducing Risks Through Flood Management, 1-12. Springer Verlag.

Brooks, S. H. (1958) A discussion of random methods for seeking maxima. Operations Research, 6, 244-251.

Calmant, S. & F. Seyler (2006) Continental surface waters from satellite altimetry. Comptes Rendus Geosciences, 338, 1113-1122.

Carpenter, T. M., J. A. Sperfslage, K. P. Georgakakos, T. Sweeney & D. L. Fread (1999) National threshold runoff estimation utilizing GIS in support of operational flash flood warning systems. Journal of Hydrology, 224, 21-44.

De Groeve, T. (2010) Flood monitoring and mapping using passive microwave remote sensing in Namibia. *Geomatics, Natural Hazards and Risk*, 1, 19 - 35.

Di Baldassarre, G., G. Schumann & P. D. Bates (2009) A technique for the calibration of hydraulic models using uncertain satellite observations of flood extent. *Journal of Hydrology*, 367, 276-282.

Entekhabi, D., E. Njoku, P. O'Neill, K. Kellogg, W. Crow, W. Edelstein, J. Entin, S. Goodman, T. Jackson & J. Johnson (2010) The Soil Moisture Active Passive (SMAP) Mission*. Proceedings of the IEEE*, 98, 704-716.

France, M. & P. Hedges. 1986. Hydrological Comparison of Landsat TM, Landsat MSS and Black & White Aerial Photography.

Friedl, M. A., D. K. McIver, J. C. F. Hodges, X. Y. Zhang, D. Muchoney, A. H. Strahler, C. E. Woodcock, S. Gopal, A. Schneider, A. Cooper, A. Baccini, F. Gao & C. Schaaf (2002) Global land cover mapping from MODIS: algorithms and early results. *Remote Sensing of Environment*, 83, 287-302.

Fujisada, H., F. Sakuma, A. Ono & M. Kudoh (1998) Design and preflight performance of ASTER instrument protoflight model. *IEEE Transactions on Geoscience and Remote Sensing*, 36, 1152-1160.

Gale, S. J. & S. Bainbridge (1990) The floods in eastern Australia. *Nature,* 345, 767-767.

Harris, A. & F. Hossain (2008) Investigating the optimal configuration of conceptual hydrologic models for satellite-rainfall-based flood prediction. *Geoscience and Remote Sensing Letters, IEEE*, 5, 532-536.

Hong, Y., R. Adler, F. Hossain, S. Curtis & G. Huffman (2007) A first approach to global runoff simulation using satellite rainfall estimation. *Water Resources Research*, 43, W08502.

Horritt, M. S. (2000) Calibration of a two-dimensional finite element flood flow model using satellite radar imagery. *Water Resources Research*, 36, 3279-3291.

Horritt, M. S. & P. D. Bates (2002) Evaluation of 1D and 2D numerical models for predicting river flood inundation. *Journal of Hydrology*, 268, 87-99.

Horritt, M. S., G. Di Baldassarre, P. D. Bates & A. Brath (2007) Comparing the performance of a 2-D finite element and a 2-D finite volume model of floodplain inundation using airborne SAR imagery. *Hydrological Processes*, 21, 2745-2759.

Huffman, G., D. Bolvin, E. Nelkin, D. Wolff, R. Adler, G. Gu, Y. Hong, K. Bowman & E. Stocker (2007a) The TRMM Multisatellite Precipitation Analysis (TMPA): Quasi-global, multiyear, combined-sensor precipitation estimates at fine scales. *Journal of Hydrometeorology*, 8, 38-55.

Huffman, G. J., R. F. Adler, D. T. Bolvin, G. J. Gu, E. J. Nelkin, K. P. Bowman, Y. Hong, E. F. Stocker & D. B. Wolff (2007b) The TRMM multisatellite precipitation analysis (TMPA): Quasi-global, multiyear, combined-sensor precipitation estimates at fine scales. *Journal of Hydrometeorology*, 8, 38-55.

Jensen, J. 2005. Introductory digital image processing: a remote sensing perspective. Prentice Hall PTR Upper Saddle River, NJ, USA.

Jensen, J. R., M. E. Hodgson, E. Christensen, H. E. Mackey, L. R. Tinney & R. Sharitz (1986) Remote-sensing inland wetlands - A multispectral approach. *Photogrammetric Engineering and Remote Sensing*, 52, 87-100.

Jonkman, S. N. (2005) Global perspectives on loss of human life caused by floods. *Natural Hazards*, 34, 151-175.

Khan, S. I., Y. Hong, J. Wang, K. K. Yilmaz, J. J. Gourley, R. F. Adler, G. R. Brakenridge, F. Policelli, S. Habib & D. Irwin (2011) Satellite Remote Sensing and Hydrologic Modeling for Flood Inundation Mapping in Lake Victoria Basin: Implications for Hydrologic Prediction in Ungauged Basins. *IEEE Transactions on Geoscience and Remote Sensing,* 49, 85-95.

Kugler, Z. & T. De Groeve. 2007. The Global Flood Detection System. Office for Official Publications of the European Communities.

Lang, R. L., G. F. Shao, B. C. Pijanowski & R. L. Farnsworth (2008) Optimizing unsupervised classifications of remotely sensed imagery with a data-assisted labeling approach. *Computers & Geosciences*, 34, 1877-1885.

Lehner, B., K. Verdin & A. Jarvis (2008) New global hydrography derived from spaceborne elevation data. *Eos Transactions*,, 89.

Marcus, W. & M. Fonstad (2008) Optical remote mapping of rivers at sub-meter resolutions and watershed extents. *Earth Surface Processes and Landforms*, 33, 4-24.

McCarthy, J. 2001. Climate change 2001: impacts, adaptation, and vulnerability: contribution of Working Group II to the third assessment report of the Intergovernmental Panel on Climate Change. Cambridge University Press.

Nash, J. E. & J. V. Sutcliffe (1970) River flow forecasting through conceptual models part I -- A discussion of principles. *Journal of Hydrology*, 10, 282-290.

Pronzato, L., E. Walter, A. Venot & J. Lebruchec (1984) A general-purpose global optimizer: Implimentation and applications. Mathematics and Computers in Simulation, 26, 412-422.

Puech, C. & D. Raclot (2002) Using geographical information systems and aerial photographs to determine water levels during floods. *Hydrological Processes*, 16, 1593-1602.

Rabus, B., M. Eineder, A. Roth & R. Bamler (2003) The shuttle radar topography mission - a new class of digital elevation models acquired by spaceborne radar. Isprs *Journal of Photogrammetry and Remote Sensing*, 57, 241-262.

Rasid, H. & M. Pramanik (1993) Areal extent of the 1988 flood in Bangladesh: How much did the satellite imagery show? Natural Hazards, 8, 189-200.

Reed, S., J. Schaake & Z. Zhang (2007) A distributed hydrologic model and threshold frequency-based method for flash flood forecasting at ungauged locations. *Journal of Hydrology*, 337, 402-420.

Sandholt, I., L. Nyborg, B. Fog, M. Lô, O. Bocoum & K. Rasmussen (2003) Remote sensing techniques for flood monitoring in the Senegal River Valley. Geografisk Tidsskrift, *Danish Journal of Geography*, 103, 71.

Schumann, G., P. Bates, M. Horritt, P. Matgen & F. Pappenberger (2009) Progress in integration of remote sensing–derived flood extent and stage data and hydraulic models. *Reviews of Geophysics*, 47.

Schumann, G., R. Hostache, C. Puech, L. Hoffmann, P. Matgen, F. Pappenberger & L. Pfister (2007) High-resolution 3-D flood information from radar imagery for flood hazard management. *IEEE Transactions on Geoscience and Remote Sensing*, 45, 1715-1725.

Shiklomanov, A., R. Lammers & C. Vorosmarty (2002) Widespread decline in hydrological monitoring threatens pan-Arctic research. *EOS Transactions*, 83, 13.

Sivapalan, M. (2003a) Prediction in ungauged basins: a grand challenge for theoretical hydrology. *Hydrological Processes*, 17, 3163-3170.

Sivapalan, M., K. Takeuchi, S. Franks, V. Gupta, H. Karambiri, V. Lakshmi, X. Liang, J. McDonnell, E. Mendiondo & P. O CONNELL (2003b) IAHS Decade on Predictions in Ungauged Basins (PUB), 2003–2012: Shaping an exciting future for the hydrological sciences/La décennie de l'AISH sur les prévisions en bassins non jaugés (PBNJ), 2003–2012: émergence d'un futur passionnant pour les sciences hydrologiques. *Hydrological Sciences Journal*, 48, 857-880.

Smith, E., G. Asrar, Y. Furuhama, A. Ginati, A. Mugnai, K. Nakamura, R. Adler, M.-D. Chou, M. Desbois, J. Durning, J. Entin, F. Einaudi, R. Ferraro, R. Guzzi, P. Houser, P. Hwang, T. Iguchi, P. Joe, R. Kakar, J. Kaye, M. Kojima, C. Kummerow, K.-S. Kuo, D. Lettenmaier, V. Levizzani, N. Lu, A. Mehta, C. Morales, P. Morel, T. Nakazawa, S. Neeck, K. i. Okamoto, R. Oki, G. Raju, J. Shepherd, J. Simpson, B. Sohn, E. Stocker, W.-K. Tao, J. Testud, G. Tripoli, E. Wood, S. Yang & W. Zhang. 2007. International Global Precipitation Measurement (GPM) Program and Mission: An Overview. In Measuring Precipitation From Space, eds. V. Levizzani, P. Bauer & F. J. Turk, 611-653. Springer Netherlands.

Smith, L. C. (1997) Satellite remote sensing of river inundation area, stage, and discharge: A review. *Hydrological Processes*, 11, 1427-1439.

Stancalie, G., A. Diamandi, C. Corbus & S. Catana (2004) Application of EO data in flood fore-casting for the Crisuri Basin, Romania. Flood Risk Management: Hazards, Vulnerability and Mitigation Measures, 101.

Stokstad, E. (1999) HYDROLOGY: Scarcity of Rain, Stream Gages Threatens Forecasts. *Science*, 285, 1199.

Su, F., Y. Hong & D. Lettenmaier (2008) Evaluation of TRMM multisatellite precipitation analysis (TMPA) and its utility in hydrologic prediction in the La Plata basin. *Journal of Hydrometeorology*, 9, 622-640.

Swenson, S. & J. Wahr (2009) Monitoring the water balance of Lake Victoria, East Africa, from space. *Journal of Hydrology*, 370, 163-176.

Wang, Y. (2004) Using Landsat 7 TM data acquired days after a flood event to delineate the maximum flood extent on a coastal floodplain. *International Journal of Remote Sensing*, 25, 959-974.

Wang, Y., J. D. Colby & K. A. Mulcahy (2002) An efficient method for mapping flood extent in a coastal floodplain using Landsat TM and DEM data. *International Journal of Remote Sensing*, 23, 3681-3696.

Wang, J., H. Yang, L. Li, J. J. Gourley, K. Sadiq I, K. K. Yilmaz, R. F. Adler, F. S. Policelli, S. Habib & D. Irwn (2011) The coupled routing and excess storage (CREST) distributed hydrological model. *Hydrological Sciences Journal,* 56**,** 84-98.

Watson, J. P. (1991) A visual interpretation of a LANDSAT mosaic of the Okavango-delta and surrounding area*. Remote Sensing of Environment*, 35, 1-9.

Xiao, Q. & W. Chen (1987) Songhua River ood monitoring with meteorological satellite imagery. *Remote Sensing Information*, 37–41.

Yamaguchi, Y., A. B. Kahle, H. Tsu, T. Kawakami & M. Pniel (1998) Overview of Advanced Spaceborne Thermal Emission and Reflection Radiometer (ASTER). *IEEE Transactions on Geoscience and Remote Sensing*, 36, 1062-1071.

Yilmaz, K., R. Adler, Y. Tian, Y. Hong & H. Pierce (2010) Evaluation of a satellite-based global flood monitoring system. *International Journal of Remote Sensing*, 31, 3763-3782.

CHAPTER 5 : OVERALL CONCLUSION

Flood forecasting for early warning systems is crucial for risk management strategies. However, the effectiveness of an early warning depends on the robustness as well as accurate extent where the impacts will be felt. In view of the ever increasing flood disasters and their hazards to human security, there is an urgent need to reassess how to respond and prevent the potential of catastrophic loss of life and economic damage from flood risks. Satellite observations are crucial for future improvement of the understanding and monitoring of floods with better spatiotemporal resolution. Remotely sensed data provides potential for flood monitoring particularly over many data poor regions.

5.1 Remote sensing products for flood monitoring

Global monitoring of earth system process with satellite remote sensing improved our understanding of the water cycle both in the atmosphere and on the land surface. Both active and passive sensors are used as sources of observations, particularly in regions where in-situ networks are sparse. Many hydrological state variables and fluxes can be estimated through satellite remote sensing. Multispectral and microwave remote sensing detect reflected or emitted energy from an object in a number of different spectral bands of the electromagnetic spectrum. In remote sensing this spectral signature is the most diagnostic tool in remotely identifying the composition of an object. Generally

there is a trade-off between the spectral resolution, spectral coverage, radiometric resolution, and temporal resolution.

Freely available remote sensing data are an excellent resource for the mapping of spatially distributed disasters. Satellite based disaster monitoring systems have become an integral part of disaster management activities in many developed and some developing countries. NASA's Earth Observing Systems (EOS) provides seamless data that can be used for flood detection and mapping research. Therefore, data from multiple missions and sensors (e.g. SRTM, TRMM, MODIS, ASTER, AMSR-E) can be used with existing hydrologic models such as the CREST model for hydrologic analysis and flood prediction in ungauged basins.

The development of satellite rainfall estimates offers the potential to address flood prediction problems in poorly gauged basins. The current TRMM mission particularly contributes towards this effort. One of the goals of this mission is to enable improved hydrological modeling for flood prediction applications over South Asia, Mesoamerica and Africa. Multispectral satellite sensors such as MODIS and ASTER can be used to evaluate and validate hydrologic model predictions. Quantification of flooding through orbital sensors can help to evaluate hydrologic models and, hence, potentially improve hydrologic predictions and flood management strategies in un-gauged catchments.

This research work demonstrates the utility of remotely sensed data for hydroclimatologic studies at a catchment scale with sparse ground observations. Simulation of the key hydrological processes and their interconnection with climate and basin characteristics is a critical step in estimating catchment water balance. Therefore, a distributed hydrologic model (CREST) is implemented to simulate hydrological states and flux variables such as runoff, evapotranspiration, precipitation and soil moisture at a spatial resolution of 30 arc seconds at three hour intervals. The hydrologic model is forced by satellite-based precipitation and evapotranspiration estimates and other remote sensing products. The hydrologic model calibrated with satellite precipitation TMPA 3B42 V6 displayed agreement with gauge observations.

The proof of concept study has demonstrated the efficacy of satellite remote sensing data for flood forecasting in poorly and ungauged basins. In particular, a distributed rainfall-runoff model is calibrated with satellite based river discharge proxy, which implicitly simulate the varying runoff response for a given rainfall event. Contrary to the traditional data types that represent point measurements, passive microwave sensor shows flood evolution at the pixel level. This spatially continuous and daily data can be used to implement distributed hydrological models. Novel geospatial framework that can incorporate satellite-rainfall estimates and other remote sensing data into a hydrologic model can be helpful to develop flood forecasting systems in ungauged regions. Operationally implementing this strategy in those areas will provide flood

managers and international aid organizations, a realistic decision-support tool in order to better assess flood risks.

5.2 Key Limitations

1. The research work for this study is focused on major floods that occur due to longer duration storms systems lasting for more than several days. Results from this study are limited to large scale (>1,000 km2) watersheds. Therefore, findings from this study cannot be generalized to small scale runoff generation mechanisms.

2. The other limitation is the cloud contamination in optical remote sensing data for other basins that can lead to noise in the flood pixel classification.

5.3 Future Research Direction

The next generation precipitation satellite constellations “Global Precipitation Measurement” (GPM) mission will address the need for accurate global precipitation measurement. With the availability of satellite precipitation data at fine spatial scales in the coming years, there is currently an urgent need to better assess the utility of these satellite products for flood predictions. On the other hand, statistical downscaling of current TRMM data to GPM’s 4-km resolution will provide insight into the potential utility of future GPM products for flood prediction applications.

Future research will address these issues by systematically applying the

approach to a wider range of flooding events in different basins with a variety of climatic and land cover characteristics. Moreover, near future satellite missions such as the Soil Moisture Active and Passive (SMAP) mission (Entekhabi et al. 2010) for global soil moisture, Surface Water and Ocean Topography (SWOT) mission for river discharge estimates (Alsdorf, Rodríguez and Lettenmaier 2007b) and the Global Precipitation Measurement (GPM) mission integrated into the proposed framework can materialize flood forecasting systems in ungauged basins throughout the globe.

APPENDICES

Appendix 1. CREST Model Parameters that require optimization.

Symbol	Unit	Brief description	Default values
B	-	Exponent of variable infiltration curve	0.2
K_c	-	Coefficient of land cover's CIC	0.5
k_I	-	Interflow reservoir discharge parameter	0.1
k_O	-	Overland reservoir discharge parameter	0.5
k_X	-	Runoff velocity coefficient varying in overland, channel and interflow	50/100/15
Th	km^2	Threshold between overland and channel	30
W_{m1}	mm	Maximum cell mean water capacity of soil layer 1	20
W_{m2}	mm	Maximum cell mean water capacity of soil layer 2	50
W_{m3}	mm	Maximum cell mean water capacity of soil layer 3	80

Appendix 2. Input and output Hydrologic Variables of CREST model.

Symbol	Unit	Description
A	-	Upstream point of profile along several cells
CI	mm	Intercepted water in canopy layer
CIC	mm	Canopy interception capacity
E_a	mm h^{-1}	Actual evaporation of bare soil
E_c	mm h^{-1}	Actual evaporation from intercepted water in canopy layer
E_p	mm h^{-1}	Potential evapotranspiration
E_{p1}	mm h^{-1}	Potential evaporation from soil layer 1
E_{p2}	mm h^{-1}	Potential evaporation from soil layer 2
E_{p3}	mm h^{-1}	Potential evaporation from soil layer 3
E_{s1}	mm h^{-1}	Actual evaporation from soil layer 1
E_{s2}	mm h^{-1}	Actual evaporation from soil layer 2
E_{s3}	mm h^{-1}	Actual evaporation from soil layer 3
i_m	mm	Maximum i of a cell
I	mm h^{-1}	Infiltration water simulated from variable infiltration curve

$\hat{I}$	mm h^{-1}	Adjusted I considering horizontal input water from routing
P	mm h^{-1}	Precipitation
P_{soil}	mm h^{-1}	Precipitation input to soil surface
$\hat{P}_{soil}$	mm h^{-1}	Adjusted P_{soil} considering horizontal input water from routing
R	mm h^{-1}	Excess rain generated by variable infiltration curve
R_O	mm h^{-1}	Overland excess rain
R_I	mm h^{-1}	Interflow excess rain
$R_{I,in}$	mm h^{-1}	Interflow runoff entering a cell from routing
$R_{I,out}$	mm h^{-1}	Interflow runoff leaving a cell
$R_{O,in}$	mm h^{-1}	Overland runoff entering a cell from routing
$R_{O,out}$	mm h^{-1}	Overland runoff leaving a cell
S_I	mm	Interflow reservoir storage
S_O	mm	Overland/channel reservoir storage
$\hat{S}_O$	mm	Adjusted S_O considering horizontal input water from routing
Sto	mm	Total cell water storage, including soil water and free water
T	h	Concentration time from cell to its downstream adjoining cell

W	mm	Total cell mean water of three soil layers
W_1	mm	Cell mean water in soil layer 1
W_2	mm	Cell mean water in soil layer 2
W_3	mm	Cell mean water in soil layer 3
W_m	mm	Maximum cell mean water capacity